DEVELOPMENT OF AN EARTH PRESSURE MODEL FOR DESIGN OF RETAINING STRUCTURES IN PIEDMONT SOILS

FINAL REPORT

University of North Carolina at Charlotte
Department of Civil and Environmental Engineering

October, 2008

J. Brian Anderson, Ph.D. P.E., Principal Investigator
Vincent Ogunro, Ph.D., Co-Principal Investigator

Jonathan M. Detwiler, Graduate Student
James R. Starnes Jr., Graduate Student
Richard E. Burrage Jr., Graduate Student

TECHNICAL REPORT DOCUMENTATION PAGE

1. Report No. **FHWA/NC/2006-51**	2. Government Accession No.	3. Recipient's Catalog No.
4. Title and Subtitle **Development of an Earth Pressure Model for Design of Earth Retaining Structures in Piedmont Soil**		5. Report Date **October 2008** 6. Performing Organization Code
7. Author(s) **J. B. Anderson and V. O. Ogunro**		8. Performing Organization Report No.
9. Performing Organization Name and Address **University of North Carolina at Charlotte College of Engineering** **9201 University City Boulevard** **Charlotte, NC 28223-0001**		10. Work Unit No. (TRAIS) 11. Contract or Grant No.
12. Sponsoring Agency Name and Address **North Carolina Department of Transportation** **Research and Development Unit** **1549 Mail Service Center** **Raleigh, 27699-1549**		13. Type of Report and Period Covered **Final Report** **July 2004 – June 2007** 14. Sponsoring Agency Code **2005-16**
Supplementary Notes:		

16. Abstract

Anecdotal evidence suggests that earth pressure in Piedmont residual soils is typically over estimated. Such estimates of earth pressure impact the design of earth retaining structures used on highway projects. Thus, the development of an appropriate model for estimating earth pressure would result in more rational design of retaining structures in Piedmont residual soils. Accordingly, the objective of this research was to develop an earth pressure model for Piedmont residual soil.

An experimental program to estimate, model, and measure earth pressure in Piedmont residual soils was carried out by the University of North Carolina at Charlotte. This study centered around the instrumentation, construction, and load testing of four sheet pile retaining walls at two sites in the Charlotte Belt and Carolina Slate belt regions of the Piedmont. The scope of work included extensive insitu and laboratory soil testing to estimate soil strength parameters for the residual soils; and numerical models to plan the load testing program and evaluate the results. Results of the load tests showed little or no earth pressure due to Piedmont residual soil. Interpretation of data from the sites using theoretical and numerical methods supports this findings.

Conclusions from this study include: 1) The earth pressure currently used in design of retaining structures in Piedmont soils is greater than earth pressure measured during load tests. Field measurements from the instrumented wall load tests demonstrated that the retained soils exerted little or no pressure on the structure. 2) The Piedmont soils that were tested in this research had significant strength. The average drained friction angle was 28^o and the average drained cohesion intercept was above 300 psf. These values were consistent with those found in the literature for similar soils. 3) Based on the soil test results as well as the minimal earth pressure detected during the load tests, the soil strength parameters, ϕ'and c' should be used together in Rankine's earth pressure equation to predict the earth pressure in Piedmont soils. And 4) Triaxial tests provided the most consistent measurement of ϕ' and c'. The borehole shear tests also measure ϕ and c' but should only be used when triaxial testing is unavailable.

17. Key Words **Retaining structure, residual soil, sheet pile, insitu test, load test, instrumentation, dilatometer, borehole shear, triaxial**	18. Distribution Statement		
19. Security Classif. (of this report) **Unclassified**	20. Security Classif. (of this page) **Unclassified**	21. No. of Pages **147**	22. Price

Form DOT F 1700.7 (8-72) **Reproduction of completed page authorized**

DISCLAIMER

The contents of this report reflect the views of the Authors and not necessarily the views of the University. The Authors are responsible for the facts and the accuracy of the data presented herein. The contents do not necessarily reflect the official views or policies of the North Carolina Department of Transportation or the Federal Highway Administration. This report does not constitute a standard, specification, or regulation.

ACKNOWLEDGMENTS

This project would not have been possible without major contributions from several individuals and groups. The researchers would like to express their sincerest gratitude to following individuals and organizations:

The North Carolina Department of Transportation
Geotechnical Engineering Unit
Njoroge Wainaina, Mohammed Mulla, Chris Kreider, Scott Hidden, Chris Chen, Scott Webb, Clint Little, Jay Stickney, Chad Smith, and Mike Smith.
Materials and Tests Unit
C.K. Su and Randy Privette
Division 12 Construction and Operations
Max Buchanan, Dan Grissom, and Marty Plyler.
Division 10 Construction and Operations
Barry Moose, Garland Haywood, Gary Huneycutt, and Mark Smith.

S&ME, Inc.
Billy Camp and Tim Cleary

Insitu Soil LLC.
Roger Failmezger

SUMMARY

Anecdotal evidence suggests that earth pressure in piedmont residual soils is typically over estimated. Increased or overly conservative estimates of earth pressure impact the design of earth retaining structures used on highway projects. Thus, the development of an appropriate model for estimating earth pressure would result in more rational design of retaining structures in Piedmont residual soils. Accordingly, the objective of this research was to develop an earth pressure model for Piedmont residual soil.

The University of North Carolina at Charlotte carried out an experimental program to estimate, model, and measure earth pressure in Piedmont residual soils. This study centered around the instrumentation, construction, and load testing of four sheet pile retaining walls at two sites in the Charlotte Belt and Carolina Slate belt regions of the Piedmont geologic province. The scope of work included extensive insitu and laboratory soil testing to determine soil strength parameters for the residual soils. Numerical models were used to both plan the load testing program and evaluate the results. Results of the load tests showed little or no earth pressure due to Piedmont residual soil. Data interpretation through theoretical and numerical methods supports this findings. Conclusions from this study include:

1) The earth pressure currently used in design of retaining structures in Piedmont soils is significantly greater than earth pressure measured during load tests. Field measurements from the instrumented wall load tests demonstrated that the retained soils exerted little or no pressure on the structure.

2) The Piedmont soils that were tested in this research had significant strength. The average effective friction angle was 28^{o} and the average drained cohesion

intercept was above 300 psf. These values were consistent with those found in the literature for similar soils.

3) Based on the soil test results as well as the minimal earth pressure detected during the load tests, the soil strength parameters ϕ'and c' should be used together in Rankine's earth pressure equation to predict the earth pressure in Piedmont soils.

4) Triaxial tests provided the most consistent measurement of ϕ' and c'. The borehole shear tests also measure ϕ and c' but should only be used when triaxial testing is unavailable.

TABLE OF CONTENTS

page

APPENDICES

CHAPTER 1
INTRODUCTION

1.1 Introduction

Earth retention is an integral part of transportation infrastructure. Mechanically stabilized earth, sheet pile, soldier pile, pile panel, soil nail, gravity and cantilevered are different types of retaining structures utilized by the North Carolina Department of Transportation. Regardless of the earth retaining method, the design of a retaining structure is driven by the earth pressure exerted by the soil that must be retained.

Normal and shearing stresses exist within soil masses as well as at the interface between soil and structure. The magnitude and orientation of the resultant forces depend upon the strength and compressibility properties of the soil mass. In the case of a retaining wall, the amount of soil stress that is transmitted to the structure is the net amount that is not carried by the shearing strength within the soil mass. In the worst case, the entire stress due to the soil overburden is imposed on the wall, this would be the hydrostatic stress. However, most soils have internal shearing strength that will carry the stress and reduce the amount of lateral earth pressure. Therefore, knowing the strength and compressibility properties of the soil, the earth pressure on a retaining structure can be determined theoretically or analytically.

Of course, the magnitude of earth pressure is affected by the type and nature of soil. North Carolina has a diverse geologic footprint. Subsurface materials in the state range from rock found in the mountains to sands of the coastal plain. However, several zones of residual soils, known collectively as the Piedmont Physiographic Province, underlay a large portion of the state. Figure 1.1 shows the location of the Piedmont and that a

number of major U.S. cities, from Trenton, New Jersey to Atlanta, Georgia, are all located in the zone.

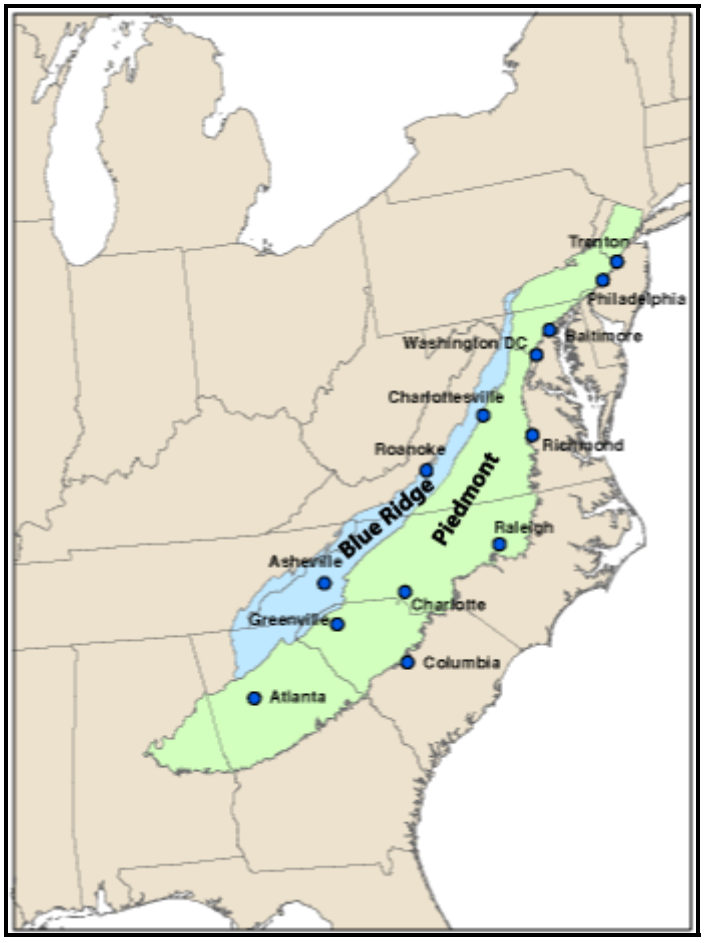

Figure 1.1 - Map of the Piedmont physiographic province (USGS 2001)

Within North Carolina, the Piedmont soils can be divided into three major zones: the Inner Piedmont (Alexander, Buncombe, Burke, Caldwell, Catawba, Cleveland, Henderson, Iredell, Lincoln, McDowell, Polk, Rockingham, Rutherford, Stokes, Surry, Transylvania, Yadkin, and Wilkes counties), the Charlotte Belt (Cabarrus, Davidson, Davie, Gaston, Guilford, Forsyth, Iredell, Lincoln, Mecklenburg, and Rowan counties) and the Carolina Slate Belt (Alamance, Anson, Cabarrus, Caswell, Chatham, Davidson, Durham, Granville, Guilford, Montgomery, Moore, Orange, Person, Randolph, Rowan,

Stanley, Union, and Vance counties). Figure 1.2 is a rough geologic map of North Carolina showing the Piedmont zones with county and NCDOT division boundaries.

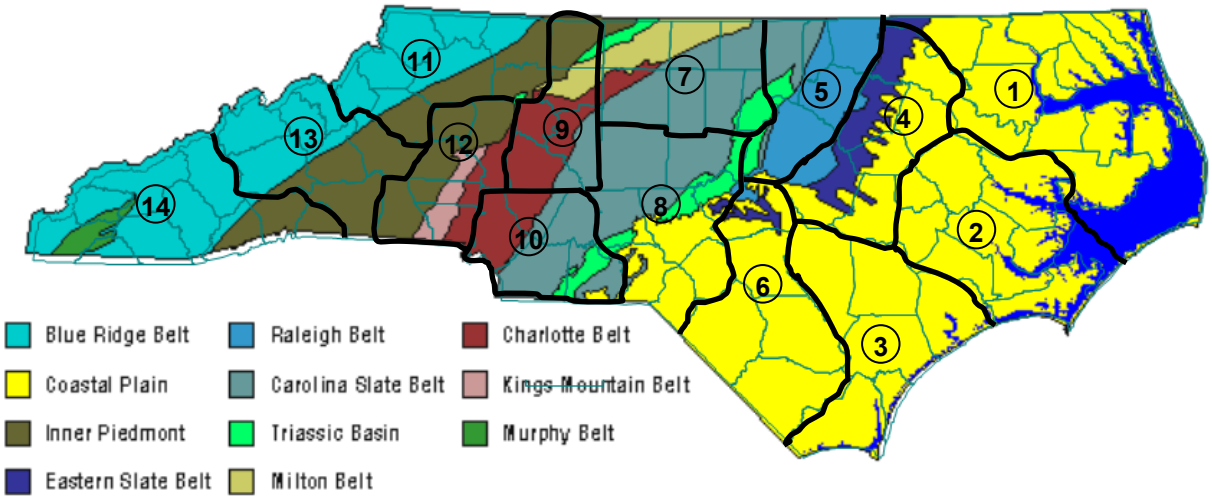

Figure 1.2 - County and NCDOT Division maps over North Carolina geology.

As a consequence of the formation process, residual soil often exhibits an increased strength over comparable transported materials. However, this strength often goes undetected by traditional sampling and insitu testing methods. Thus, the strength of residual soil is often poorly characterized and underestimated. This is particularly apparent when performing the standard penetration test, where many strength correlations were developed for transported soils that were assumed to either be cohesive or cohesionless, but not both. This assumption could mean that though a residual soil may be classified as a cohesionless material, the additional strength available due to the fabric structure and particle to particle bonding is ignored.

In terms of an engineering equation, the shearing strength of soil is represented by the Mohr-Coulomb criteria $\tau = c' + \sigma' \tan\phi'$, where the shear strength τ is the sum of a

cohesive component c' and geostatic stress σ' multiplied by the tangent of the drained friction angle ϕ'. Within this context, most soils are typically assumed to have c' = 0. However, residual soils tend to possess an appreciable amount of drained cohesion that can have a substantial impact on the design of retaining structures.

1.2 Background

1.2.1 Retaining Structures

Retaining structures are used when a difference in elevation is required and a constraint such as right of way, limited horizontal distance, or excessive elevation change, prevents utilizing a slope. In terms of typical highway applications, retaining structures are often used in bridge abutments, culverts and pipe wing walls, and roadway cuts and fills.

Retaining structures can be categorized by construction method as either bottom up or top down type. Bottom up would commonly be used for retaining walls required for fills, but can be used in cut applications with temporary shoring. Such walls include gravity, cantilevered concrete, mechanically stabilized or reinforced earth. Top down walls are used for cut applications where the wall is installed during the cut process without the need for shoring. Common examples include soldier pile/pile panel (cantilevered or tied back), soil nails, and sheet piling.

1.2.2 Methods for Estimating Lateral Earth Pressure

Common to methods for retaining structure design is the determination of lateral earth pressure. In the majority of cases, this is provided through the use of limiting equilibrium earth pressure coefficients. When the displacement of the structure is critical, the use of numerical techniques may be required.

1.2.2.1 Theoretical Approaches

There are three categories of lateral earth pressure - earth pressure at-rest, active earth pressure, and passive earth pressure. Earth pressure at rest, σ_0, refers to lateral earth pressure caused by an unyielding wall preventing earth from any lateral movement. If a wall is permitted to move away from the retained soil mass a slight distance, the soil will expand laterally following the wall. Shearing resistance developed within the soil mass acts opposite to the direction of the expansion, resulting in a decrease in lateral earth pressure. The minimum lateral earth pressure is the active pressure, σ'_a. Conversely, if a wall moves into the retained soil mass, the soil will be compressed laterally with the soil shearing resistance acting to oppose the lateral compression. The maximum lateral earth pressure condition is the passive pressure, σ'_p. The relationship between vertical stress and the active and passive lateral stress for a soil with cohesion and internal friction is shown on the Mohr's circle presented in figure 1.3.

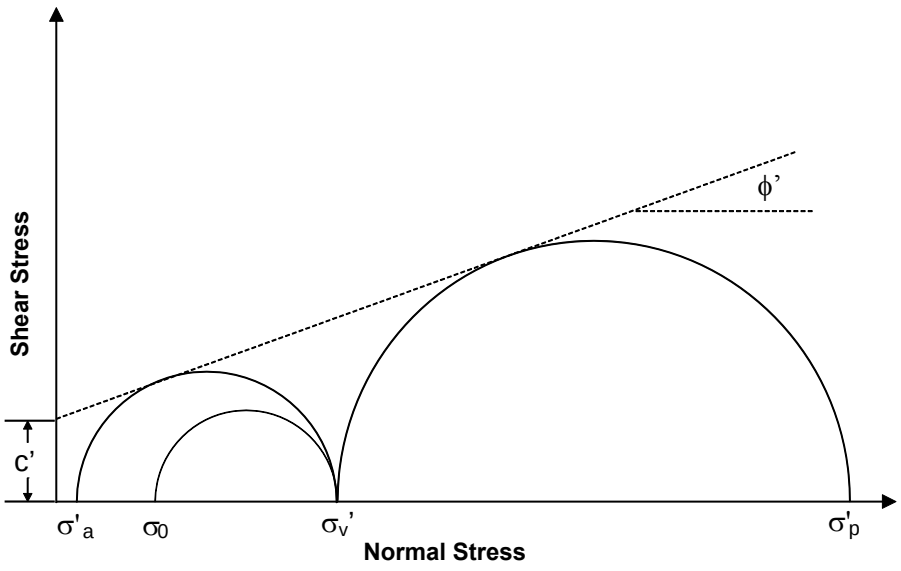

Figure 1.3 - Mohr's circle relationship for soil with cohesion and internal friction

The ratio of horizontal effective stress to vertical effective stress in a soil mass is referred to as the coefficient of lateral earth pressure, K. For the at-rest condition the earth pressure coefficient is designated K_0. For the active and passive pressure conditions the earth pressure coefficient is designated K_a and K_p, respectively. Therefore,

$$\sigma_h' = K\sigma_v' \pm 2c'\sqrt{K} \tag{1.1}$$

where K is the appropriate earth pressure coefficient, depending on stress conditions. The at-rest stresses for cohesionless soils are often determined using the modified Jaky (1948) equation:

$$\sigma_0' = \sigma_v'(1 - \sin\phi') \tag{1.2}$$

Traditionally, two general methods are used to estimate lateral earth pressure – the Rankine (stress) and Coulomb (force). Use of these theories has resulted in successful retaining wall design, but measured lateral earth pressure often differs largely from the expected values calculated from these models. These methods and many others are presented in a comprehensive text by Hansen (1961).

The Rankine theory for determining lateral earth pressure is based on several assumptions, but the most important is that there is no adhesion or friction between wall and soil. Pressures computed from Rankine theory are limited to vertical walls (with vertical blackface), and failure is said to occur in the form of a sliding wedge along an assumed failure plane that is a function of the friction angle of the soil. The equations derived from these assumptions are widely used and, propitiously, the results may not differ appreciably from those from other more fundamentally accurate analyses. Results obtained from the Rankine method generally are slightly more conservative, resulting in a small additional safety factor (Liu and Evett 2001).

The Rankine earth pressure model is illustrated in figure 1.4. The general equation for the magnitude of the resultant lateral force, P_a, in the active pressure case is given as:

$$P_a = \frac{1}{2}(H - z_c)(\gamma H K_a - 2c'\sqrt{K_a}) \tag{1.3}$$

where:

$$K_a = \tan^2\left(45 - \frac{\phi'}{2}\right) \tag{1.4}$$

$$z_c = \frac{2c'}{\gamma\sqrt{K_a}} \tag{1.5}$$

The resultant force acts at $(H-z_c)/3$ from the base of the wall.

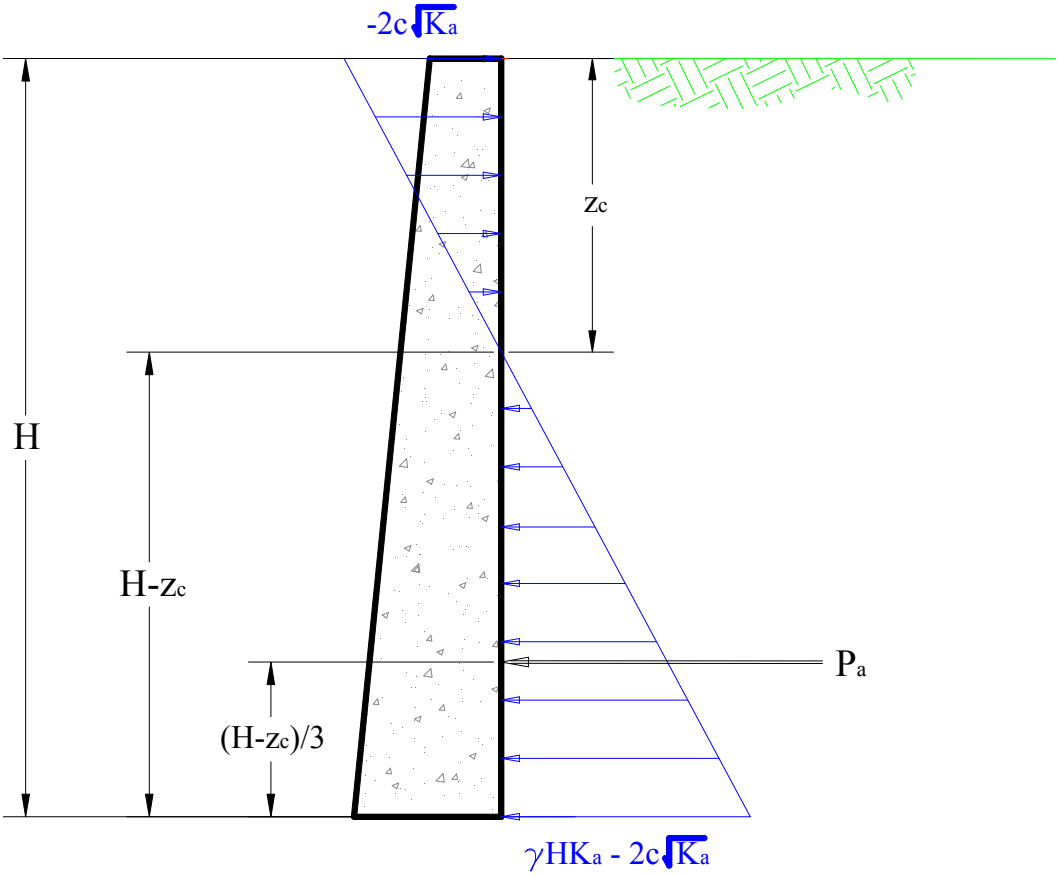

Figure 1.4 – Rankine earth pressure theory

Coulomb's theory for lateral earth pressure resulting from a retained mass of cohesionless soil considers that a failure wedge forms behind the wall by sliding along a plane. As the retaining structure moves away from the soil mass, lateral expansion is permitted and results in a relative movement between the wall and soil causing friction to develop on the back face of the wall (McCarthy, 2002). And so Coulomb, like Rankine, assumed that the failure surface due to lateral earth pressure would be planar. The key difference in these two methods, however, is that Coulomb took into account friction between the back face of the wall and retained soil. For Coulomb's method, the resultant of this friction and lateral pressure, P_A, acts at an angle, δ, measured normal to the back face of the wall. When the failure wedge is satisfactorily retained by the wall, the forces acting on the wedge are in equilibrium. Therefore, when the unit weight, γ_t, and friction angle, ϕ, for a retained soil are known, the force imposed on the wall as a result of the active pressure wedge, P_A, can be determined by vector addition, shown in figure 1.5. This force is calculated using the following equation:

$$P_A = \frac{1}{2}\gamma_t H^2 K_A = \frac{1}{2}\gamma_t H^2 \left[\frac{\cos^2(\phi' - \theta)}{\cos^2\theta\cos(\delta+\theta)\left[1+\sqrt{\frac{\sin(\delta+\phi')\sin(\phi'-\alpha)}{\cos(\delta+\theta)\cos(\theta-\alpha)}}\right]^2} \right] \qquad (1.6)$$

Similarly, the force imposed by the passive earth pressure wedge, P_p, can be calculated for the Coulomb case using the following equation:

$$P_p = \frac{1}{2}\gamma_t H^2 K_p = \frac{1}{2}\gamma_t H^2 \left[\frac{\cos^2(\phi' + \theta)}{\cos^2\theta\cos(\theta-\delta)\left[1-\sqrt{\frac{\sin(\delta+\phi')\sin(\phi'+\alpha)}{\cos(\theta-\delta)\cos(\theta-\alpha)}}\right]^2} \right] \qquad (1.7)$$

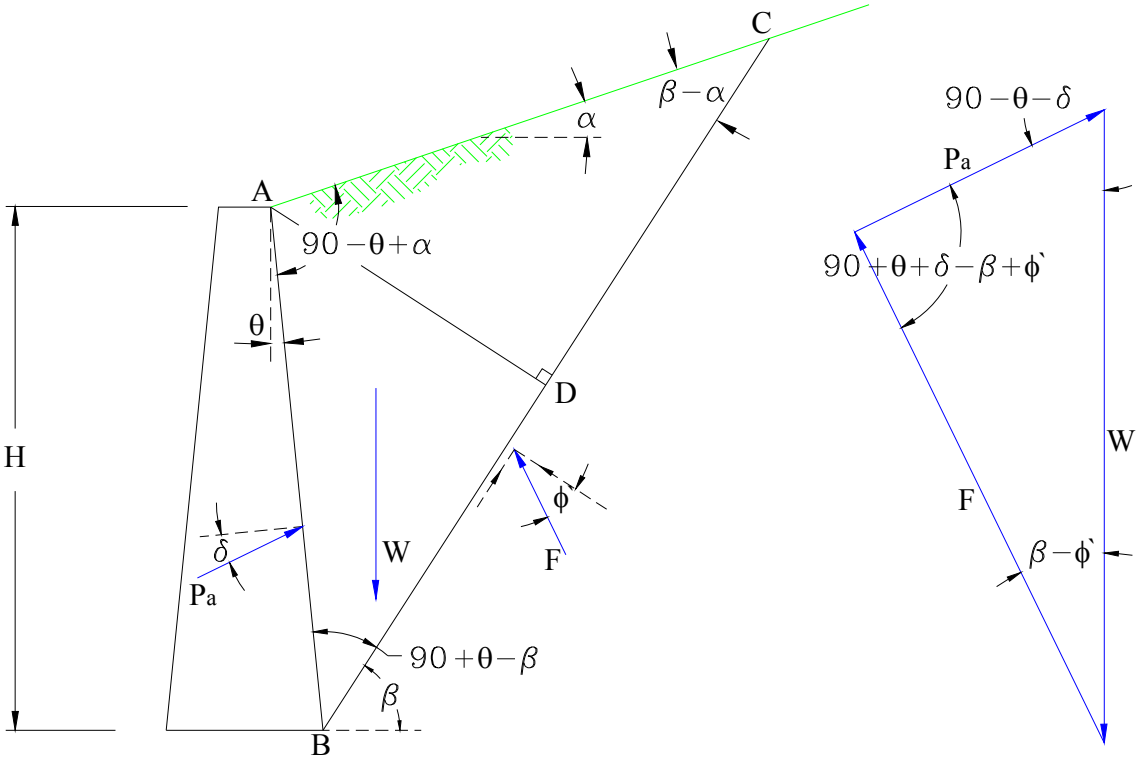

Figure 1.5 – Coulomb's active pressure trial failure wedge and force polygon

The actual active pressure condition for a given wall results from a unique failure wedge that provides the largest numerical value for the force P_A. But the above equation is only true for a uniform backfill slope and where the retaining wall is a plane surface. If this is not the case, P_A can be determined by trial-and-error analyzing a series of different sized failure wedges (McCarthy 2002).

When the retained soil mass has both cohesion and friction, the vector addition representing equilibrium forces acting on the failure wedge must include the additional vector of cohesive resistance, cL, acting on the failure plane.

Because the Coulomb theory assumes a planar failure, whereas the actual failure surface is typically curved, the lateral force calculated is slightly low. This discrepancy is typically minor, and so the Coulomb procedure for active pressure determination

provides a practical accuracy. The value of P_A computed from the Coulomb method will be slightly larger than that of the Rankine method, but due to the difference in direction that these forces act, the Rankine method typically creates the more severe condition and results in a slightly more conservative value (McCarthy 2002).

1.2.2.2 Soil Structure Interaction Approach

Given that Rankine and others have provided a convenient method for determining the lateral earth pressure, in any case, the soil mass must translate to achieve the minimum active pressure. If the soil mass does not translate one of two cases develop: either the at-rest pressure dominates or there is no lateral earth pressure on the structure. The soil structure interaction approach (SSI) can take this effect into account. Furthermore, this method allows for the beam behavior of a flexible wall to be included, which is essential to this study.

The most common application of the SSI method is for laterally loaded piles. Wang and Reese (1993) popularized the solution of the differential equation governing the response of a pile under lateral load in COM624. The soil in that case was reduced into a set of nonlinear slip springs connected to nodes on the pile, like those shown in figure 1.7. The pile was treated as a bending element. The response curves (p-y curves) represent a combination of active, passive, and shearing stresses on a single pile.

1.2.2.3 Finite Element Method

The finite element method (FEM) is often used in the analysis of complicated geotechnical problems based on the stress-deformation concept. In addition, it provides a rational method of attacking problems that are not readily solved using classic limiting equilibrium analysis under elastic conditions in infinite half spaces.

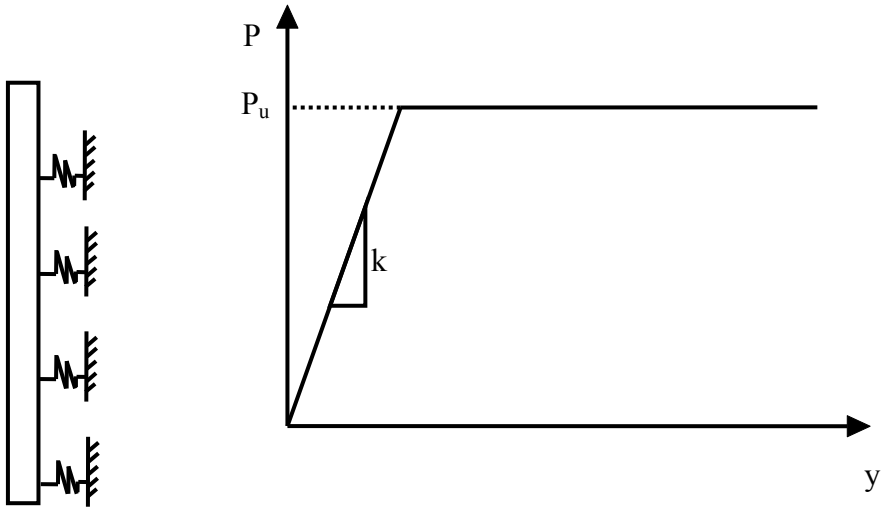

Figure 1.7 - Simple p-y relationship

Simply stated, the FEM is a way to solve partial differential equations (PDEs) numerically. Extended to civil-structural-geotechnical problems, the PDEs arise from complex elemental shape functions, the determination of strain from stress, and constitutive models that incorporate viscosity, plasticity, and pore fluid dynamics. Taking a step back, a simpler perspective is that the finite element method is nothing more than a complex way of expressing Hooke's Law $E = \frac{\sigma}{\varepsilon}$. A model is developed where either forces or displacements are imposed on boundaries. The resulting displacements and stresses are determined based on the shape functions and constitutive models selected.

In the context of the determination of earth pressure on a retaining structure, the stresses are then determined based upon the propagation of stresses within continuum, rotation of planes of primary stress, and deformation/translation of the soil mass. This method allows for the behavior of discrete soil layers to be included while at the same time considering the stress and deformation and their impact on one another.

1.3 Retaining Structure Design

Given the methods for determination of lateral earth pressure, the design of a retaining structure is typically completed using limiting equilibrium concepts. Take for example a gravity retaining wall. The wall is sized to resist overturning and sliding, while the base is safe for bearing and settlement. MSE structures use similar concepts. Sheet pile and solider pile walls are designed using a mixture of limiting equilibrium and soil-structure-interaction. In any case, the driving horizontal earth pressure is typically determined using Rankine's active earth pressure coefficient.

1.4 North Carolina Department of Transportation Retaining Structures

According to the 2002 NCDOT Roadway Design Manual, the NCDOT allows the use of gravity/semi-gravity, cantilever concrete, mechanically stabilized earth (MSE), prefabricated modular, and pile/panel (can be cantilevered or tieback) wall systems. A sampling of recent wall design projects within the Piedmont are shown in table 1.1. The majority of these are soldier pile or gravity structures. The standard parameters used in the design are also reported. It is worth noting that for the projects, the walls were designed to retain cohesionless soils with the drained friction angles between 30 and 35 degrees.

Table 1.1 Recent retaining wall projects in the Piedmont

Project #	County	Type	γ (pcf)	ϕ'	c' (psf)
B-3119	Buncombe	Soldier	110	34	0
B-1019	Anson	Soldier	120	30	0
B-3157	Davidson	Soldier	120	30	0
B-3406	Durham	Fabric			
B-3446	Davidson	Gravity	120	35	0
B-3601	Alamance	Soldier	120	30	0
B-3667	Davie	Gravity	120	35	0
B-3872	McDowell	MSE	120	30	0
B-4011	Ashe	Soldier	120	30	0
B-4043	Burke	Gravity	120	35	0
B-4095	Davidson	Gravity	120	35	0
B-4258	Rutherford	Soil Nail			
B-4317	Watauga	Gravity	120	35	0
B-3340	Haywood	Soldier	120	30	0
I4025A	Yad/Sur	Soldier	120	30	0
NC112	Buncombe	Soil Nail	120	30	
R-2107B	Montgomery	Gravity	120	35	0
R-2233AA	Rutherford	MSE	120	30	0
R-2248D	Mecklenburg	Soldier	120	30	0
R-2518A	Yancey	Soldier	120	30	0
R-2710	Watauga	Fabric	120	30	0
R-3415	Yadkin	Soldier	120	30	0
R-4758	Jackson	Soldier	120	30	0
R-3101	Alleghany	Soil Nail			
U-2510A	Mecklenburg	Gravity	120	35	0
U-3401	Randolph	MSE/Gravity	120	35	0
U-3456	Richmond	Soldier	120	30	0
U-3601	Buncombe	Gravity	120	35	0

CHAPTER 2
PROJECT OVERVIEW

2.1 Objectives

The main objective of this research program was to develop a model for lateral earth pressure in Piedmont residual soil. In order to develop the model, this program examined both the properties of Piedmont residual soils and the field performance of retaining structures at two research sites.

2.2 Research Methodology & Tasks

Since direct measurement of lateral earth pressures by earth pressure cells was ruled out due to construction complications and survivability concerns, instrumented sheet piles were used as "moment-cells" adapted from the analysis of deep foundations under lateral loading. Measured earth pressure was correlated back to insitu and laboratory determined soil parameters. Figure 2.1 shows a schematic diagram of the walls and the excavation.

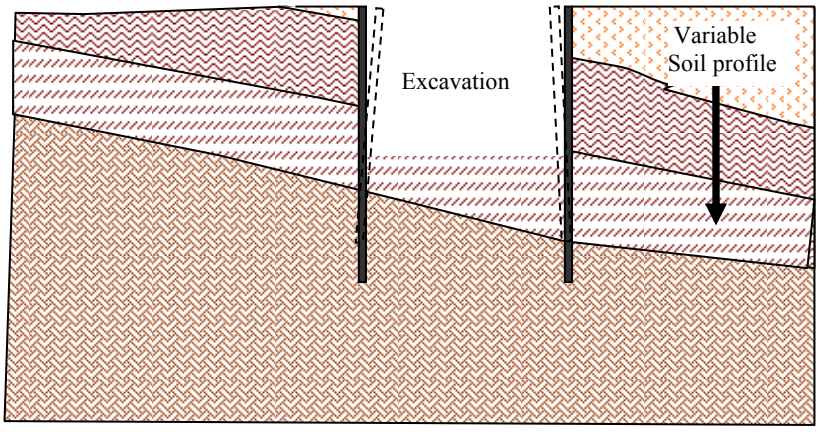

Figure 2.1 - Conceptualization of the field test walls

The following outlines the different tasks of the project, and explains the variations between the proposed and actual scope of work where applicable

1. Overview Retaining Structures: A detailed and extensive review of widely accepted works and literature associated with retaining structures will be completed.

   Commentary: This task was completed unchanged.

2. Collection of Existing Data: The historic records of earth retaining structures implemented in Piedmont residual soils and their performance will be collected and analyzed. The performance of these structures will be examined and correlated with the corresponding soil parameters

   Commentary: This task was completed unchanged.

3. Site Selection: Working in close partnership with engineers and personnel of the NCDOT Geotechnical Engineering Unit, three suitable test sites located in the Carolina Slate Belt, the Charlotte Belt and the Inner Piedmont will be selected. The selection of these sites will be based on the thickness of residual soils, bedding and joint structure.

   Commentary: Two sites, one in Statesville in the Carolina Slate Belt and the other in Monroe in the Charlotte Belt were chosen by the NCDOT Geotechnical Engineering Unit in cooperation with UNCC based on availability of funds.

4. Insitu and Laboratory Soil Testing: After the wall sites are selected, a rigorous site investigation program will be completed. NCDOT and UNCC personnel will work to perform standard penetration tests, Iowa Borehole Shear Tests, additional specialized insitu soil tests to determine the engineering properties and geologic

fabric of the residuum. In addition, the probable penetration depth of the sheet piles will be evaluated. Where possible, undisturbed samples of residual materials will be collected for determination of engineering properties.

Commentary: Additional specialized insitu soil tests successfully carried out included Dilatometer (Statesville and Monroe), Cone Penetration Test (Statesville). Specialized tests to determine soil fabric were not available.

5. Preliminary Numerical Simulations: Finite element method models will be developed to predict the earth pressure behind and deflection of the sheet pile walls based on insitu test parameters and geologic information at each site. These models will help fine tune the instrumentation and measurements for each test wall to best match the field conditions.

   Commentary: Finite element analyses were used to simulate the behavior and response of walls for different excavation depths. The simulations were used to select the sheet pile wall sizes, and assess wall deformation prior to field instrumentation.

6. Prototype Wall Testing: In order to verify the function of field instrumentation, two prototype sheet piles, one strain instrumented and one with the slope inclinometer casing, will be tested in the laboratory. The sheets will be installed with a fixed base and a point load will be applied at the opposite end to induce a moment. The strain gages will be checked and monitored during the loading process. The function of the slope inclinometer will also be verified. A third uninstrumented sheet will be tested in series with the prototype sheets to compare

the bending stiffness of the instrumented and non instrumented sheet pile sections and the effects of other environmental factors on the measurement system.

Commentary: This task was not performed because of delays in project implementation.

7. Full-Scale Instrumented Field Test Walls: The primary task of the research project will be the construction and excavation of the test retaining walls. At each of the selected sites from task 3, a pair of parallel instrumented retaining walls will be constructed, approximately 20 feet apart. Each wall will be 20 to 30 feet in length and will be constructed of sheets driven 20 feet into the ground or refusal. The soil between the two walls will be excavated 10 feet from the original ground surface. Each wall will contain three strain instrumented sheets and two slope instrumented sheets. Prior to and after excavation, slope inclinometer readings will be taken. The strain gages continually will be monitored over the duration of the excavation. After completing the excavation, the sheets will be removed and transported to the next site.

   Commentary: Apart from installation of the walls and constraints due to subsurface soil conditions, this task was carried out as planned with some changes to ensure for practical constructability of walls and safety.

8. Analysis of Results: Based on the results from task 6 and the research strategy discussed above, lateral earth pressure distribution for each field sheet pile test will be determined. The results obtained for each test site will be compared and correlated to characteristics of the residual soil (thickness, bedding and joint

structure). A simple displacement and earth pressure relationship based on the joint structure orientation will be proposed.

Commentary: This task was completed unchanged. It should be noted that characteristics of the residual soil such as joint structure orientation could not be determined.

9. Model Validation: The models developed in task 7 above will be correlated to the engineering properties of the residuum obtained from both laboratory and insitu tests. A relationship among earth pressure and measurable insitu soil properties will be developed and recommended. Results of the models will also be compared with classical earth pressure theory.

   Commentary: This task was completed in accordance with the plan.

10. Reporting and Publication: The data from each phase of the study, the results of analysis, and the project findings will be documented in a comprehensive report to the NCDOT. In addition, findings will be presented as publications and presentation to the TRB, STGEC, and Geo^3 T^2.

11. Commentary: This task was completed in accordance with the plan.

2.3 Significance of Work

Anecdotally speaking, this project was suggested based on the observation that Piedmont residual soils produce little or no lateral earth pressure. This can be seen in steep natural slopes or temporary cuts in these soils that appear to be stable over long periods of time. Most engineers recognize this and account for some reduction in earth pressure in their designs, however, this effect is almost purely by judgment.

The objective of this project was to develop a model that predicts earth pressure in Piedmont residual soils for use in the design of typical retaining structures. Classical earth pressure theory as well as numerical modeling using parameters derived from soil tests at both research sites were used to predict earth pressure at these sites. The results of the full scale load tests were used to validated the findings.

Based on these findings, the use of a reduced amount of earth pressure for retaining structures in Piedmont soils appears justified. This will impact the type and size of earth retaining structures that are available on a given project.

2.4 Limitations of Research

The limitations of this program bear mention. The original two-year duration of the overall project, as well as the finite schedule of the sheet pile wall construction projects, did not allow time to assess the long term changes in lateral earth pressure. Unaccounted aspects of unsaturated soil behavior may have contributed to the behavior observed. The second significant limitation was the number of research sites tested. The proposed research program involved installation of sheet pile walls at three or more sites. However, due to multiple factors, only two research sites were tested. Findings and conclusions herein are limited by these factors.

CHAPTER 3
REVIEW OF RELEVANT LITERATURE

3.1 Residual Soil

Previous studies of residual soils have been performed by researchers in the mid-Atlantic and southeastern United States, as well as the tropics, Europe, and China. The bulk of the published research, in the United States and Europe, falls into one of three groups: investigation at a research farm location by North Carolina State University (1980s), field and laboratory testing at a National Geotechnical Research Site in Alabama by Auburn University and Georgia Institute of Technology (1990s), and recent activity on Portuguese soils attributed to Viana de Fonseca and Cruz (2000s).

3.1.1 Comprehensive test site studies

An extensive investigation of a single Piedmont residual soil test site was documented in a doctoral dissertation by Heartz (1986) and a technical publication by Lambe and Heartz (1988). The work was performed at a research farm near the North Carolina State University campus, in Raleigh, NC. The goal was to characterize the site by measuring compressibility, shear strength, and permeability, with special emphasis on the effects of anisotropy, mica content, stress history, suction, and sample disturbance.

The soil at the site was found to be composed primarily of flat kaolinized biotite particles oriented parallel to each other in fairly distinct tilted bands. One-dimensional consolidation tests, drained triaxial tests, and unconfined compression tests along with classification and index testing were performed on Shelby tube and hand trimmed block specimens. The drained triaxial tests were isotropically consolidated, and falling head permeability tests were performed before and after consolidation. Suction was measured

on unconfined compression test specimens before loading using a fine porous stone mounted in a triaxial cell. Results revealed suction was well below one atmosphere.

Exploration efforts by Wilson (1988) and Harshman (1989) expanded on work by Heartz at the test site. Wang (1995) and Wang and Borden (1996) describe the weathering profile and deformation characteristics of the soils and attempted to evaluate pressuremeter, dilatometer, standard penetration tests, and oedometer tests to predict foundation settlements. The laboratory testing program included oedometer, triaxial stress path and multistage compression, resonant column, and torsional shear tests. From the same site, Gupta (1995) and Borden et al. (1996) developed relationships for residual soil shear modulus, damping ratio, and volume change/densification characteristics based on the influencing parameters of confining pressure, shear strain amplitude, and number of loading cycles.

Similar effort was conducted by Vinson and Brown (1997) at a level III National Geotechnical Experimentation Site near Opelika, Alabama at the southern extent of the Piedmont province (Mayne et al. 2000). The original work was intended to serve as a reference for soil characteristics for other research at the site and to compare different types of insitu and laboratory measurements of physical properties of the soils at the site. The insitu testing program included standard penetration, piezocone penetration, pressuremeter, cone pressuremeter, dilatometer, borehole shear, cross- hole seismic, seismic cone penetration, and seismic dilatometer tests. The laboratory testing program included undrained triaxial tests, unconsolidated undrained triaxial tests, routine water content, unit weight, grain size analysis, Atterberg limits, and other classification tests. The results provide a basis for comparison of strength and stiffness measurements.

Analyses of the results of insitu and dynamic laboratory tests on soils from the site are included in Martin and Mayne (1998), Hoyos and Macari (1999), Finke et al. (1999), Finke et al. (2001), and Schneider et al. (1999).

3.1.2 Other works involving insitu and laboratory testing of residual soils

Some of the earliest published work on engineering aspects of residual soils was by Sowers (1954 and 1963). Masters theses at the Georgia Institute of Technology during the same period were published by Miller (1957) who investigated the behavior of a shear vane in Piedmont residual soil and Crowther (1963) who correlated data from cone and standard penetration testing in Piedmont residual soil to the bearing capacity of shallow foundations.

In 1982, a conference was held on "Engineering and Construction in Tropical and Residual Soils" that generated 37 papers (ASCE, 1982). The goal of the conference was to discuss the unique properties of tropical residual soils by emphasizing aspects such as composition and structure. The conference focused on the geotechnical properties, soil investigation and field testing, slope stability, excavation and dewatering, along with construction case histories.

In 1985, Brand and Phillipson (1985) published Sampling and Testing of Residual Soils which included current practices from 19 countries around the world. The goal of the book was to detail localized residual soil classifications, insitu and laboratory testing, geotechnical issues, and specialized residual soil problems. One of the main conclusions was that several authors place a larger reliance on insitu tests for residual soils than other soil types, because of sampling and testing problems. The difficulty of sampling reduces the reliability of lab testing and creates a discontinuity in results.

During the 1990s there was an increase in the use of insitu tests to characterize residual soils. Frank (1990) at the Georgia Institute of Technology revisited the relationship between SPT N and CPT q_c values. A conference track at the ASCE annual meeting in Charlotte, North Carolina in October of 1999 resulted in published GSP with 14 papers on residual soils. Of those, Failmezger et al. (1999) took a critical look at the misuse of the standard penetration test for residual soil characterization and the use of alternative insitu tests to characterize residuum. Kelley and Lutenegger (1999) used the standard penetration test with torque and dynamic cone penetrometer to develop relationships for engineering properties.

In the current decade, a great deal of literature has been generated concerning insitu testing of Portuguese residual soils. These soils are derived from some of the same ancient rocks as the Piedmont. Viana da Fonseca (2001) details a load testing of a shallow foundation in residual soil. Cruz et al. (2004a) used dilatometer and cone penetration tests to estimate the effective cohesive intercept, c', in Portuguese residual soils. Cruz et al. (2004b) took the same approach and developed it a step further to conclude that residual soils are characterized by a true drained cohesion as well as a multi-level yielding behavior that reflects the breaking down of residual structure under stress. Gomes Correia et al. (2004) used insitu tests to obtain geotechnical parameters. They reported that the bonded structure and fabric of residual saprolitic soils from granite have a significant influence on geomechanical behavior. Rodrigues and Lemos (2004) performed standard penetration, cone penetration, and cross-hole seismic tests and discovered significant differences between those correlations and the ones established for transported soils with identical grading curves. Viana da Fonseca et al. (2004) details the

investigation of a research site by extensive insitu and laboratory tests and presents correlative results of q_c/N and shear modulus (G_0). Cruz and Viana da Fonseca (2006) used the dilatometer to estimate the at rest earth pressure coefficient (K_0), shear strength parameters (c' and ϕ'), and stiffness parameters (G_0, E, and M).

3.1.3 Specific Literature on Triaxial Testing in Residual Soils

Between 1988 and 2006, 13 triaxial shear test studies have been published specifically in residual soils. A summary of these authors, date, location, soil type, and triaxial shear type are presented in Table 3.1.

3.2 Load Testing of Retaining Structures

Researchers such as Peck (1969) and Clough and O'Rourke (1990) have investigated retaining wall pressure and earth movements due to excavations. Other case studies of worldwide experience are also presented by Long (2001). In addition, studies seeking to determine lateral earth pressures have been presented by researchers like Fang et al. (1994) who utilized a movable model retaining wall to study passive pressures. The same moveable retaining wall was presented by Fang et al. (1997) to study the effect of sloping backfill on earth pressures. Similarly, Georgiadis and Anagnostopoulos (1998) used a model cantilever sheet pile wall in a tank to study surcharge effects. Both studies dealt with carefully placed sand in a controlled environment.

Full scale tests have been rare. A case was discovered where a full scale sheet pile supported excavation was instrumented. Kort (2002) presents a study carried out on an anchored sheet pile wall in Rotterdam, Holland. The soils were predominantly weak clay and peat, and the study was concerned with oblique bending and plastic hinging of sheet piles. However, there is extensive documentation of the field instrumentation plan.

Table 3.1 - Comprehensive summary of published residual soils triaxial testing

Author	Date	Location	Soil Type	Test Type	Numerical Results
Gan	1996	Hong Kong	Undisturbed completely decomposed granite and fine ash tuff (saprolite)	CD Saturated and Unsaturated	Remolded: c' = 1.45 psi and $\phi' = 35.5^o$ CDG: c'=3.05 psi and $\phi' = 31^o$
Garga	1988	Brazil	"Dense" Basaltic soil and "vesicular" basalt	CU	Peak CU Dense: c'= 8.53 psi and $\phi' = 32^o$ Vesicular: c'= 5.26 psi and $\phi' = 23^o$
Heartz	1986	North Carolina	Piedmont (Gneiss and Schist bedrock)	CD	
Lambe and Heartz	1988	North Carolina	Piedmont	CD	
Lee and Coop	1995	Korea	Decomposed granite (Compacted samples, highly organized)	CD	
Mayne et al.	2000	Alabama	Piedmont	CD; CU Disturbed and Undisturbed	c' = 2.47 psi and $\phi' = 31^o$ if c'=0 psi then ϕ = 35.3 degrees
Mohamedzein and Mohammed	2006	Sudan	sandstone and mudstone	UU, CIU	(Depth < 4m) c' = 0 psi and ϕ = 29 -35^o (Depth > 4m) c' = 0 psi and average $\phi' = 42^o$
Rahardjo et al.	2004a	Singapore	Reconstituted	CD	$\phi' = 31.5^o$
Rahardjo et al.	2004b	Singapore	Residual	CD Saturated and Unsaturated	$\phi' = 41.3^o$ or $\phi' = 36^o$
Viana da Fonseca et al.	2006	Portugal	Granite (saprolite with weak relict structure)	CD	c' = 0.65 psi and $\phi' = 45.8^o$
Vinson and Brown	1997	Alabama	Piedmont (micaceous sandy silt)	CD, CU, UU	
Wang	1996	North Carolina	Igneous and Metamorphic rocks	CD Unsaturated	
Wang and Yan	2006	Hong Kong	2 Saprolites Weathered volcanic tuff an Weathered Granite	CD CU	WT: $\phi' = 36.6^o$ WG: $\phi' = 34.1^o$

CHAPTER 4
SITE LOCATION AND CHARACTERIZATION

4.1 Site Selection and Investigation Plan

Selection of the research sites was based on multiple criteria that were not necessarily evident at the outset of the project. Foremost, the sites were to be located in the Piedmont physiographic province. Based on the geology and funding opportunities, research sites were suggested by the NCDOT Geotechnical Unit in the Charlotte Belt/Inner Piedmont near Statesville and the Carolina Slate Belt, outside of Monroe. Figure 4.1 shows the same map from figure 1.2 with the locations of the selected sites. The Statesville site was located in a borrow pit being excavated for the adjacent (project R-2911) US 70 bypass project. The Monroe site was part of the right of way being purchased for the US 601 widening, (project R-2616). Other sites that had been initially considered but were ruled out for various reasons included the Shelby Bypass, Monroe Bypass, and another near Winston-Salem.

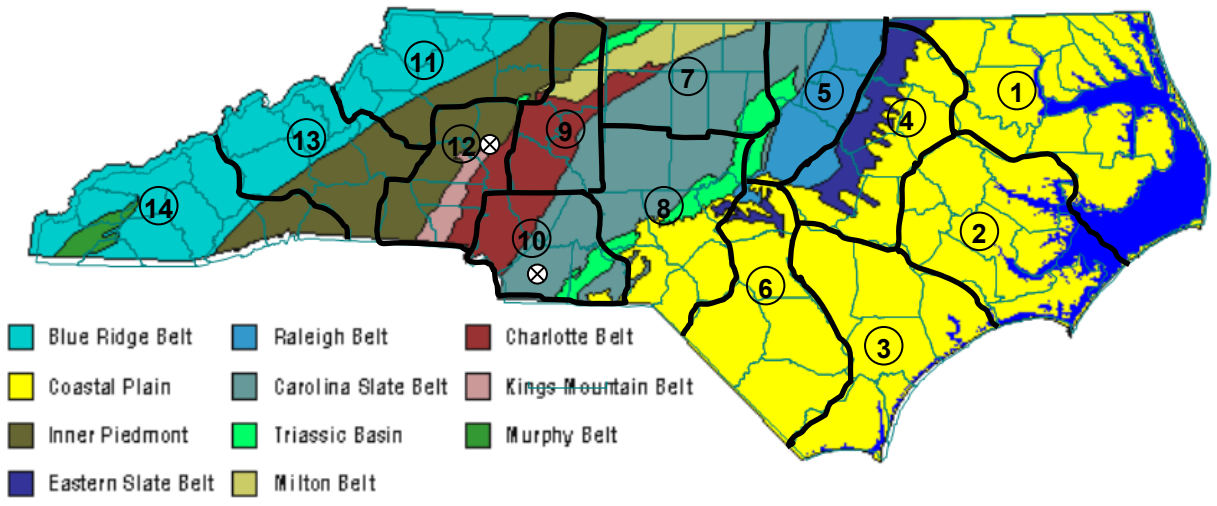

Figure 4.1 - North Carolina Geologic Map with counties, DOT divisions, and test site locations superimposed

To verify the existence of residual soils with sufficient thickness for wall testing, several Standard Penetration Test (SPT) borings were conducted at targeted locations within the test sites. Using the information from these borings, the sites were chosen and the location for each wall construction was established.

In order to pinpoint the stratigraphy, a second round of SPT was completed at the approximate location of measuring elements of the test walls. These borings were extended forty feet below the ground surface. Further insitu tests included Marchetti Dilatometer (DMT) to determine soil properties including lateral stiffness and earth pressure coefficients as well as Iowa Borehole Shear Tests (BST) to determine insitu strength. Cone Penetration Tests (CPT) and K_0 Stepped Blade (K_0SBT) were conducted only at the Statesville Site with the latter being ineffective.

Shelby tube specimens that were collected in the preparation of boreholes for the BST were sent to the Materials and Tests Unit for consolidated undrained triaxial and consolidation testing. The same soils were classified and their specific gravities were determined. The full complement of data is included in Appendices A and B for Statesville and Monroe, respectively.

4.2 Statesville

4.2.1 Insitu Tests

The first test site was near Statesville inside a contractor controlled borrow pit being excavated for use as fill for the US 70 Bypass. Three initial boring locations indicated thick horizons of Piedmont Residual soil ideal for installation of sheet piles for the project. Any of the tested locations would have been suitable for wall installation.

Targeted site exploration began just after the contractor began site clearing operations. Due to the anticipated use of the site, the contractor dictated that only a small

portion of the borrow pit was available for the research project, and thus the location was constrained near the northwest corner of the property. The approximate location for the test walls was laid out and the second phase SPT was conducted. The boring locations overlain on the walls that were eventually constructed are shown in Figure 4.2.

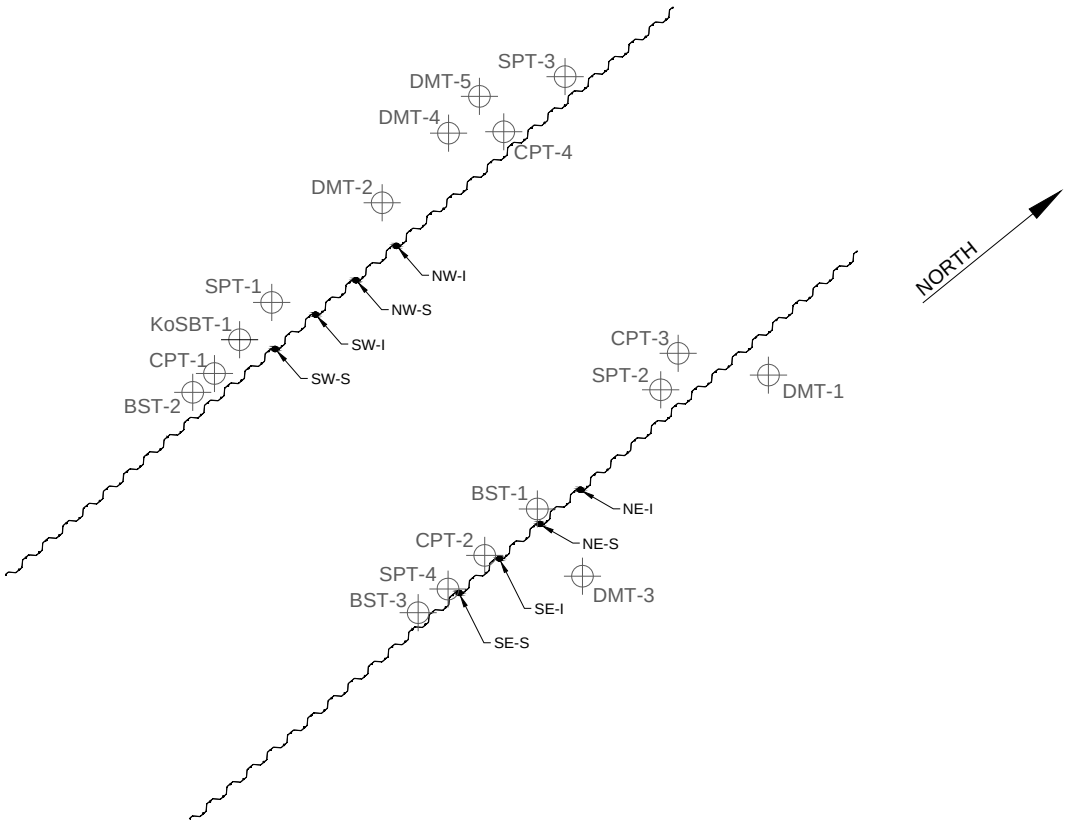

Figure 4.2 - Location of in-situ soil tests with respect to wall placement

Four SPT showed a profile consisting of tan and red clayey silt. Uncorrected blowcounts ranged from 5 to 15 with an average around 8. The raw and corrected numerical results of the SPT are show in Table 4.1. Two Marchetti Dilatometer (DMT) soundings were completed to determine strength and compressibility parameters. Three additional DMT soundings, including thrust measurements that were not available during

the initial tests, were conducted after the wall load tests. All of the soundings were consistent as seen in Figure 4.3. Borehole shear tests (BST) were performed at several depths in three boreholes. Key to the performance of the BST was the creation of a test pocket using a Shelby tube. Of the twelve potential BST locations, eight were successful. Results of these tests show generally friction angle of 30-40^{o} and cohesion intercept averaging 250 psf. The results are shown graphically and numerically in figure 4.4 and table 4.2, respectively.

Additional tests, only conducted at the Statesville site were the Cone Penetration Test (CPT) and the K_0 Stepped Blade Test (K_0SBT). S&ME Inc. performed four CPT soundings with their truck mounted 20 ton rig, the results of which are shown in figure 4.5. The CPT showed a consistent tip resistance value of 20 tsf and sleeve friction between 2 and 5 tsf. Only one K_0SBT test was attempted. Multiple pressure cells were damaged during penetration, therefore test was abandoned and not considered further.

Table 4.1 - SPT results (Statesville)

SPT-1			SPT-2			SPT-3			SPT-4		
Depth (ft)	N	N'_{60}	Depth (ft)	N	N'_{60}	Depth (ft)	N	N'_{60}	Depth (ft)	N	N'_{60}
4.2	7	18.2	4.5	7	18.2	4.3	6	15.6	3.4	11	28.6
9.2	5	9.1	9.5	8	14.4	9.3	6	10.9	8.4	14	26.8
14.2	6	8.8	14.5	10	14.6	14.3	6	8.8	13.4	13	19.7
19.2	5	6.4	19.5	8	10.0	19.3	8	10.1	18.4	9	11.6
24.2	5	6.1	24.5	8	9.0	24.3	6	6.9	23.4	16	18.3
29.2	5	5.8	29.5	8	8.2	29.3	5	5.5	28.4	11	11.5
34.2	7	7.8	34.5	8	7.6	34.3	8	8.5	33.4	10	10.1
39.2	8	8.5	39.5	7	6.4	39.3	10	10.2	38.4	11	10.7

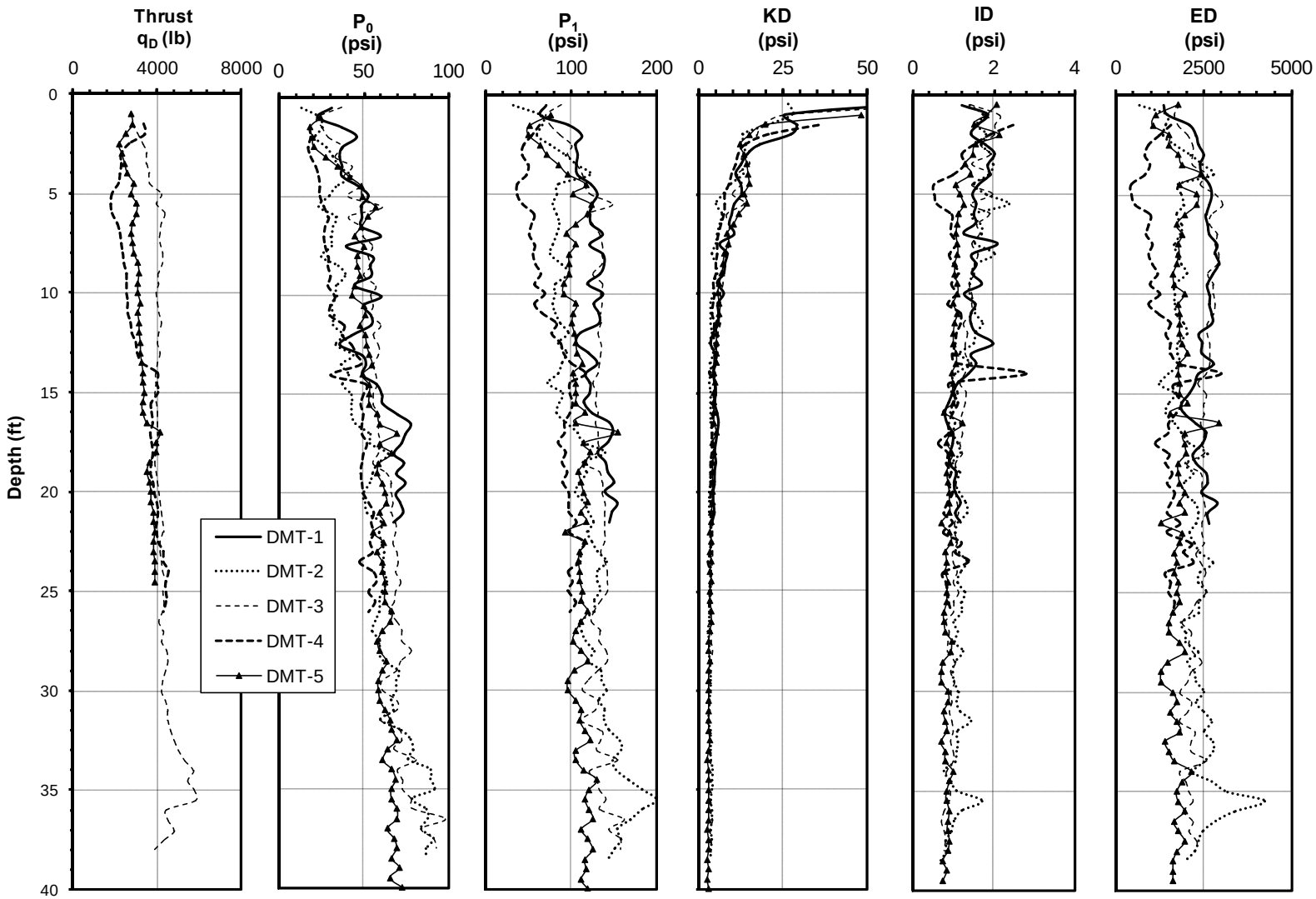

Figure 4.3 - Summary of DMT results (Statesville)

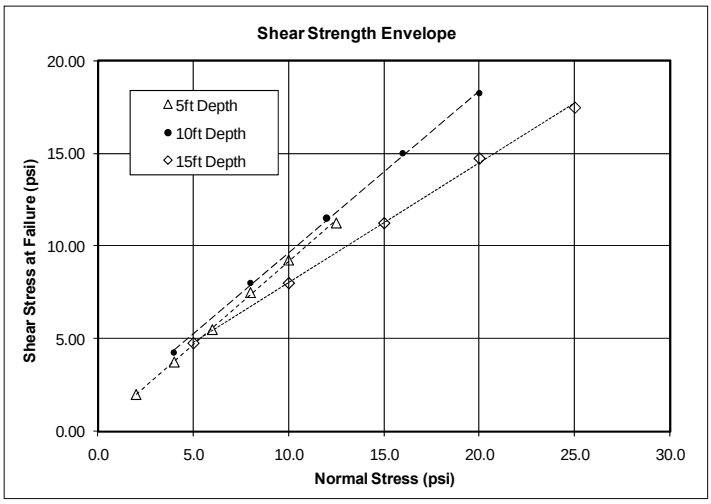

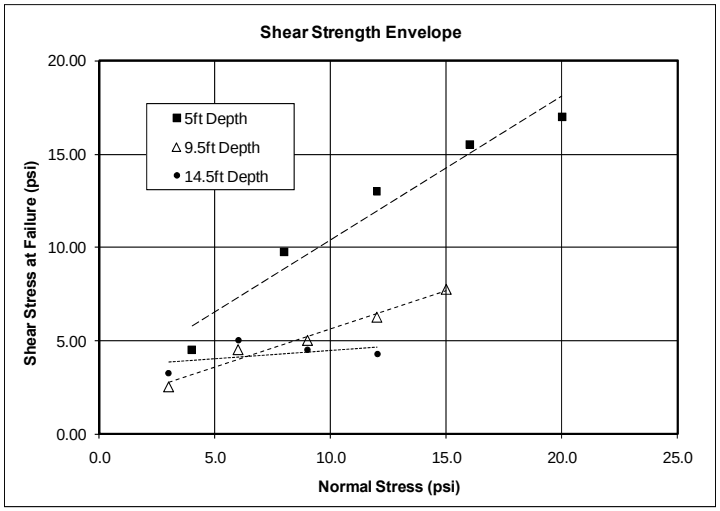

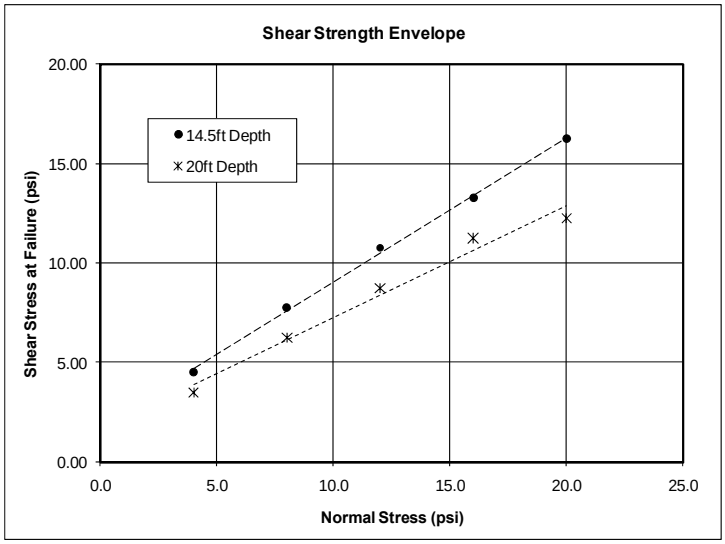

Figure 4.4 – Summary of Statesville BST results

Table 4.2 - BST Measured ϕ and c (Statesville)

Test	Depth (ft)	ϕ (deg)	c (psf)
BST #1	5	41.7	32
BST #1	10	41.2	130
BST #1	15	32.8	227
BST #2	5	31.2	767
BST #2	9.5	23.4	166
BST #2	14.5	4.8	522
BST #3	14.5	36	259
BST #3	20	32.8	144

4.2.2 Laboratory Tests

The specimens tested were from depths between 5 and 21 feet below ground level, and all were collected in preparation of pockets for the BST. Classification tests were performed on nineteen samples using Atterberg limits, sieve, and hydrometer analysis. The specific gravity was determined as well.

Six one dimensional consolidation tests were conducted to determine compressibility parameters. Nineteen triaxial tests, representing seven test locations, were completed for the Statesville Site. All but three of these specimens were saturated and tested in the consolidated-undrained (CU) condition. The others, from a shallow depth, above the water table, were not saturated and tested consolidated drained (CD) condition to ascertain the impact of unsaturated behavior.

The index tests, summarized in table 4.3, showed that the vast majority of the soils were A-7. Consolidation tests suggest that the soils were all highly over-consolidated, especially at shallow depths. Triaxial tests reported effective friction angles between 25^o and 35^o with cohesion ranging between 200 and 400 psf. Modulus, $E_{50,}$ values ranged from 200 to 3000 psi, for the confining pressures between 5 and 35 psi. Tables 4.4 and 4.5 show the consolidation and triaxial test results, respectively.

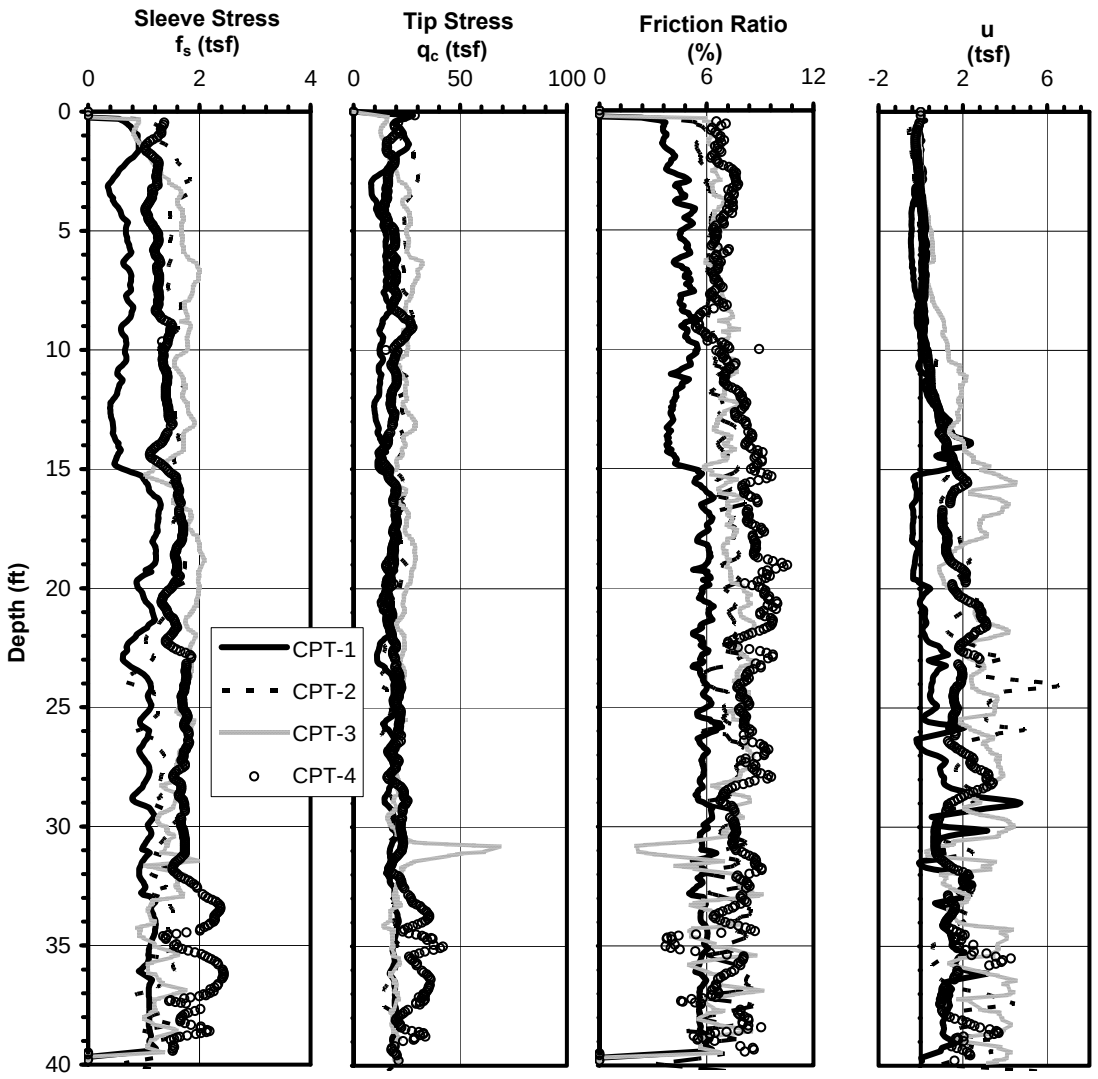
Sleeve Stress
f_s (tsf)
Tip Stress
q_c (tsf)
Friction Ratio
(%)
u
(tsf)
Depth (ft)
CPT-1
CPT-2
CPT-3
CPT-4

Figure 4.5 – Summary of CPT results (Statesville)

Table 4.3 - Summary of index properties and classification testing (Statesville)

Borehole No.	Sample No.	Sample Depth	Specimen No.	Grain-Size Analysis								Atterberg Limits			AASHTO	Specific Gravity, G_s
								Minus #10 Fraction				Liquid Limit, *LL*	Plastic Limit, *PL*	Plasticity Index, *PI*		
				#4	#10	#40	#200	#60	#270	Silt	Clay					
[-]	[-]	[ft]	[-]	[% passing]								[%]	[%]	[%]	[-]	[-]
BST-1	ST-1	5.0 - 7.0	1	100	99	78	28	39.5	37.5	21	2	54	NP	NP	A-2-5(0)	2.643
			2	-	100	89	52	22.6	30.8	36.6	10.1	53	42	11	A-7-5(5)	2.717
			3													
	ST-2	9.3 - 11.3	1	-	100	94	65	13.9	31.8	38.3	16.1	52	36	16	A-7-5(11)	2.74
			2													
			3													
	ST-3	19.3 - 21.3	1	-	100	89	58	18.2	34.2	35.5	12.1	56	40	16	A-7-5(9)	2.715
			2													
BST-2	ST-2	9.0 - 11.0	1	-	100	97	82	6.3	16.2	41.2	36.4	73	43	30	A-7-5(31)	2.723
			2													
	ST-3	14.0 - 16.0	1	-	100	96	81	8.5	13.3	35.7	42.5	72	42	30	A-7-5(30)	-
			2	-	100	94	65	14.8	25.5	29.6	30.1	51	32	19	A-7-5(12)	2.671
			3	100	99	93	59	15.6	32.4	35.9	16.2	51	42	9	A-5(6)	2.678
BST-3	ST-3	14.0 - 16.0	1	100	90	78	49	26.6	23	18.1	32.3	52	33	19	A-7-5(7)	2.684
			2	100	96	80	44	31.1	29.1	21.7	18.2	48	38	10	A-5(2)	2.668
			3	-	100	94	54	15.7	39	33.2	12.1	54	47	7	A-5(4)	2.643
	ST-4	19.0 - 21.0	1	-	100	93	54	18.2	34.9	26.7	20.2	53	40	13	A-7-5(6)	2.713
			2	-	100	91	50	19.6	39	29.4	12.1	53	39	14	A-7-5(5)	
			3													

Table 4.4 - Summary of consolidation testing (Statesville)

Borehole No.	Sample No.	Depth	AASHTO	Compression Index, c_c	Recompression Index, c_r	Pre-consolidation Pressure, P_c	Over-consolidation Ratio, *OCR*
[-]	[-]	[ft.]	[-]	[-]	[-]	[psf]	[-]
BST-1	ST-1	5.0 – 7.0	A-2-5(0)	0.528	0.011	7,000	12.1
	ST-3	19.3 – 21.3	A-7-5(9)	0.515	0.035	9,000	4.0
BST-2	ST-2	9.0 - 11.0	A-7-5(31)	0.225	0.003	6,400	5.8
	ST-3	14.0 - 16.0	A-7-5(30)	0.266	0.005	6,000	3.5
BST-3	ST-3	14.0 - 16.0	A-7-5(7)	0.264	0.005	4,000	2.3
	ST-4	19.0 - 21.0	A-7-5(6)	0.421	0.006	7,000	3.3

Table 4.5 - Summary of triaxial shear testing (Statesville)

Location	**Depth (ft)**	**Type**	**Saturated**	**c' (psf)**	**ϕ' (deg)**	**E_{50} (psi)**
BST-1	6	CD	No	318	24.3	933, 1791, 926
BST-1	10.3	CU	Yes	255	29.5	1219, 2256, 2596
BST-1	20.3	CU	Yes	410	28.7	2126, 3346
BST-2	10	CU	Yes	411	27.1	588, 673
BST-2	15	CU	Yes	0	34.4	192, 1477, 2459
BST-3	15	CU	Yes	300	27.8	266, 1765, 2361
BST-3	20	CU	Yes	404	26.1	607, 1861, 2372

4.3 Monroe

4.3.1 Insitu Tests

The second research site was chosen using a different set of criteria from Statesville. The selection of the Monroe site was done primarily to be in line with the future US601 widening project. Within that project, two locations of highest elevation along the alignment were identified as potential test sites. One was a small field and the other was a residence, both of which would be part of the right-of-way to be acquired in the widening project. Based upon the initial SPT borings, both sites were potential test locations. However, due to delays in the US601 project, right-of-way would not be purchased in time, therefore, the southerly of the two potential sites was chosen and the small amount of right-of-way was pre-purchased for use on the project.

Beginning in June of 2006, in depth insitu testing and soil sampling program was carried out at the Monroe site. As before, the location of the test walls was established before testing. Figure 4.6 shows the locations of the insitu tests with respect to the final walls installed. Four SPT, depicted in table 4.6, were conducted down to 40 feet with SPT1 refusing at around 28.5 feet. The soil type at the Monroe site appeared to be a mixture of red clayey silt with uncorrected blowcounts that ranged between 9 and 19 blows per foot. The soils were markedly stiffer than those found in Statesville and more pockets of quartz were found than previously. Four DMT were performed in proximity to the test walls. In several cases, the DMT pushing was refused, however, the obstruction was easily augered through and the test resumed. The results of the DMT are shown in figure 4.7. Finally, BST at four depths were conducted in two locations. The data in table 4.7 and figure 4.8 includes friction angles near 40^{o} and cohesion as high 200 psf for the Slate Belt soil.

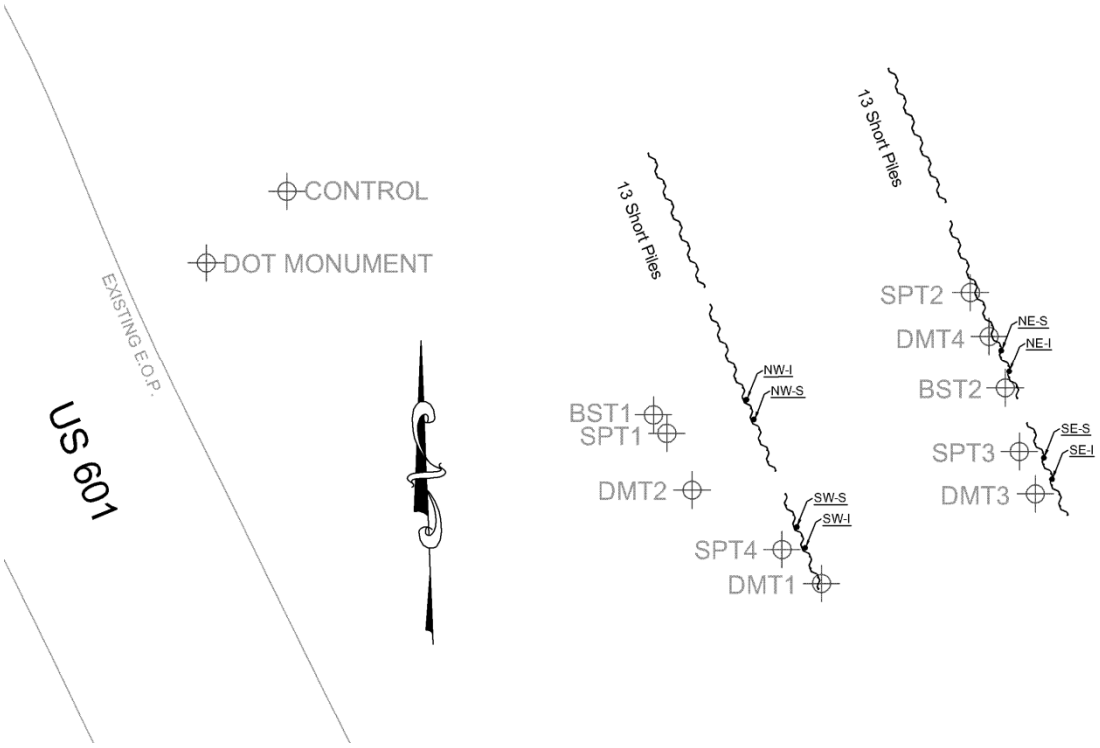

Figure 4.6 – Monroe soil test locations

Table 4.6 - SPT results (Monroe)

SPT-1			SPT-2			SPT-3			SPT-4		
Depth (ft)	N	N'_{60}	Depth (ft)	N	N'_{60}	Depth (ft)	N	N'_{60}	Depth (ft)	N	N'_{60}
3.5	30	78.0	3.9	17	44.2	4	17	44.2	4.1	10	26
8.5	15	28.5	8.9	13	24.2	9	15	27.7	9.1	9	16.5
13.5	11	16.6	13.9	11	16.4	14	13	19.3	14.1	12	17.7
18.5	10	12.9	18.9	9	11.5	19	14	17.8	19.1	12	15.2
23.5	10	11.4	23.9	9	10.2	24	10	11.3	24.1	15	16.9
28.5	*100		28.9	13	13.4	29	17	17.5	29.1	10	10.3
*Refusal			33.9	18	17.1	34	16	15.2	34.1	11	10.4
			38.9	19	16.9	19	15	13.3	39.1	19	16.8

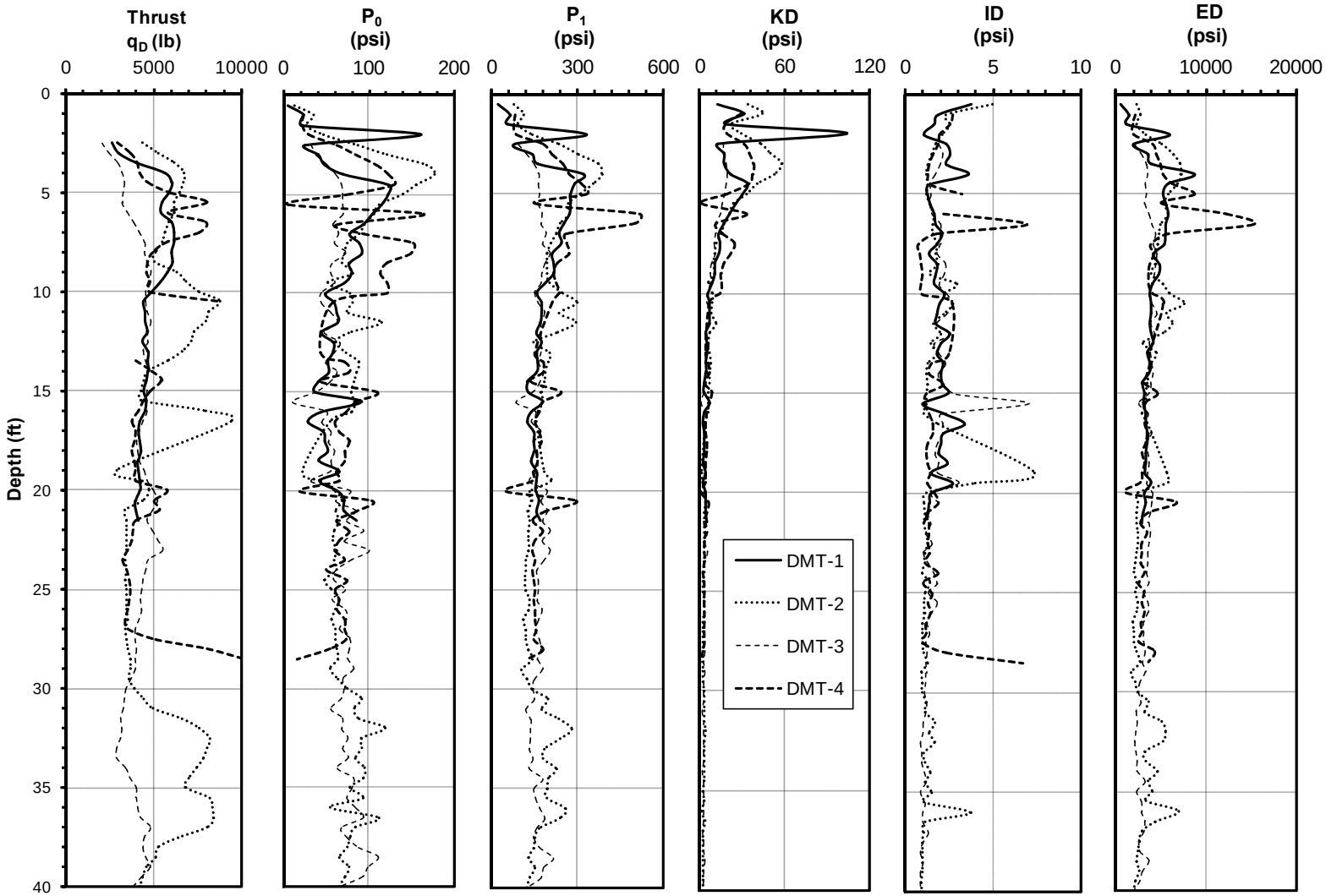

Figure 4.7 - Summary of DMT results (Monroe)

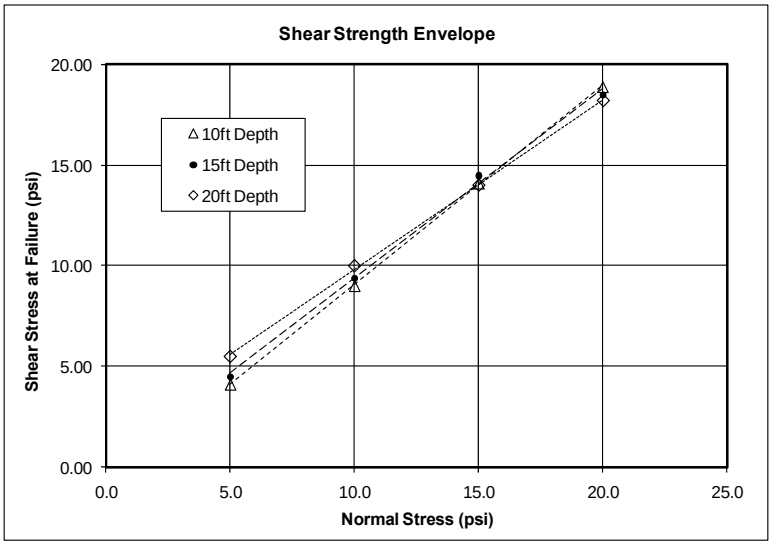

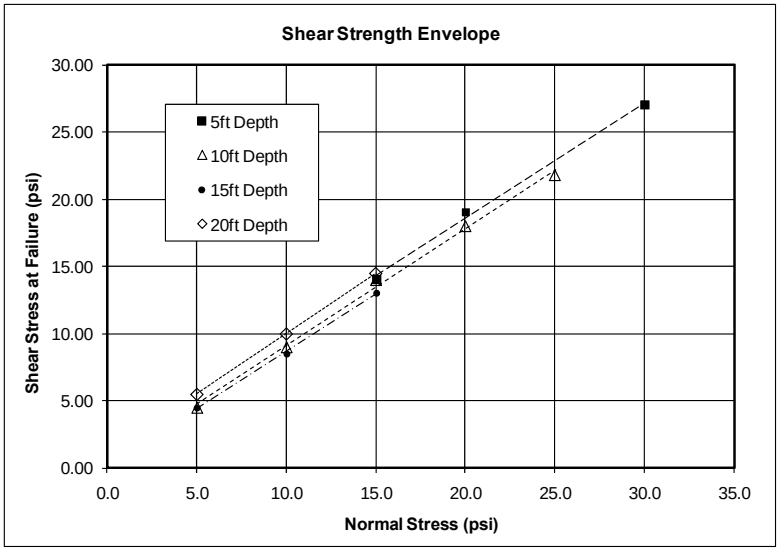

Figure 4.8 - Summary of Monroe BST results

Table 4.7 - BST calculated ϕ and c (Monroe)

Test	Depth (ft)	ϕ (deg)	c (psf)
BST #1	10	43.0	0
BST #1	15	43.2	0
BST #1	20	40.1	201.6
BST #2	5	40.6	205.9
BST #2	10	23.4	165.6
BST #2	15	40.4	24.5
BST #2	20	42.0	144.0

4.3.2 Laboratory Tests

The specimens tested were from depths between 5 and 21 feet below ground level, and were all collected in preparation of pockets for the BST. Classification tests were performed on nine samples using Atterberg limits, sieve, and hydrometer analysis. The specific gravities were determined as well.

Three one dimensional consolidation tests were conducted to determine compressibility parameters. Nineteen triaxial tests, representing seven test locations, were completed for the Monroe Site. All specimens were saturated and tested in the consolidated-undrained (CU) condition.

The index tests, summarized in table 4.8, showed that the soils were predominantly A-7. Consolidation tests suggest that the soils were all apparently highly overconsolidated. Triaxial tests reported drained friction angle between 30 and 40^{o} with cohesion intercepts ranging between 100 and 500 psf. Modulus, E_{50}, values ranged from 700 to 4000 psi, for confining pressures between 5 and 15 psi. Tables 4.9 and 4.10 show the consolidation and triaxial test results, respectively.

4.4 Summary of Soil Testing

It is worth noting that even though both sites were in different sections of the Piedmont, soil parameters determined from both were remarkably similar. The insitu and laboratory tests both showed friction angles and a cohesive component to the strength. Soils at both sites were AASHTO A-7 and appeared highly over consolidated.

Table 4.8 - Summary of index properties and classification testing (Monroe)

Borehole No.	Sample No.	Sample Depth	Specimen No.	Grain-Size Analysis								Atterberg Limits			AASHTO	Specific Gravity, G_s
								Minus #10 Fraction				Liquid Limit, *LL*	Plastic Limit, *PL*	Plasticity Index, *PI*		
				#4	#10	#40	#200	#60	#270	Silt	Clay					
[-]	[-]	[ft]	[-]	[% passing]								[%]	[%]	[%]	[-]	[-]
BST-1	ST-1	9.2-11.2	1	1	97	94	85	4.4	11.7	37.4	46.5	56	43	13	A-7-5(16)	2.8
	ST-2	14.2-16.2	1	-	98	89	73	13	20.1	38.6	28.4	43	29	14	A-7-6(10)	2.78
			2	2	96	93	80	6.1	14.2	33.1	46.6	63	43	20	A-7-5(21)	2.77
	ST-3	19.2-21.2	1	-	100	98	84	4.2	15.3	46.1	34.3	46	38	8	A-5-(10)	2.76
BST-2	ST-1	4-6	1	-	97	92	81	8.1	10.9	26.2	54.7	58	35	23	A-7-5(22)	2.83
	ST-2	9-11	1	-	99	97	88	4.0	9.1	24.4	62.5	65	46	19	A-7-5(24)	2.84
	ST-3	14-16	1	8	84	75	66	13.8	9.6	27.8	48.8	67	41	26	A-7-5(19)	2.77
			2	-	100	100	94	1.4	6.9	36.8	54.9	75	50	25	A-7-5(34)	2.82
	ST-4	19-21	1	-	99	98	90	1.6	9.9	43.8	44.7	64	50	14	A-7-5(21)	2.82

Table 4.9 - Summary of consolidation testing (Monroe)

Borehole No.	Sample No.	Depth	AASHTO	Compression Index, c_c	Recompression Index, c_r	Pre-consolidation Pressure, P_c	Over-consolidation Ratio, *OCR*
[-]	[-]	[ft.]	[-]	[-]	[-]	[psf]	[-]
BST-2	ST-1	4.0 - 6.0	A-7-5(16)	0.171	0.029	9000	16.3
	ST-2	9.0-11.0	A-7-5(24)	0.350	0.042	3800	3.45
	ST-3	14.0-16.0	A-7-5(19)	0.353	0.032	3600	2.18

Table 4.10 - Triaxial results (Monroe)

Location	**Depth (ft)**	**Type**	**Saturated**	**c' (psf)**	**ϕ' (deg)**	**E_{50} (psi)**
BST-1	10.2	CU	Yes	122.4	28.6	4029, 1518, 1945
BST-1	15.2	CU	Yes	230.4	36.9	3404, 1683, 1301
BST-1	20.2	CU	Yes	0	41.4	1078, 1559
BST-2	5	CU	Yes	504	30.5	1765, 1071, 2604
BST-2	10	CU	Yes	382	29.9	1760, 1051, 1505
BST-2	15	CU	Yes	295.2	36.0	2229, 984, 1351
BST-2	20	CU	Yes	417.6	28.6	722, 1283

CHAPTER 5
INSTRUMENTED WALL LOAD TESTS

5.1 Preliminary Modeling

The selection of the wall section and geometry was based upon a preliminary numerical modeling program. Considered were length of wall, spacing between walls, depth of walls, depth of excavation, type of pile, and instrumentation. In order to simulate the plane strain condition, the walls ideally would have been several hundred feet in length, driven to a depth of one hundred feet and excavated at least sixty feet deep. This scenario, of course, was impractical from a financial standpoint, therefore the configuration was optimized by modeling the potential configurations using the finite element program PLAXIS (1998).

5.1.1 FEM Initial Conditions

Since the optimization was done before the test sites were chosen, average values for soil properties such as cohesion, friction angle, modulus, and unit weight were based on previous work in residual soils in North Carolina by Heartz (1986). Table 5.1 provides a summary of these values. Since there is some question concerning the use of cohesion in the analysis, alternative values of 270 and 0 psf were also considered in these preliminary models.

Table 5.1 - Summary of soil properties for modeling

Unit Weight	100	pcf
ϕ’	24.9	deg
c’	540	psf
Permeability	0.85	ft/day
E	1.440E+05	psf
ν	0.15	

Three sheet piles, PZ27, PZ22, and a lightweight 5-5 arch pile were considered. The PZ27 was the sheet pile most commonly used by NCDOT. The PZ22 sheet pile had

the same cross sectional area as the PZ27, but wider section resulting in a lower moment of inertia. The lightweight 5-5 arch pile, a flat sheet, was considered as a low cost and high deflection option. Table 5.2 summarizes the structural properties of the sheet piles.

Table 5.2 – Summary of key pile properties used for modeling

PZ27		
Moment of Inertia (I)	184.2	in^4
Cross Sectional Area (A)	7.94	in^2/ft
Young's Modulus (E)	29000000	psi
Weight per foot of wall (w)	27	lb/ft
PZ22		
I	84.7	in^4
A	6.46	in^2/ft
E	29000000	psi
W	22	lb/ft
5-5		
I	5.7	in^4
A	3.35	in^2/ft
E	29000000	psi
W	11.3	lb/ft

5.1.2 FEM Modeling

FEM models were created for pile lengths of 20 ft., 25 ft., 30 ft. 35 ft. and 40 ft. Excavation of the soil behind the sheet piles was simulated by removing 2.5 ft. increments of soil to within 5 ft. of the tip of the pile. Each model was analyzed using the full c' = 540 psf, a half c' = 270 psf, and a worst case scenario of c' = 0. The maximum deflection was compiled for each scenario, The results are shown in Table 5.3.

The models showed the PZ22 and PZ27 were similar in behavior, though as expected the PZ22 exhibited greater deflection at the same length and excavation depth. The 5-5 arch sheet pile, a much more flexible pile than the PZ22 and PZ27, was modeled at 20 ft only. The 5-5 pile deflects much more than the PZ22 and PZ27.

Table 5.3- Summary of deflection versus depth

Pile Information													Excavation Details (Δ_h = Horizontal Deflection (in))												
Pile Type	Pile Length (ft)	E (ksi)	Soil Cohesion (lb/ft²)	Soil Friction	I (in^4)	S (in³)	Yield Stress (ksi)	M_p (ft*lb)	A_{cs} (in²/ft)	Pile Width	Weight (lb/ft)	Wall Spacing (ft)	Δ_h @ 2.5'	Δ_h @ 5'	Δ_h @ 7.5'	Δ_h @ 10'	Δ_h @ 12.5'	Δ_h @ 15'	Δ_h @ 17.5'	Δ_h @ 20'	Δ_h @ 22.5'	Δ_h @ 25'	Δ_h @ 27.5'	Δ_h @ 30'	Δ_h @ 32.5'	Δ_h @ 35'
5-5	20	29000	0	24.9	5.7	3.4	50	14167	4.85	18	11.3	40	0.0	0.8	3.9	6.9	n/a	n/a								
5-5	20	29000	270	24.9	5.7	3.4	50	14167	4.85	18	11.3	40	-0.1	0.1	0.5	1.1	2.1	4.5								
5-5	20	29000	540	24.9	5.7	3.4	50	14167	4.85	18	11.3	40	-0.1	0.1	0.4	0.9	1.7	2.9								
PZ22	20	29000	0	24.9	84.4	18.1	50	75417	6.47	18	22	40	0.0	0.2	1.0	3.9	4.1	0.0								
PZ22	20	29000	270	24.9	84.4	18.1	50	75417	6.47	18	22	40	-0.1	0.0	0.2	0.7	1.3	3.0								
PZ22	20	29000	540	24.9	84.4	18.1	50	75417	6.47	22	22	40	-0.1	0.0	0.1	0.5	1.1	2.1								
PZ22	25	29000	0	24.9	84.4	18.1	50	75417	6.47	22	22	40	0.0	0.1	0.8	2.4	5.2	7.1	7.2	n/a						
PZ22	25	29000	270	24.9	84.4	18.1	50	75417	6.47	22	22	40	-0.1	0.0	0.2	0.5	1.0	1.8	3.0	n/a						
PZ22	25	29000	540	24.9	84.4	18.1	50	75417	6.47	22	22	40	-0.1	0.0	0.1	0.4	0.9	1.5	2.4	3.9						
PZ22	30	29000	0	24.9	84.4	18.1	50	75417	6.47	22	22	40	0.0	0.1	0.7	2.0	5.2	5.5	n/a	n/a	n/a	n/a				
PZ22	30	29000	270	24.9	84.4	18.1	50	75417	6.47	22	22	40	-0.1	0.0	0.1	0.5	1.0	1.6	2.6	4.8	4.9	n/a				
PZ22	30	29000	540	24.9	84.4	18.1	50	75417	6.47	22	22	40	-0.1	0.0	0.1	0.4	0.8	1.4	2.0	2.9	4.2	7.9				
PZ22	35	29000	0	24.9	84.4	18.1	50	75417	6.47	22	22	40	0.0	0.1	0.6	1.8	4.5	9.2	10.2	n/a	n/a	n/a	n/a	n/a		
PZ22	35	29000	270	24.9	84.4	18.1	50	75417	6.47	22	22	40	-0.1	0.1	0.1	0.4	0.9	1.5	2.4	3.7	6.5	6.8	n/a	n/a		
PZ22	35	29000	540	24.9	84.4	18.1	50	75417	6.47	22	22	40	-0.1	0.1	0.1	0.4	0.7	1.3	2.0	2.8	3.7	5.2	7.4	9.8		
PZ22	40	29000	0	24.9	84.4	18.1	50	75417	6.47	22	22	40	0.0	0.1	0.6	1.8	4.5	8.2	8.2	n/a	n/a	n/a	n/a	n/a	n/a	n/a
PZ22	40	29000	270	24.9	84.4	18.1	50	75417	6.47	22	22	40	-0.1	0.1	0.1	0.4	0.9	1.5	2.2	3.5	5.7	10.0	10.6	n/a	n/a	n/a
PZ22	40	29000	540	24.9	84.4	18.1	50	75417	6.47	22	22	40	-0.1	0.1	0.1	0.4	0.7	1.2	1.8	2.7	3.7	4.6	5.9	9.0	9.6	n/a
PZ27	20	29000	0	24.9	184.2	30.2	50	125833	7.94	18	27	40	0.0	0.2	0.8	0.9	n/a	n/a								
PZ27	20	29000	270	24.9	184.2	30.2	50	125833	7.94	18	27	40	-0.1	0.0	0.2	0.6	1.2	3.0								
PZ27	20	29000	540	24.9	184.2	30.2	50	125833	7.94	18	27	40	-0.1	0.0	0.1	0.4	1.0	2.0								
PZ27	25	29000	0	24.9	184.2	30.2	50	125833	7.94	18	27	40	0.0	0.1	0.6	1.8	4.4	8.0	n/a	n/a						
PZ27	25	29000	270	24.9	184.2	30.2	50	125833	7.94	18	27	40	0.0	0.0	0.1	0.5	0.9	1.6	3.4	8.7						
PZ27	25	29000	540	24.9	184.2	30.2	50	125833	7.94	18	27	40	0.0	0.0	0.1	0.3	0.8	1.4	2.2	3.7						
PZ27	30	29000	0	24.9	184.2	30.2	50	125833	7.94	18	27	40	0.0	0.1	0.5	1.4	3.6	8.2	8.3	n/a	n/a	n/a				
PZ27	30	29000	270	24.9	184.2	30.2	50	125833	7.94	18	27	40	0.0	0.0	0.1	0.4	0.8	1.4	2.2	4.3	5.6	n/a				
PZ27	30	29000	540	24.9	184.2	30.2	50	125833	7.94	18	27	40	0.0	0.0	0.1	0.3	0.7	1.2	1.8	2.8	4.0	7.6				
PZ27	35	29000	0	24.9	184.2	30.2	50	125833	7.94	18	27	40	0.0	0.1	0.4	1.2	2.9	6.1	n/a	n/a	n/a	n/a	n/a	n/a		
PZ27	35	29000	270	24.9	184.2	30.2	50	125833	7.94	18	27	40	0.0	0.0	0.1	0.4	0.8	1.3	2.0	3.1	5.4	12.1	12.7	n/a		
PZ27	35	29000	540	24.9	184.2	30.2	50	125833	7.94	18	27	40	0.0	0.0	0.1	0.3	0.6	1.1	1.7	2.5	3.4	4.8	7.3	15.0		
PZ27	40	29000	0	24.9	184.2	30.2	50	125833	7.94	18	27	40	0.0	0.1	0.4	1.2	2.8	5.6	n/a	n/a	n/a	n/a	n/a	n/a	n/a	n/a
PZ27	40	29000	270	24.9	184.2	30.2	50	125833	7.94	18	27	40	0.0	0.1	0.1	0.4	0.7	1.3	1.9	2.9	4.1	n/a	n/a	n/a	n/a	n/a
PZ27	40	29000	540	24.9	184.2	30.2	50	125833	7.94	18	27	40	0.0	0.1	0.1	0.3	0.6	1.0	1.6	2.4	3.2	4.3	5.5	8.2	8.7	n/a

5.2 Selected Wall Section

The PZ22 appeared to be the best pile to use because it was similar to the PZ27 typically used by DOT and still provided ample measurable deflection. Though an extreme amount of deflection was not desirable, for safety reasons, the larger the safe deflection that could be obtained the better because the measurements are more distinct and easier to interpret. The Arch 5-5 was ruled out because of the large deflections at short pile lengths. Through additional models, the minimum separation between the parallel walls was found to be 30 ft. for PZ22 sheet piles to prevent the overlap of the passive soil wedges inside the excavation.

The appropriate length for the walls was determined by engineering judgment and economic considerations. The wall length needed to be sufficient to ensure that the instrumented piles in the center would exhibit plane strain behavior. If the walls were not long enough, the piles at the end of the excavation, that were embedded in the access slopes, would influence the wall sections. Thus, through discussion it was decided that the test sections would be 40 feet.

Based on the results of the finite element simulations, 35ft. PZ 22 sheet piles were selected. The minimum separation between the parallel walls was 30 feet. The test walls would be 40 feet long and the soil between the walls would be excavated to 20 ft. When working with the Geotechnical Engineering Unit to develop a plan for the excavation, the issues of safety and access were raised. Therefore, in order to provide a 40 foot test section, the walls would need to be extended further to make provision for safe access for equipment and personnel to perform the excavation. The final plan included the addition of 20 foot wing walls on each end of the test walls to protect slopes angled at 2:1 into the excavation. There would be a total of 132 PZ 22 sheet piles (66 each side). Of the total,

80 were the full 35 feet long to be used for the test sections and partially for the access ramps. The remaining 52 piles were 20 feet long reflecting the decreasing depth of the access ramps.

5.3 Instrumentation Plan

5.3.1 Overview

The data acquisition program was comprised of three components, each designed to provide redundant measurements that would allow for earth pressure calculations or estimation. The most involved component was a network of strain gages on four piles intended to give a representation of the strain along the length of the piles. The second component was an inclinometer to determine the deflection and slope of four additional piles. For redundancy, and a general check, points on the wall and within the excavation were surveyed using conventional equipment. The strain monitoring system and inclinometer are described in the following sections.

5.3.2 Strain Gages and Data Acquisition System

Measurement of bending moment was done indirectly through the measurement of strain. Since the piles were steel and likely to remain in the elastic range throughout the test, the bending moment was determined through conversion of strain to curvature (Equation 5.1) then multiplying the curvature by the EI (Equation 5.2).

$$\kappa = \frac{\varepsilon_C - \varepsilon_T}{\bar{y}} \tag{5.1}$$

where κ is the curvature of the beam/pile,
ε_C and ε_T are compression and tension strains,
$\bar{y}$ is the distance between the gages (8.825 in)

$$M = \kappa EI \tag{5.2}$$

where M is the bending moment
E is Young's modulus
I is the moment of inertia

Strain was measured using arc weldable vibrating wire (VW) strain gages manufactured by Geokon Inc. like the one shown in figure 5.1. The gages were installed in tension-compression pairs on the flanges of the sheet piles, as shown in figure 5.2, at regular intervals of length. The mounts were welded using a gauging block and blank. After the mounts cooled, the gage was inserted into the mounts and set at the appropriate amount of pre-strain by stretching or compression before locking with set screws. The "plucker" which causes the wire to vibrate, and measures the frequency, was slipped over the gage and secured with a hose clamp. When all of the gages and pluckers were attached to the pile, the gages were covered with steel angle to protect them from damage during pile driving. The strain was recorded using a pair of Campbell Scientific CR1000 dataloggers.

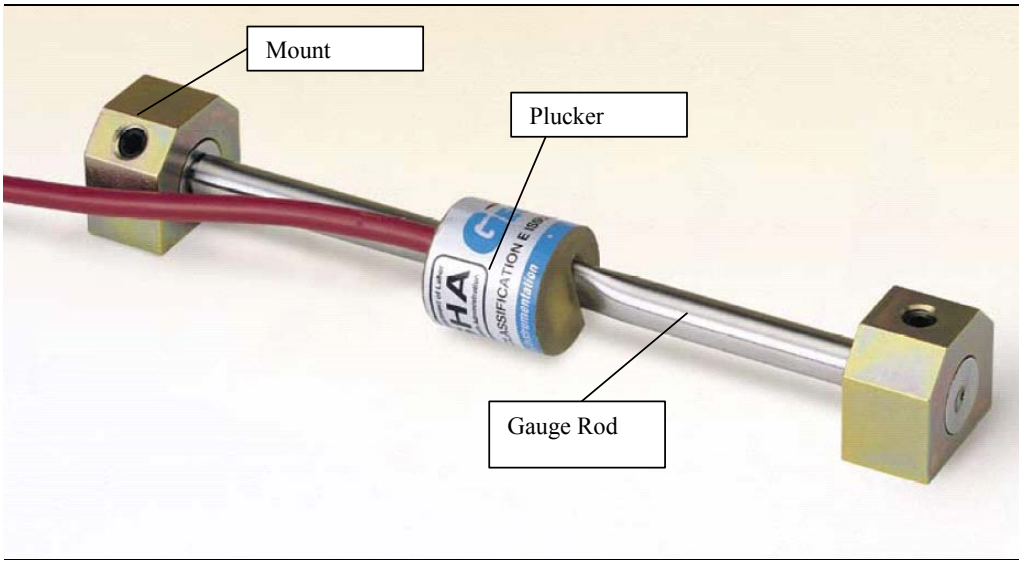

Figure 5.1 - Geokon model 4000 strain gage

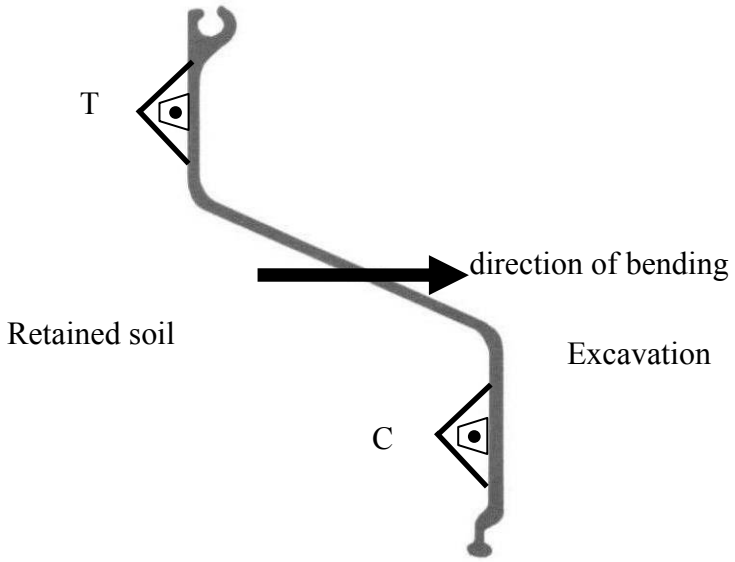

Figure 5.2 – Diagram of strain gage attachment

5.3.3 Inclinometer

In addition to the strain gages, the pile displacements were measured with an inclinometer. Typically, an inclinometer operates by lowering the instrument into a grooved PVC pipe set into soil. In the case of a sheet pile, a square steel tube section was welded directly to the piles to substitute for the inclinometer casing, like the one shown in figure 5.3. The measurement of deflection is made along the diagonal of the tube instead of the oriented casing grooves. This skew was accounted for in the inclinometer reduction software by mathematically rotating the readings such that the output was the deflection along the bending axis of the wall. The primary measurement is along the A axis and the rotated measurement is the X axis.

In the field, the A direction was always toward the northwest corner of the steel tube. Therefore to rotate west side measurements to the wall bending axis, the skew angle is 135^{o}. Similarly east side measurements are rotated -45^{o}. Figures 5.4 and 5.5 demonstrate this.

Figure 5.3 - Steel tube welded to a sheet pile as an inclinometer casing

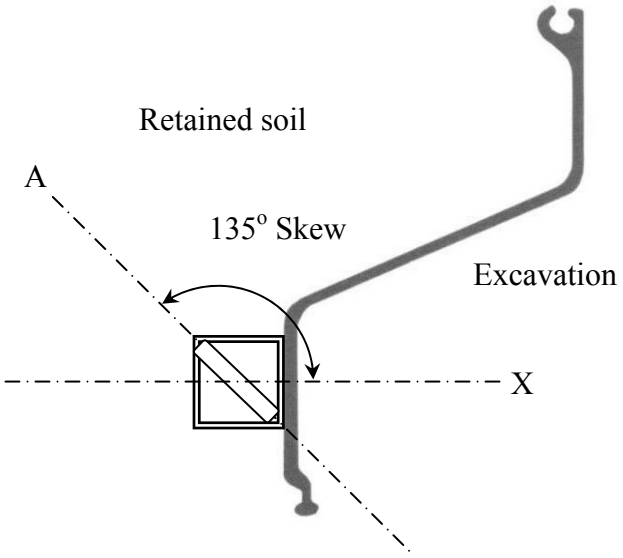

Figure 5.4 - Rotation of west side measurements to the axis of wall bending

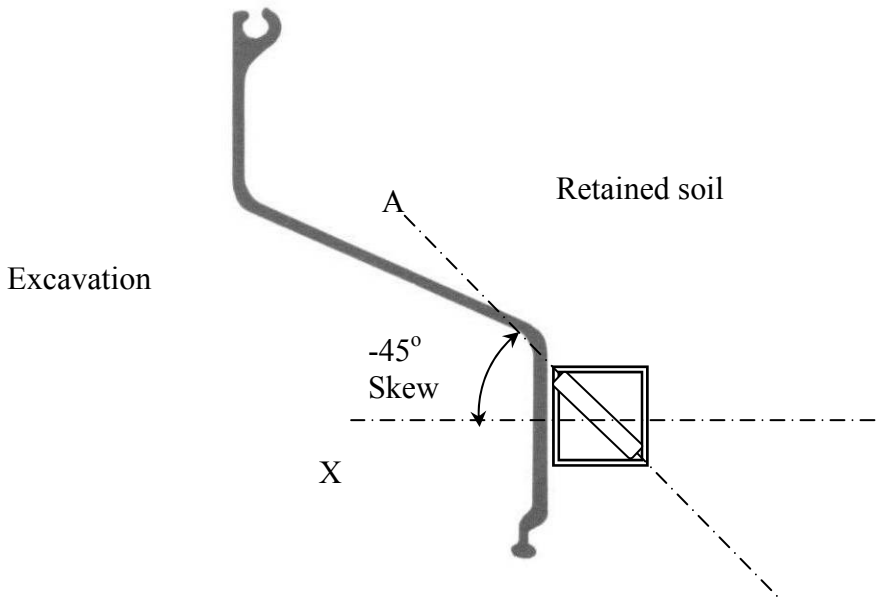

Figure 5.5 - Rotation of east side measurements to the axis of wall bending

5.4 Statesville Load Test

The test site at Statesville was the first opportunity to put the concept into action. Installation of the sheet piles was done through a purchase order contract between Division 12 Construction/Bridge Maintenance and Burns and Sons Construction.

5.4.1 Instrumentation System

The initial instrumentation plan at the Statesville site included strain gages on four piles and inclinometer tubes on four additional piles. Each side of the excavation had four instrumented piles, 2 for strain and 2 for displacement, near the center of the wall (within the 40 foot test section). Eight strain gages were attached to the non-excavation side of both flanges of the strain instrumented piles at four foot spacing. A total of 64 gages was used – 16 per pile. Inclinometer tubes were attached to non excavation side of the outermost flange of the displacement-measurement piles. The wall layout is shown in figure 5.6.

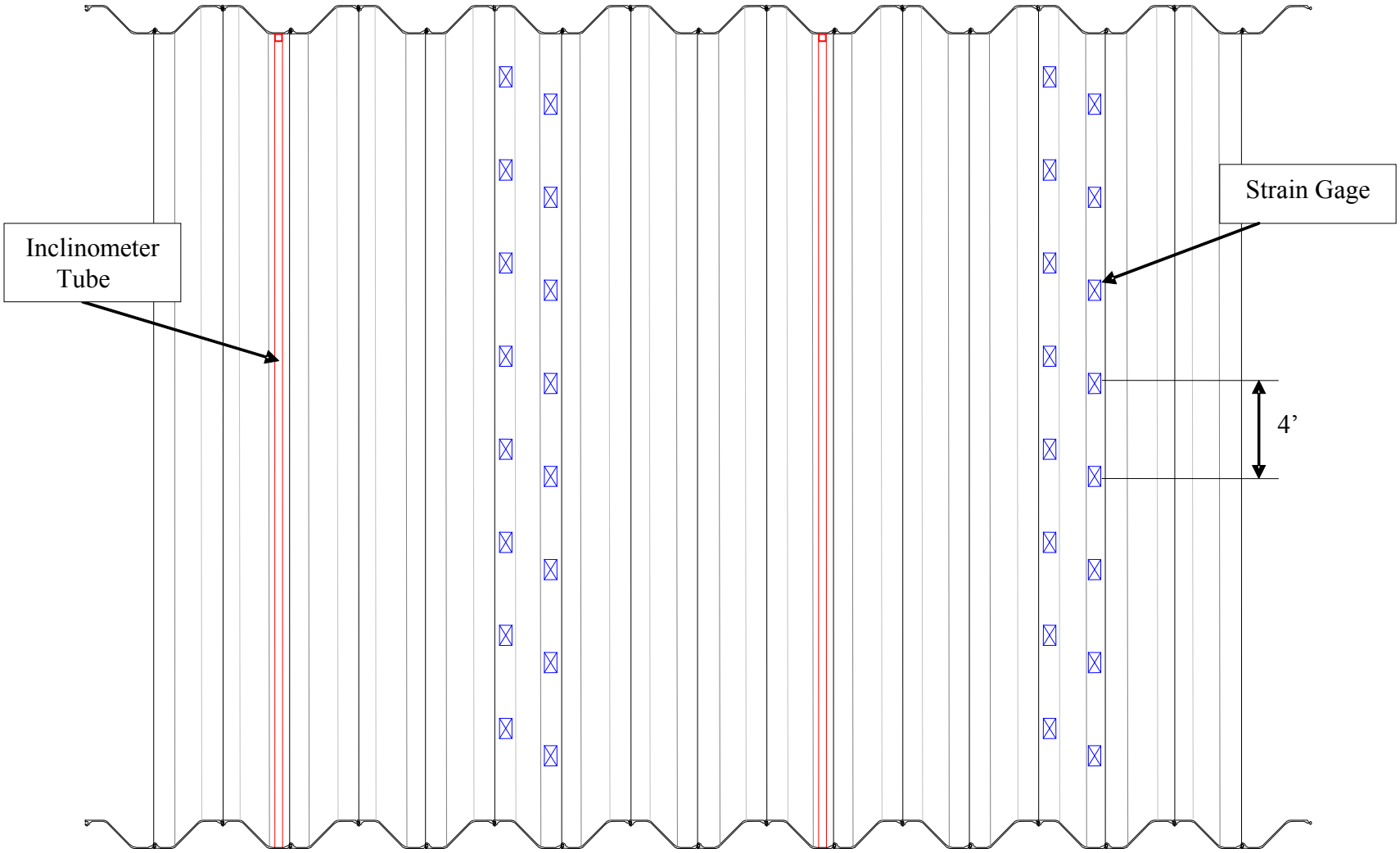

Figure 5.6 – Instrumentation system for wall

5.4.2 Pile Installation

Work at the Statesville site started on Monday September 12, 2005. While UNCC personnel were installing strain gages, the contractor began work on driving the sheet piles. Initially, the contractor leveled the site to provide a good working platform. Next, string lines were pulled to locate the walls and a jig was set up to get the first panel of piles in position and plumb prior to driving. Initial driving was done using a relatively small vibratory hammer.

The panel method of driving three piles as a set was used to help with pile alignment, decrease the chance of pile wander, and insure proper set. However, many piles refused under vibratory driving. An attempt was made to drive many of these piles further with a diesel hammer. The diesel hammer was able to drive some of the piles deeper, however due to the makeshift nature of the pile helmet, and lack of any driving criteria, several pile tops were overstressed and yielded. Near the end of driving, a proper sheet-pile driving helmet was implemented. The new helmet and maintaining a driving criteria of 10 blows per inch, made a significant difference in not over stressing the piles though several of the piles were still not able to be driven completely without damage. Thus, several of the piles were partially driven. However, all of the sheet piles on the original plan were eventually installed. Burns and Sons wrapped pile driving on September 30, 2005. Several photos from the construction phase in Statesville are shown in figure 5.7. The heights of the piles above the ground surface is shown in figure 5.8. This is also reflected in the position of the strain gages. The relative positions of the strain gages with respect to the ground surface are shown in figure 5.9.

Figure 5.7 – Photographs from wall installation in Statesville

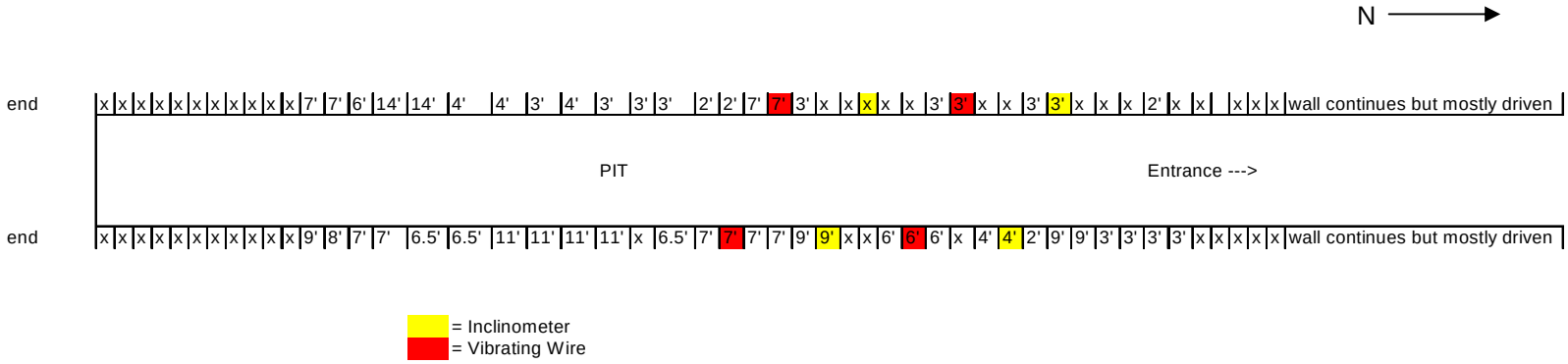

Figure 5.8 - Height of piles above ground (x = fully driven)

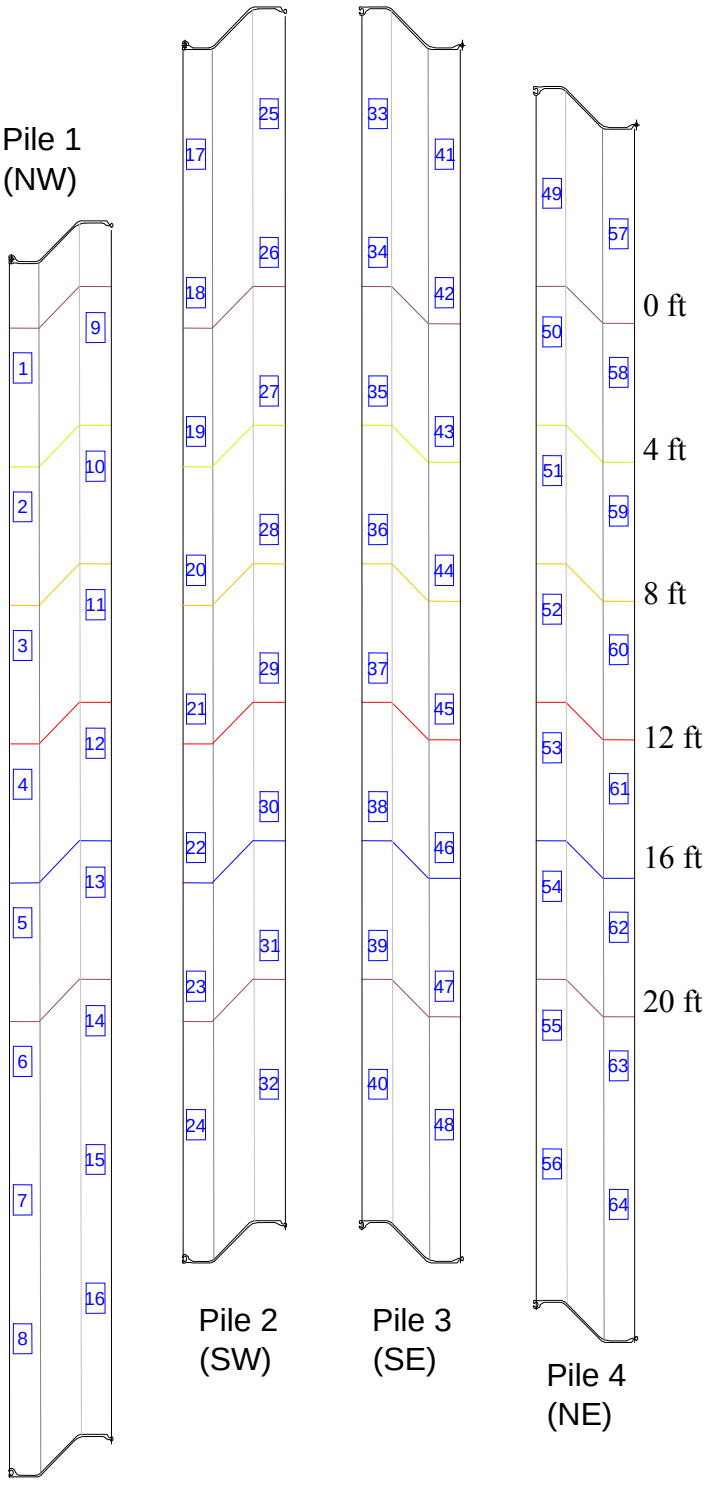

Figure 5.9 - Gage diagram of pile elevations and excavation depths

5.4.3 Excavation

After the completion of pile driving, the strain gages were connected to the dataloggers. The dataloggers and excess cabling were secured in weather resistant (traffic signal) boxes. The dataloggers were set to take readings continuously every one minute until the load test was complete. Two sets of baseline inclinometer readings were taken. Notably, heavy rains due to the remnants of Tropical Storm Ophelia delayed the start of excavation by nearly two weeks. The excavation process proceeded as follows:

- **Monday October 17, 2005 ~** Excavation began early morning but stopped at 11:00am after excavating one quarter of the first 4 ft. lift, due to a hydraulic failure. Excavation resumed in the afternoon to bring the total progress on the lift to about 1/3.
- **Tuesday October 18, 2005 ~** First lift (4 ft.) was completed by 11:00am. The second lift started around 2:00pm.
- **Wednesday October 19, 2005 ~** Excavation for the second lift was resumed in the morning and was complete by noon. The third excavation lift was started around 3:00pm.
- **Thursday October 20, 2005 ~** Third layer (12 ft.) was completed by 3:00pm..
- **Friday October 21, 2005 ~** Fourth excavation step (16 ft.) began at 7:30am and was completed at 3:00pm.
- **Wednesday October 26, 2005 ~** Excavation of final 4 ft. lift (20ft) was started and finished at 2:00pm.
- **Thursday October 27, 2005 ~** 20 ft. lift readings were taken in the morning.

After the final reading has been taken, an opportunity arose to explore the unsaturated effect in qualitative terms. The contractor working on the site agreed to flood the soil behind the east wall with several thousand gallons of water. .

- **November 1, 2005** ~ All instrumentation removed and walls decommissioned
- **November 5, 2005** ~ Burns and Sons remove sheet piles and transports them to Statesville Maintenance Facility.

Figure 5.10 shows highlights of the excavation.

5.4.4 Challenges and Lessons Learned During the Statesville Test

Being this was the first wall installation of a proposed three to four walls, there were several observations made that would be carried forward to future load tests. First, a better effort could be made to ensure the sheet piles are driven to proper depth, especially the instrumented sheets. Only one strain gage and one inclinometer sheet were driven to full depth. One inclinometer sheet pile was driven nine feet short of the required depth. Second, the test wall sheets should be disconnected from those protecting the access ramp. Next, the research team and NCDOT should have better control of the location of the test walls on the site. It was unfortunate that even though it was confirmed with the grading contractor that the area between the west wall and the property line would not be used for hauling, and any existing haul road would be abandoned when testing started, the haul road continued to be used throughout the test. It is difficult to say if the haul road had any impact on the tests. However, data collection and site access were far more challenging.

In terms of instrumentation, there should be more strain gages on the measuring piles. Near the depth where soil makes contact with the wall, there should be sufficient

Figure 5.10 – Photographs of excavation in Statesville

gages to capture the function that defines bending moment with depth. In Statesville, there were strain gages at 8 depths – spaced 4 feet apart. This was done, primarily, to provide full depth gages as well as work within the project budget. The gages should have been clustered around the potential depth of soil contact on the wall or used in a tighter configuration. In general, the inclinometer was under-used on the project. There could have been many more inclinometer instrumented piles with little additional cost to the project.

Overall, there should have been sufficient provision to try to get "the most bang for the buck" on the test walls. Since deflections, stresses, and moments were less than expected, addition of a surcharge load behind one or both walls would have given an additional learning opportunity for the test. In addition, truly saturating the backfill to relieve any negative pore pressure would help rule out soil suction as a source of the increased soil strength/decreased earth pressure.

5.5 Monroe Load Test

Building on the experience in Statesville, the instrumentation plan was modified for the Monroe test site. In addition, it was proposed to provide a surcharge on one side of the excavation to force an active earth pressure wedge to develop and drill wells through which the retained soil on the other side could be saturated. Unfortunately, insufficient right of way, unavoidable overhead utilities, the location of a drinking water well, and proximity to residences prevented these additional measures. Sheet pile installation was conducted by NCDOT Division 10 Bridge Maintenance personnel.

5.5.1 Instrumentation System

Based upon lessons learned from the Statesville test, the instrumentation plan was amended to maximize the ability to measure earth pressure at the second site. From the

previous test four of the sheet piles were already instrumented with strain gages every four feet. To increase the resolution of the data for subsequent tests, additional strain gages were installed between the original gages, such that there would be a strain gage every 2 feet along the pile (Figure 5.11). In order to install the new gages, the protective covers were removed. The new gages were welded on the sheet pile in line with the previous gages at a spacing of two feet on center. Before reinstalling the protective cover, the at-rest microstrain was set for every gage (new and existing). In addition to the amended strain gage plan, inclinometer tubes were attached to four additional piles to bring the total inclinometer piles to eight.

5.5.2 Pile Installation

After the piles were instrumented, NCDOT Division 10 bridge maintenance began driving the sheet piles on Monday October 2, 2006. A string line was set to help keep the wall aligned during the driving process. Per recommendation based on experience in Statesville, a larger vibratory hammer, ICE model 22 hydraulic, was utilized to drive the sheet piles. Unlike the previous work in Statesville, pile driving in Monroe proved to be rather difficult due to many factors. The short piles used to protect the access ramps were installed quickly. Starting with the first long piles, driving difficulties began to surface.

The most obvious factor is the piles were not “new” this time. Thus any damage from the work in Statesville, due to driving and extraction, would contribute to difficult driving. Thus, some piles were slightly bent, and had rust and other imperfections in the sockets. The balls and sockets of the sheet piles were lubricated to minimize friction in the joints, and help the piles drive easier. Geologically, thin layers of quartz that were found during the borings may have hindered driving in some locations.

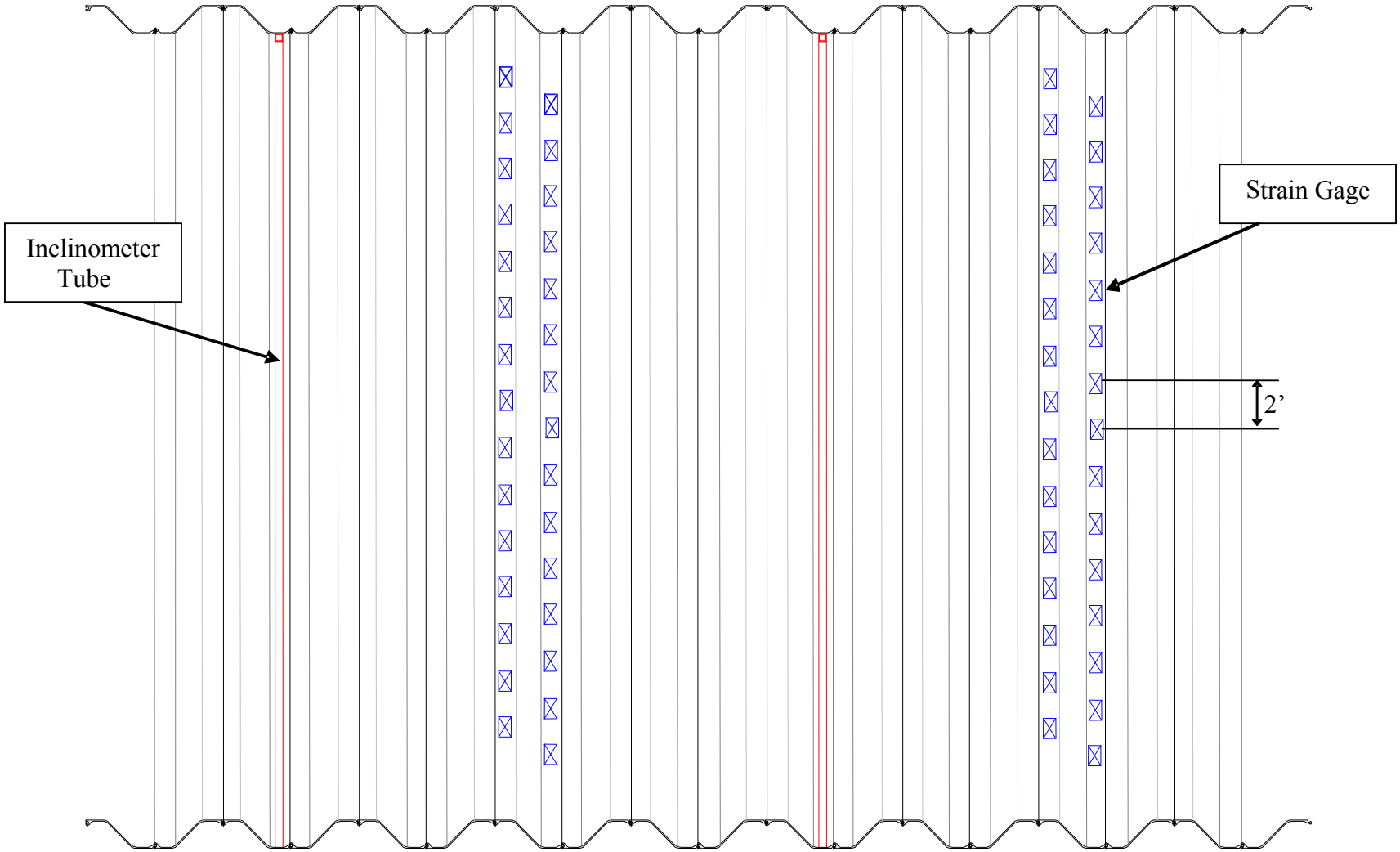

Figure 5.11 – Amended strain gage plan for Monroe test site

Thus, the ends of many piles were cut on an angle to resemble a pile point. Likely the biggest factors proved to be the lack of the panel method of driving and inexperience of the crew with sheet piling. The Division 10 team preferred using the set and drive method whereby each sheet is continuously driven to its full length without stopping. This does not provide the confinement necessary to keep the piles in line during driving.

Although the remedial measures improved the pile driving, the process was still very slow, and it became very difficult to keep the piles plumb. In several instances, the top of the pile would break off in the jaws of the hammer while driving, and the pile would have to be cut off in order to continue driving.

5.5.3 Construction Stop and Re-evaluation

After several working days attempting to drive sheet piles, the effort was stopped on October 18, 2006 in order to regroup and determine if continuation work in Monroe was feasible. During a meeting with the Division Engineer on October 19, 2006, the consensus was to make every attempt to drive the piles at the research site. To that end, additional auger borings were completed on October 26 and 27, 2006 within the wall alignment to determine the location of rock that might hinder driving. In addition, a diesel hammer was borrowed from Division 9 bridge maintenance.

Rock was found in the south western portion of the wall footprint, however the alignment of test sheets could be amended such that its impact could be minimized. Knowing that rock was not the limiting factor, pile installation was restarted on Monday October 30, 2006. Still, the driving difficulties persisted. Driving operations were suspended on Wednesday November 29, 2006 for budgetary reasons and complaints from

residents living near the site. Figure 5.13 shows photographs of the wall construction in Monroe.

The resulting test walls were far shorter that those in Statesville. Figure 5.14 shows the 26 short piles and 36 long piles that were eventually driven. Most of the long piles were damaged during installation. The NW inclinometer casing broke loose from the sheet pile and twisted rendering the data unusable. During installation of the NW strain gage pile, the protective cover vibrated loose damaging many wires in the process. The final piles were driven without supervision by UNCC and without any attempt to plumb them with a template resulting in several measuring piles being out of plumb and alignment. The stickup heights of the sheet piles installed is shown in figure 5.15, and the relative locations of the strain gages are shown in 5.16.

5.5.4 Excavation

Once the piles were driven, the strain gages were connected to the datalogger, and baseline readings were taken. Also, the baseline readings were taken with the inclinometer, and the location of each instrumented pile was surveyed using a total station. All three of these methods were used throughout the excavation sequence to determine the deflection of the wall. With all of the baseline readings taken, the excavation process was started and preceded as follows:

- **Monday December 11, 2006 ~** The excavation began in the early morning, and continued until about noon. There was a slight delay while the operator waited for a truck to haul the material on site. The first lift (4ft) was completed by 4:00pm
- **Tuesday December 12, 2006 ~** The second lift (8ft) was started in the early morning and was completed by 11:00am. The third lift (12ft) was started after lunch, and was completed by 3:30pm.

Figure 5.13 – Photographs from wall installation in Monroe

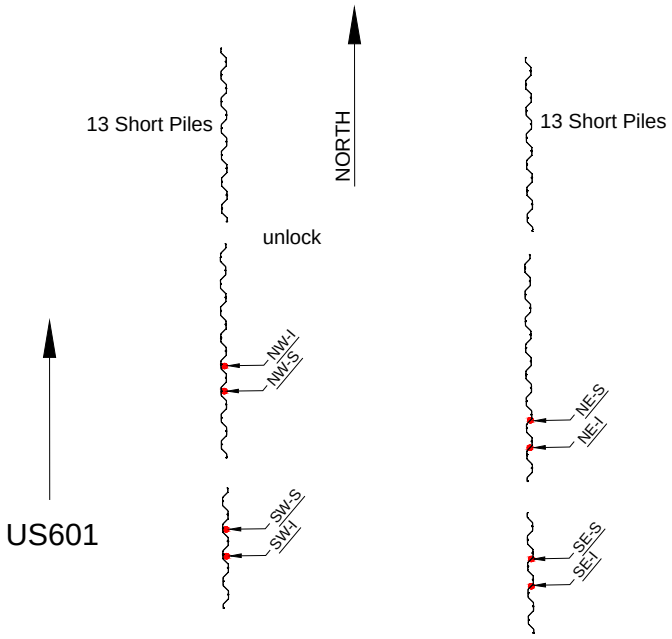

Figure 5.14 – Sheet piles as installed in Monroe

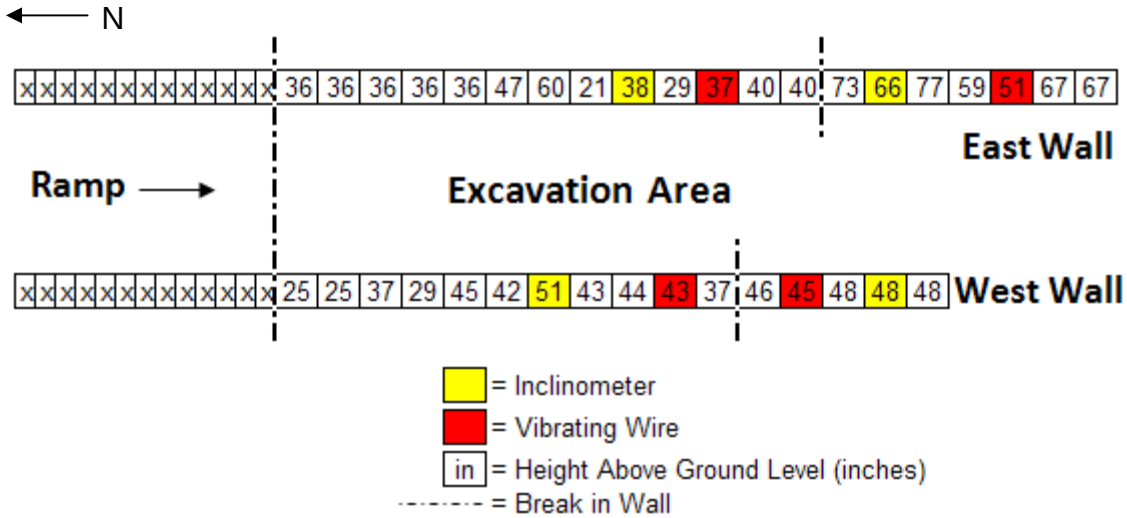

Figure 5.15 - Height of sheet piles above ground level

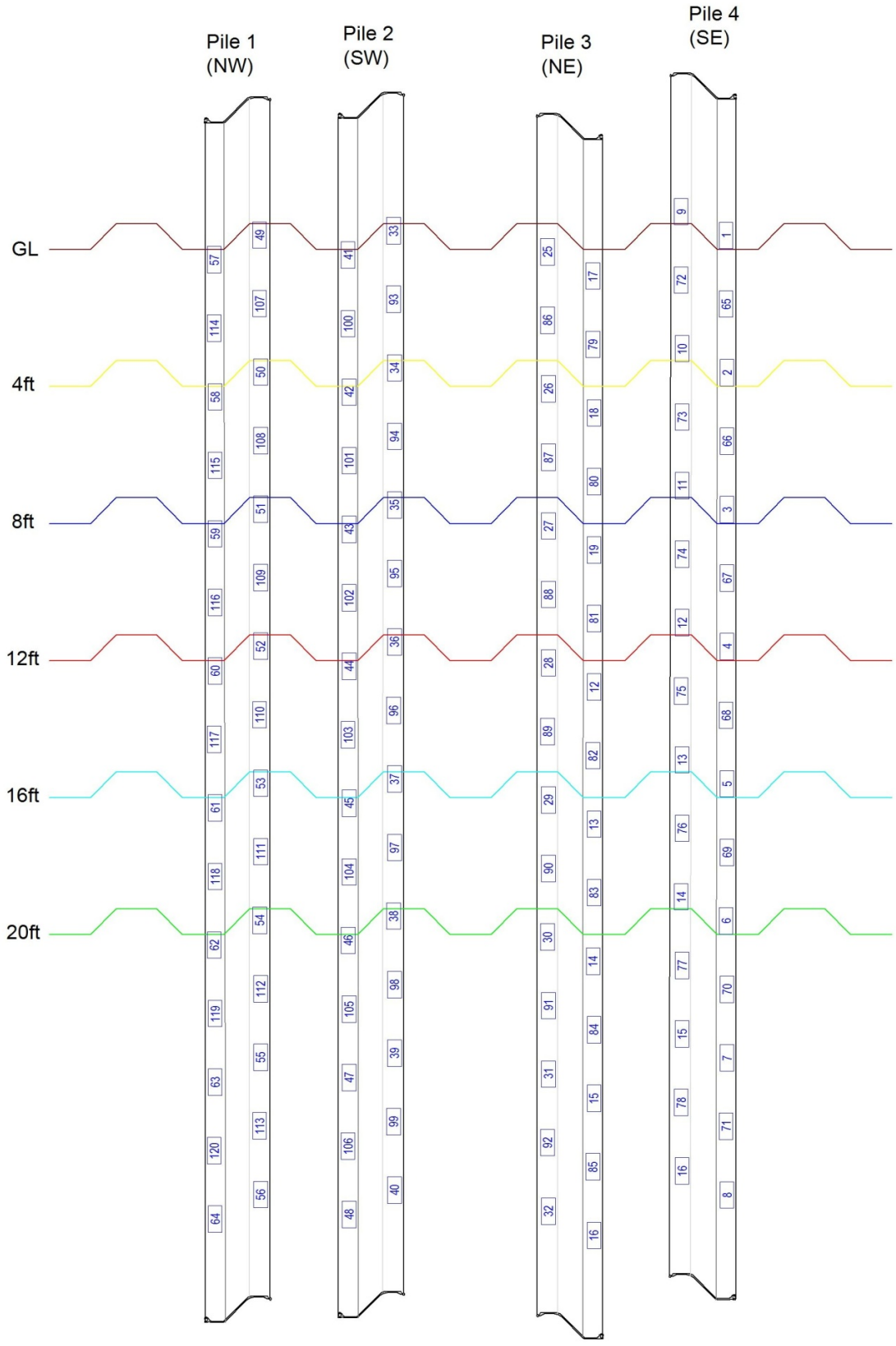

Figure 5.16 - Gage diagram of pile elevations and excavation depths

- **Wednesday December 13, 2006 ~** Excavation for the fourth lift (16ft) was started in the early morning, and was completed by 1:30pm. The fifth and final lift (20ft) was started, but the excavation was halted because one of the dump trucks was damaged in the stockpile area and required towing.
- **Thursday December 14, 2006 ~** The final lift (20ft) was continued in the early morning and completed by 12:00pm. Readings were taken after the final lift was completed. After the final readings were taken, an 8ft triangular surcharge was built behind the west wall. Readings were also taken after the surcharge was completed at 3:30pm.
- **Sunday December 17, 2006 ~** The final readings were taken in the afternoon, and the dataloggers were disconnected and walls decommissioned.

The excavation process is shown in figure 5.17.

Figure 5.17 – Photographs of excavation in Monroe

CHAPTER 6
RESULTS OF FIELD LOAD TEST PROGRAM

6.1 Statesville Test Site

As detailed in Chapter 5, the sheet piles were instrumented with strain gages and inclinometer tubes. In addition to the numerical data, there were qualitative observations that provided important information about the behavior of the soil.

6.1.1 Quantitative Results

The quantitative results are presented as plots of bending moment and lateral deflection with depth. Figure 6.1 shows the bending moments induced as the excavation was completed. Based on the sign convention shown in figure 5.2, bending into the excavation should be a positive moment. Negative moments would then mean that the wall bent backward into the wall of the excavation. In several cases, the bending moment appeared to be negative. This is likely due to the fact that the residual stresses locked in during driving were released when the soil was excavated, and there was not sufficient earth pressure on the wall to reverse this effect.

Deflections shown in figure 6.2 are affected by the pile stick-up height. The SE inclinometer pile was grossly underdriven and the deflections were magnified. The fully driven piles on the west side of the excavation showed displacements that were less than one inch.

6.1.2 Field Observations

Two important observations were made during the course of the load test. First, the sheet piles, were disconnecting from the soil mass. This was visible and could also be deduced in the strain gage data. Figure 6.3 is a magnified view of the disconnection.

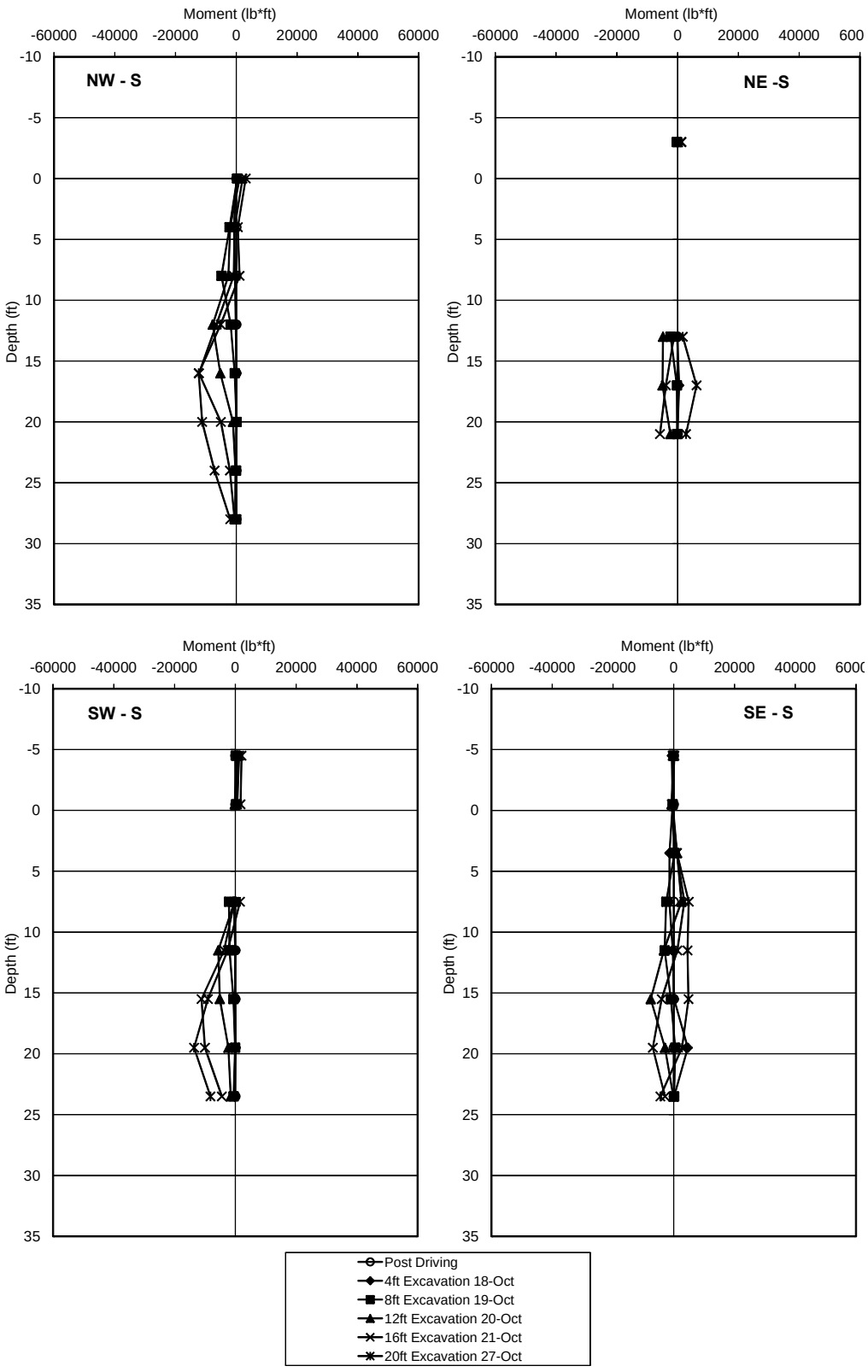

Figure 6.1 - Measured bending moments per pile and excavation step without residual stresses

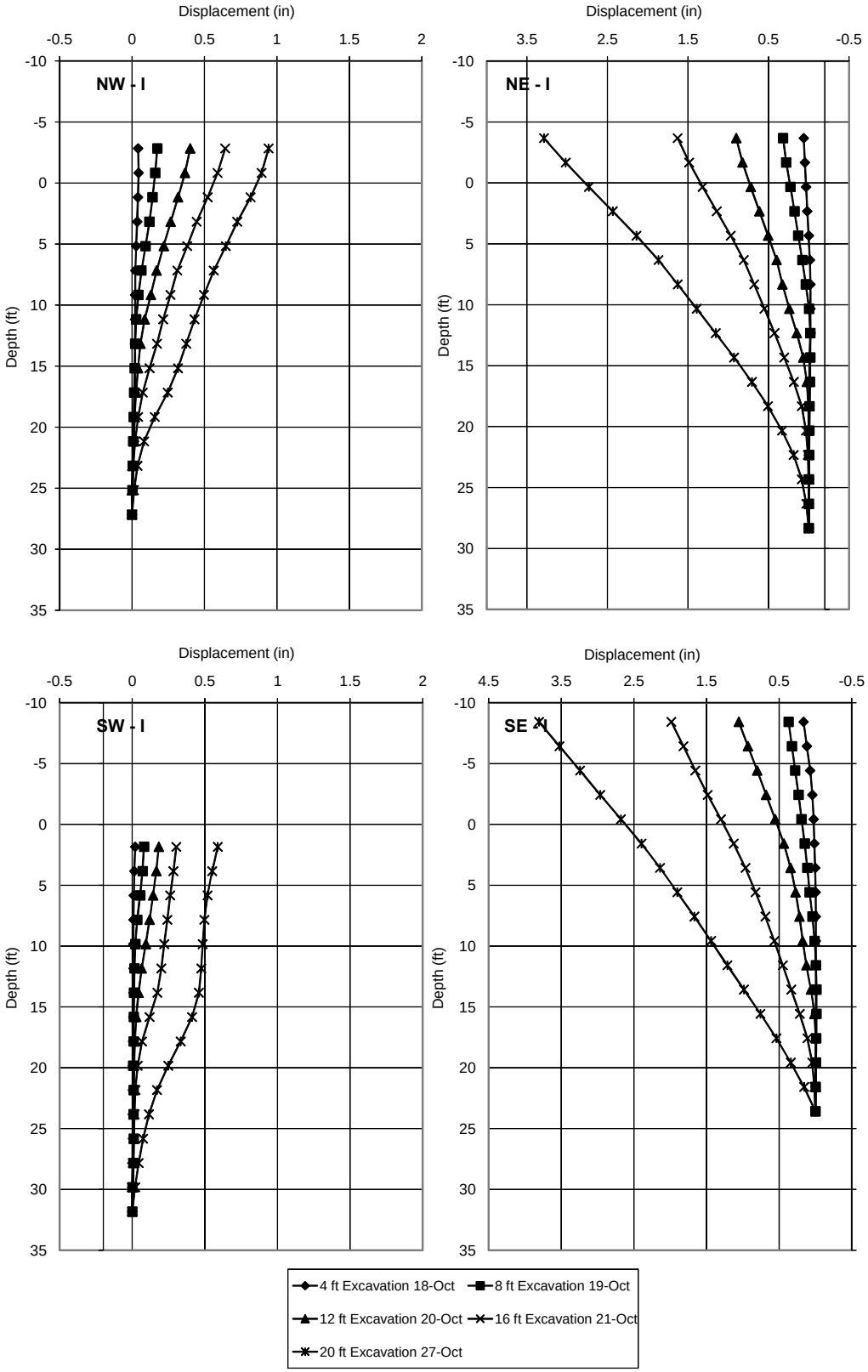

Figure 6.2 - Measured lateral displacements per pile and excavation step.

As previously mentioned, the Statesville site was inside an active borrow pit for the US 70 bypass project. The contractor planned to excavate 40 feet of material from the site through the course of the construction project. The contractor's excavator can be seen loading a truck in figure 6.4. Note the scale of the truck versus the excavated depth of the haul road.

Figure 6.3 - Disconnection of sheet piles from soil mass

Figure 6.4 - Vertical excavation of soil onsite

6.2 Monroe Test Site

As before, bending moment and lateral displacement were measured at the Monroe test site. The number of strain gages was roughly doubled in an attempt to increase the resolution of the bending moment distributions. However, the construction challenges experienced in Monroe impacted the results.

6.2.1 Quantitative Results

The quantitative results are presented as plots of bending moment and lateral deflection with depth. The first two plots show the measured bending moment versus depth for two cases. Figure 6.5 shows the bending moments induced as the excavation was completed. The detected bending moments were nearly zero. The negative bending moments again were likely due to the fact that the residual stresses locked in during driving were released as happened in Statesville.

Lateral deflections from the slope inclinometer are shown in figure 6.6. Construction difficulties resulted in damage to the sheet piles that more than likely forced them out of horizontal and vertical alignment. As mentioned previously, one of the inclinometer casings was twisted loose from the pile when installed. The most properly driven inclinometer pile was in the north east location. Measured deflections are still likely due only to release from the wall and tilting rather than earth pressure.

6.2.2 Field Observations

During the excavation, the piles were separated from the soil mass, leaving the retained soil standing without support. In order to estimate the depth of separation, the end was removed from a tape measure, and the tape was inserted behind the sheet pile wall in several locations. In every case, the tape measure extended the full 20 excavation depth

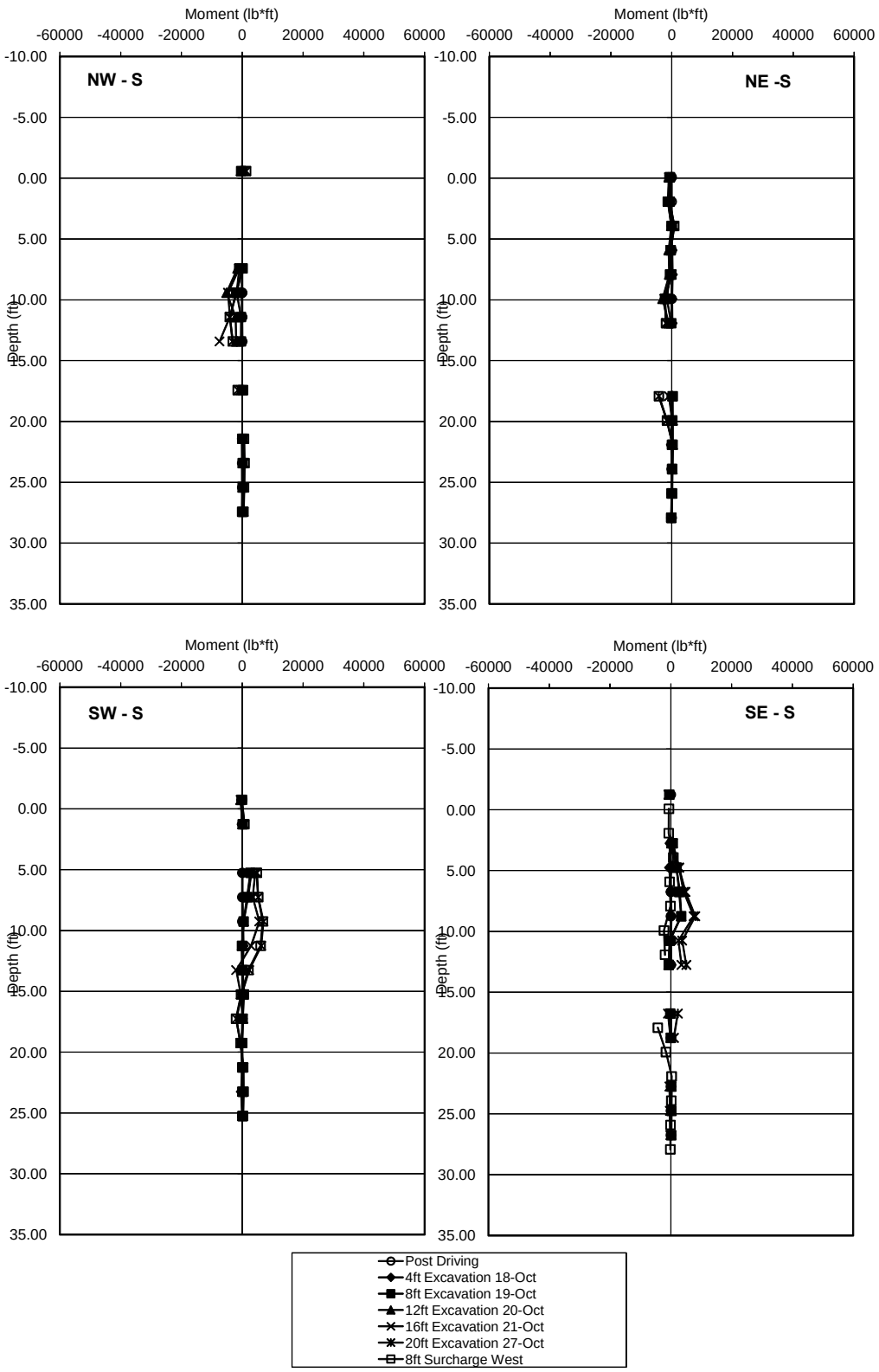

Figure 6.5 - Measured bending moments per pile and excavation step without residual stresses

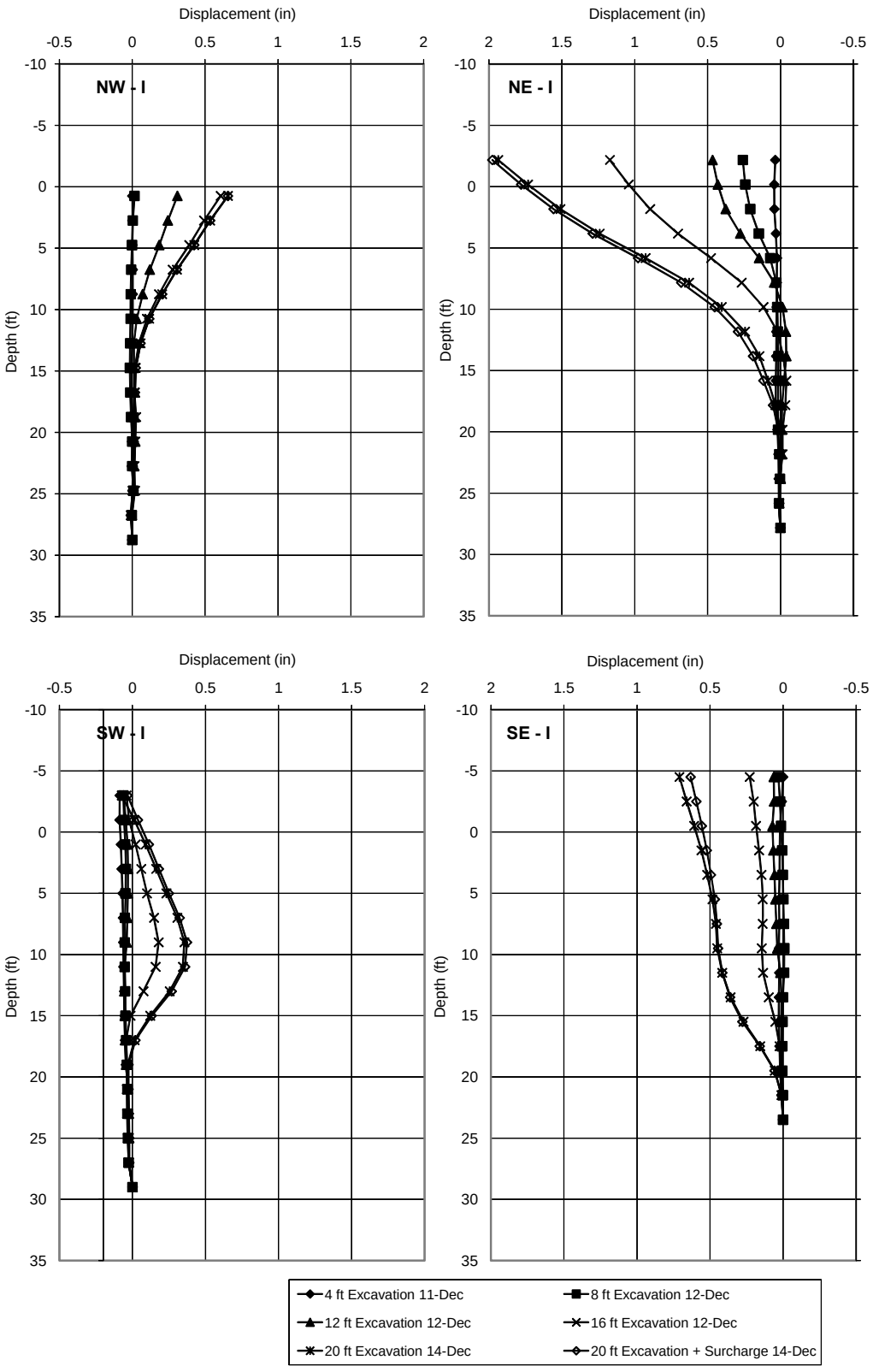

Figure 6.6 - Measured lateral displacements per pile and excavation step.

before the soil came in contact with the sheet pile wall. Figure 6.7 shows the separation of the sheet pile wall from the retained soil.

The reduced wall configuration resulted in the elimination of one of the access ramps, thus there was a section of the excavation with a near vertical slope. Figure 6.8 shows this steepened slope that illustrates the strength of the soil mass in the field.

From the field observations, it was determined that there was no lateral earth pressure acting on the retaining walls. Therefore, the soil mass would have stood by itself unrestrained.

Figure 6.7 - Wall separation

Figure 6.8 - Unsupported soil mass (20ft excavation)

CHAPTER 7
MODEL DEVELOPMENT

The strength and compressibility parameters obtained from the in-situ soil tests and lab tests were used to estimate the amount of lateral earth pressure that would occur in the field. Several methods were used to quantify the lateral earth pressure and estimate the deflection of the test wall, including Rankine's earth pressure theory, soil structure interaction, and the finite element method.

7.1 Soil Strength Parameters

Since the model would be based upon soil parameters measured in the lab or insitu, a first step was to develop composite profiles for both sites. The borehole shear or triaxial tests produced direct measurements of soil parameters c and ϕ or c' and ϕ'. However, the other insitu tests report intermediate or index parameters that must be correlated to engineering properties. There are a multitude of correlations to the SPT test. For the sake of simplicity, the equation published by Peck et al. (1974) was used to determine the friction angle from the N'_{60} value. A correlation published by Sowers (1979) was used to calculate s_u from N'_{60} as an indicator of c'. Young's modulus was determined from an equation in the Soil Properties Manual by Kulhawy and Mayne (1990). Similarly, constrained modulus, friction angle, undrained shear strength were correlated from the dilatometer soundings based upon work by Marchetti (1980, 1997). And finally, for the CPT tests in Statesville, Robertson and Campanella (1983) was employed to determine friction angle from q_c, and Baladi et al. (1981) was used to find Young's Modulus. In order to develop composite useful profiles, the soil parameters, measured and correlated, were averaged at 5 feet depth intervals. Tables 7.1 and 7.2 summarize the soil properties for Statesville and Monroe, respectively.

Table 7.1 - Summary of average soil properties for the Statesville research site

	SPT					CPT				DMT					BST		TXL			
Depth (ft)	N (bl./ft)	N'_{60} (bl./ft)	ϕ (^{o})	s_u (psf)	E (psi)	q_c (tsf)	ϕ (^{o})	s_u (psf)	E (psi)	q_D (tsf)	M (psi)	ϕ (^{o})	s_u (psf)	E (psi)	ϕ (^{o})	c (psf)	ϕ' (^{o})	c' (psf)	E (psi)	Depth (ft)
GS=0																				GS=0
5.0	7.8	20.7	33.5	1653	3015	20.6	39.3	2708	634	2.9	5219	41	717	3877	36.5	400	24.3	318	1217	5.0
10.0	8.3	15.5	31.9	1237	2256	19.2	35.3	2481	580	3.2	3924	38	803	2915	32.3	148	28.3	333	1466	10.0
15.0	8.8	13.2	31.1	1056	1926	17.4	32.8	2210	544	3.7	3309	37	913	2458	24.5	336	31.1	150	1420	15.0
20.0	7.5	9.9	30.0	793	1446	19.5	31.5	2479	616	3.9	3426	36	1079	2545	32.8	144	27.4	407	2062	20.0
25.0	8.8	10.9	30.4	875	1596	19.6	30.3	2478	616	4.7	2780	35	1235	2065	-	-	-	-	-	25.0
30.0	7.3	8.6	29.6	690	1258	20.0	30.3	2522	634	4.3	3027	36	1185	2249	-	-	-	-	-	30.0
35.0	8.3	9.4	29.8	750	1368	22.9	29.5	2893	689	6.2	3230	35	1343	2400	-	-	-	-	-	35.0
40.0	9.0	9.8	30.0	785	1432	21.4	29.0	2683	653	7.3	2302	34	1471	1710	-	-	-	-	-	40.0

GWT = 18 (ft.) below the GS (Ground Surface)

Table 7.2 - Summary of average soil properties for the Monroe research site

	SPT					DMT					BST		TXL			
Depth (ft)	N (bl./ft)	N'_{60} (bl./ft)	ϕ (^{o})	s_u (psf)	E (psi)	q_D (tsf)	M (psi)	ϕ (^{o})	s_u (psf)	E (psi)	ϕ (^{o})	c (psf)	ϕ' (^{o})	c' (psf)	E (psi)	Depth (ft)
GS=0																GS=0
5.0	18.5	48.1	40.3	3848	7018	5.4	17550	43	2511	13037	40.6	206	30.5	504	1813	5.0
10.0	13.0	24.0	34.5	1922	3505	5.8	10654	39	1469	7914	34.1	166	29.3	252	1968	10.0
15.0	11.8	17.4	32.5	1393	2540	4.5	6324	36	1006	4698	41.9	24	36.5	263	1825	15.0
20.0	11.3	14.3	31.5	1145	2087	4.7	5830	35	1028	4331	41.1	173	35	209	1161	20.0
25.0	11.0	12.4	30.9	996	1816	3.8	3849	35	975	2859	-	-	-	-	-	25.0
30.0	13.3	13.7	31.3	1098	2002	3.7	3593	34	1177	2669	-	-	-	-	-	30.0
35.0	15.0	14.3	31.5	1141	2081	5.6	4213	34	1353	3130	-	-	-	-	-	35.0
40.0	17.7	15.7	32.0	1255	2288	4.2	2553	33	1201	1897	-	-	-	-	-	40.0

GWT not present

7.2 Numerical Earth Pressure Models

The starting point for the development of an earth pressure model was numerical simulation. Two cases were considered: 1) a typical assumption of $\phi' = 30°$ and c' = 0 psf that is often used in geotechnical design in North Carolina, and 2) $\phi' = 28°$ and c' = 250 psf representing *lower bound* values from triaxial tests at the research sites. Numerical predictions were made using both SSI and FEM to show the bending moment and deflection of a 34 feet embedded PZ22 sheet pile wall with 4, 8, 12, and 16 feet excavation stages (the 20 feet excavation model as unstable when $\phi' = 30°$ and c' = 0, and therefore was not used subsequently). Figures 7.1 and 7.2 present the results of the simulations. From figure 7.1, the maximum bending moment on the sheet piles when $\phi' = 30°$ and c' = 0 psf ranges between 40,000 and 50,000 lb*ft with a maximum deflection on the order of 10 inches. In contrast, the maximum bending moment shown in figure 7.2 for $\phi' = 28°$ and c' = 250 psf is 2500 – 7500 lb*ft with pile top deflection ranging between 0.5 and 1.5 inches.

The measured bending moments and lateral displacements at an excavation depth of 16 feet for both Statesville and Monroe superimposed over the expected results from the two scenarios are shown in figure 7.3. Coupled with the qualitative observations from the load tests presented in Chapter 6, the measured response supports the behavior similar to that of soil with $\phi' = 28°$ and c' = 250 psf, or better. This follows logically from the soil test results summarized in Tables 7.1 and 7.2. The residual soils at the research sites have fiction angle that, on average, is greater than 30^o and cohesion intercept of at least 250 psf.

7.3 Earth Pressure Model Development

Rather than set out to develop a new earth pressure model using the results generated from the load tests, a more effective approach was to consider classical models using

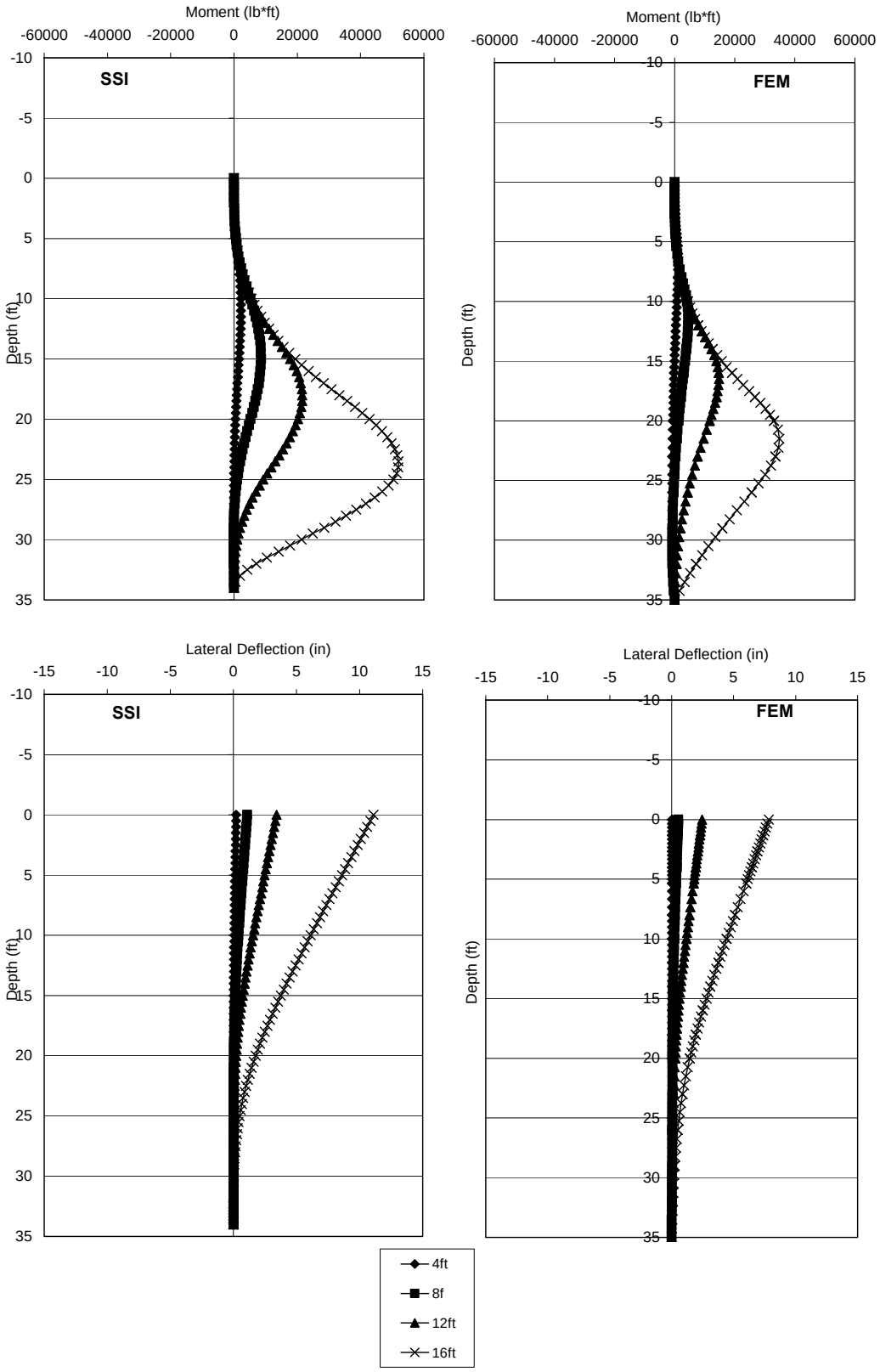

Figure 7.1 - Numerical prediction of bending moment and deflection for $\phi' = 30°$ and c' = 0

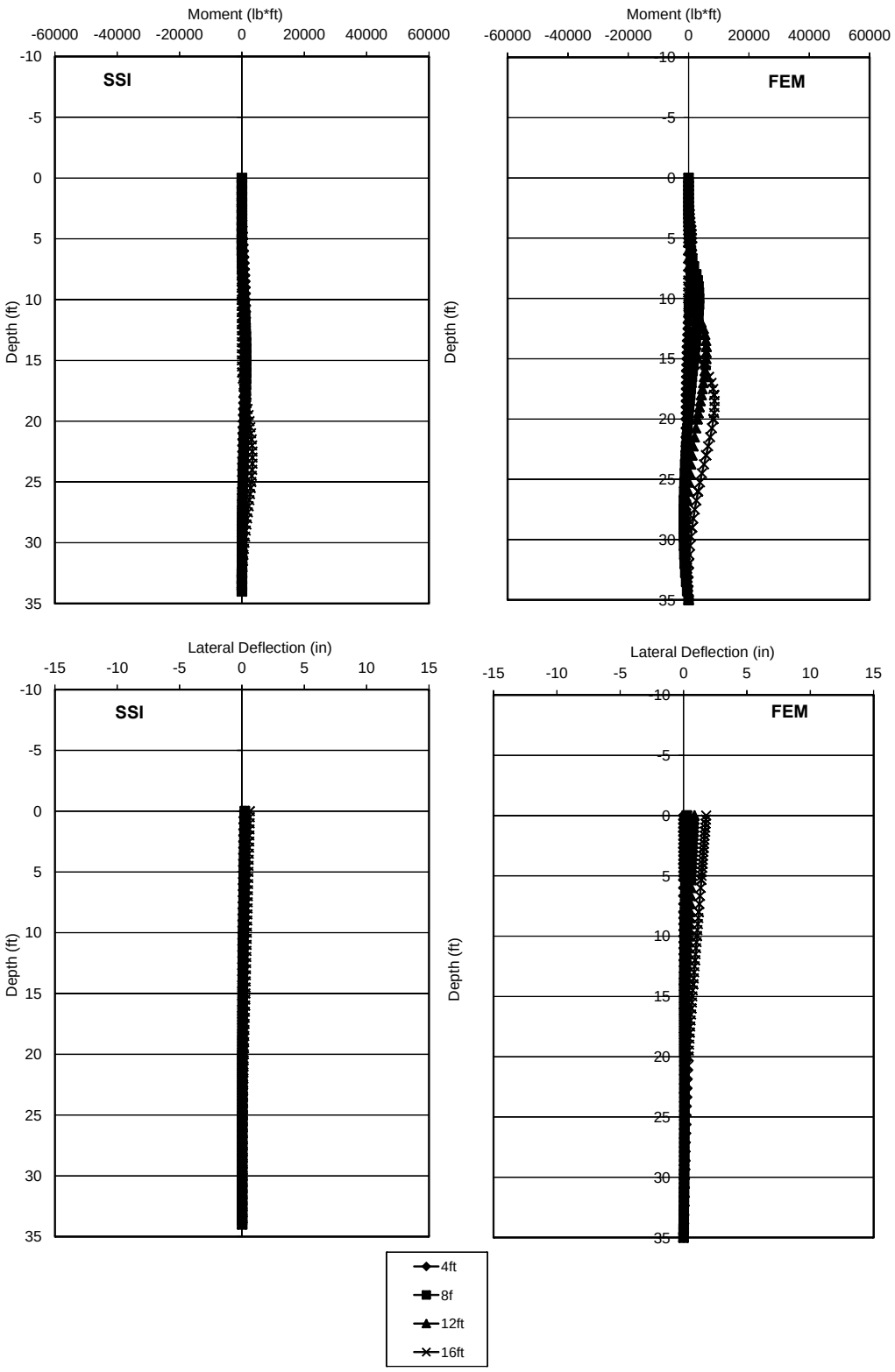

Figure 7.2 - Numerical prediction of bending moment and deflection for $\phi' = 28$ and c' = 250 psf

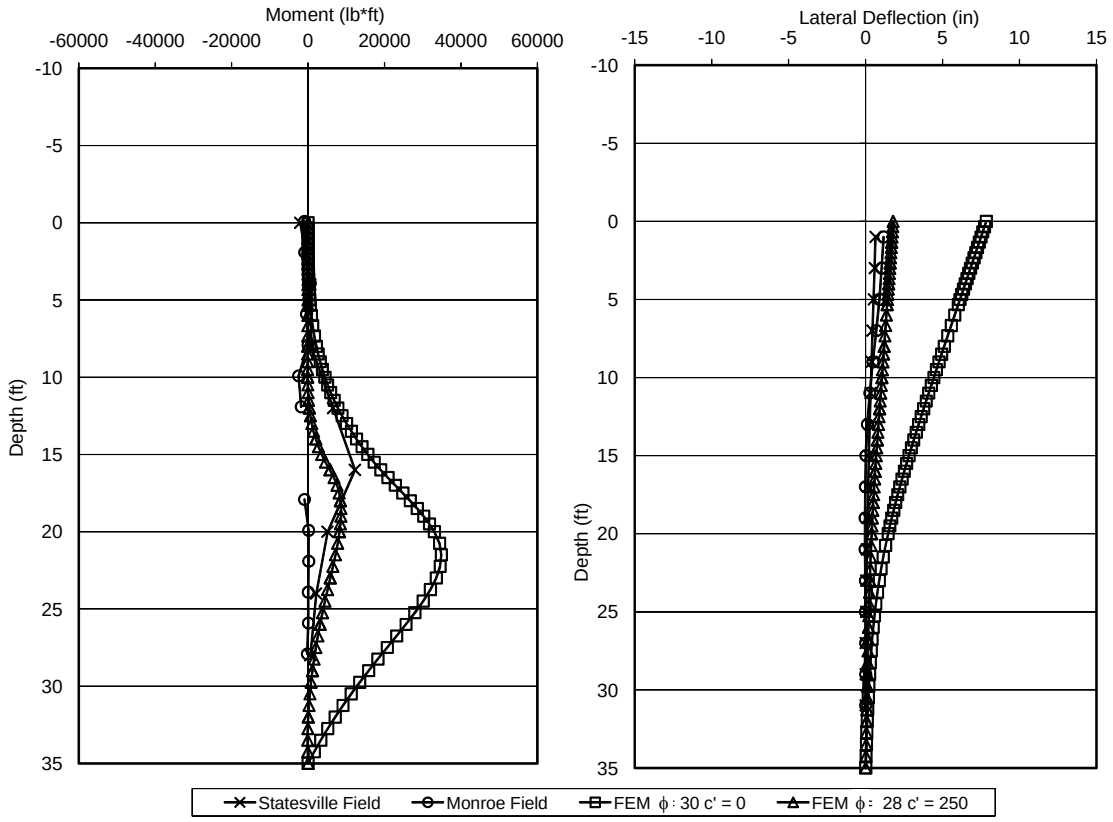

Figure 7.3 - Numerical prediction of bending moment and deflection at 16 foot excavation with field data superimposed.

parameters appropriate for the soils encountered at the sites. Rankine coefficients are often used in the determination of active earth pressure for many types of retaining structures. Furthermore, in the simplest cases, Coulomb's theory reduces to the same equations as Rankine. Therefore, Rankine's equation became the basis for the model.

First, using the ϕ and c profiles from the triaxial and BST, the Rankine earth pressure distribution is determined for a cut 20 feet deep at both Statesville and Monroe and is plotted in figure 7.4. These earth pressure distributions clearly show the impact of including c' in the analysis. The Rankine earth pressure distributions where $\phi' = 30$ and c' = 0; and $\phi' = 28$ and c' = 250 were then superimposed on top of those in figure 7.4 to obtain figure 7.5. Table 7.3 shows the same results in terms of the net earth pressure force. The resulting earth

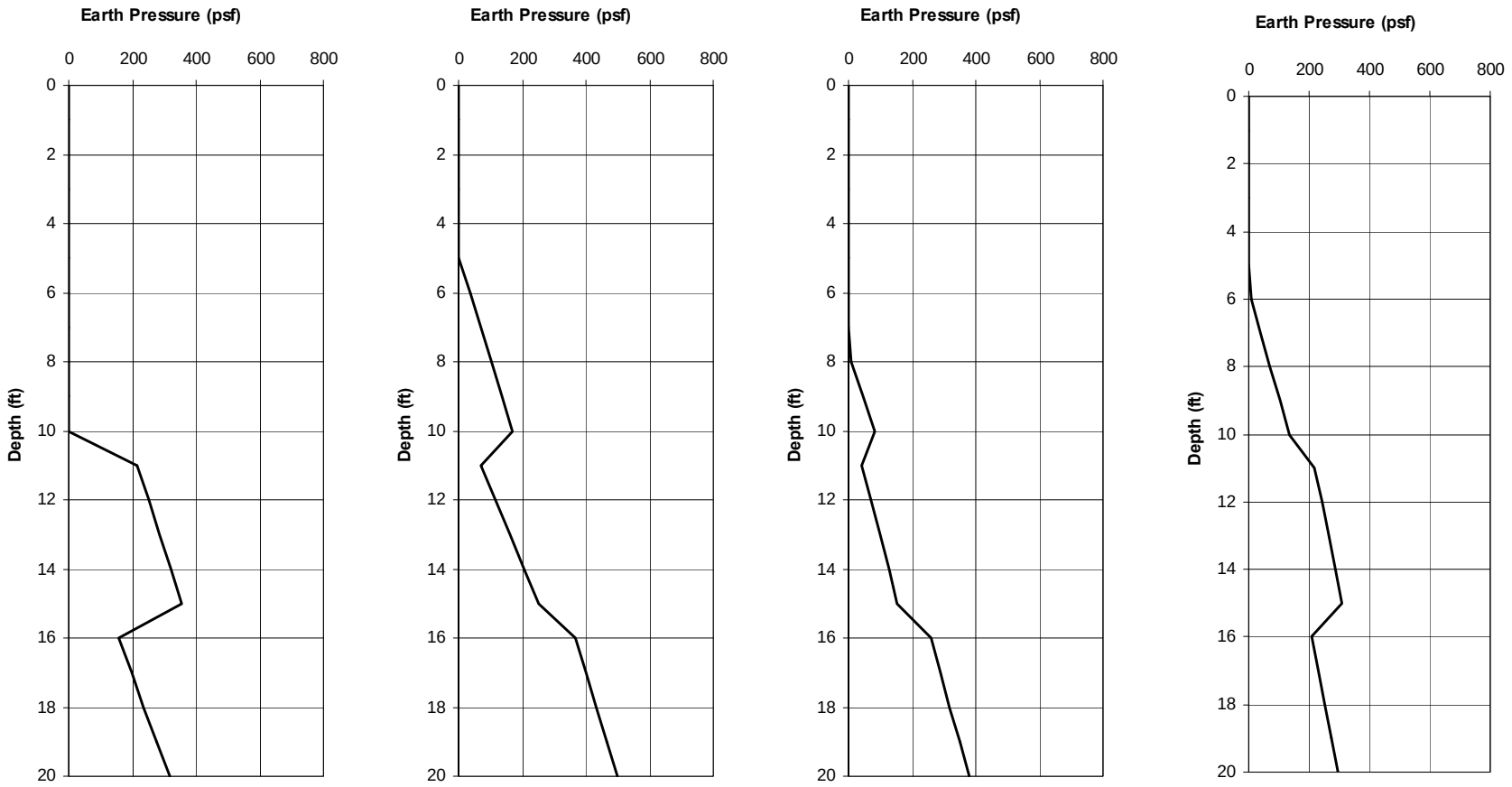

Figure 7.4 – Rankine earth pressure distributions based on triaxial and BST parameters for Statesville (a and b) and Monroe (c and d)

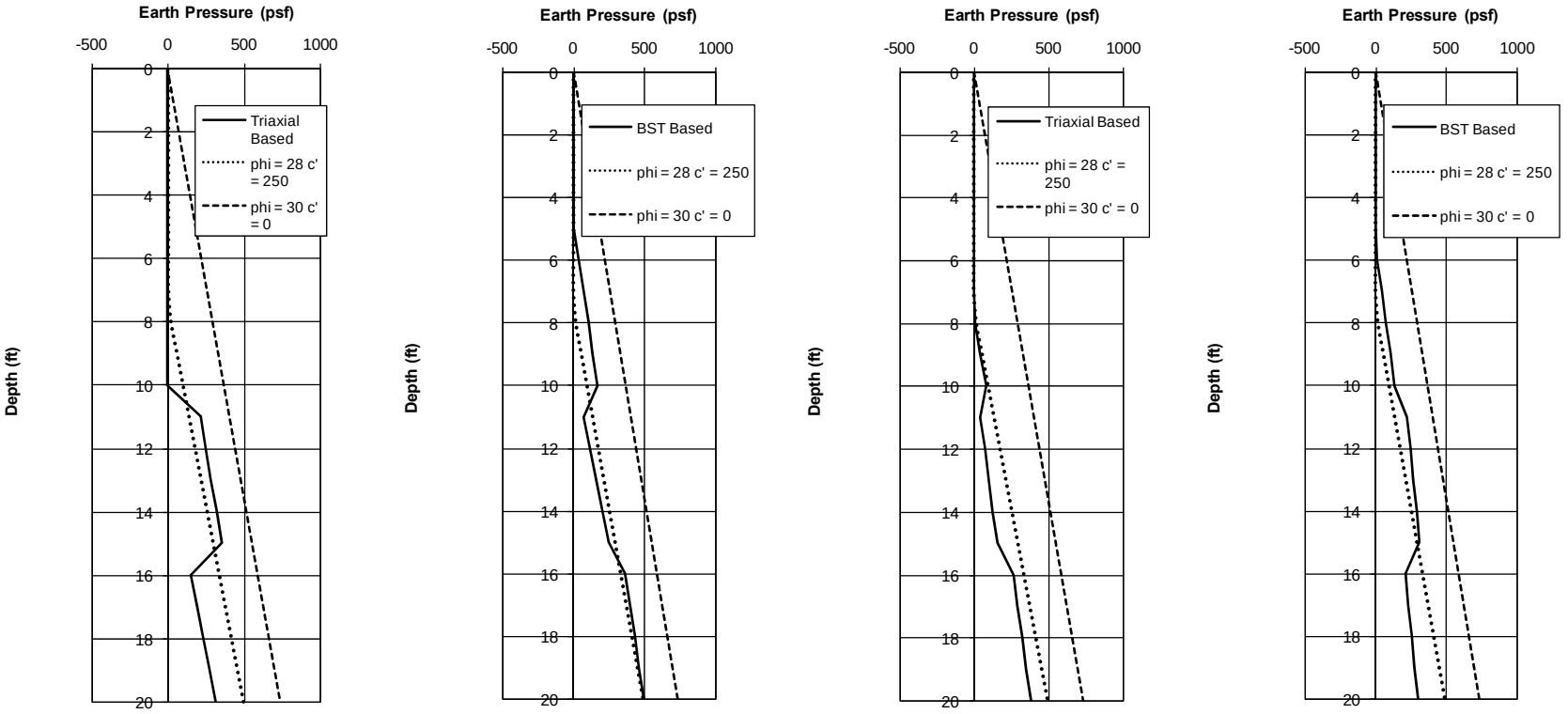

(a) (b) (c) (d)

Figure 7.5 – Rankine earth pressure distributions based on triaxial and BST parameters for Statesville (a and b) and Monroe (c and d) with superimposed predictions of distributions for cases of $\phi' = 30^o$, c' = 0 and $\phi' = 28^o$, c' = 250 psf distributions overlain

Table 7.3 – Net earth pressure forces for cases shown in figures 7.4 and 7.5.

Description		Force (lbs/ft)
Statesville		
	Triaxial	2459
	BST	3380
Monroe		
	Triaxial	2093
	BST	2904
Typical		
	$\phi' = 30°$, c' = 0 psf	7333
	$\phi' = 28°$, c' = 250 psf	3075

pressure forces for the 2-parameter Triaxial and BST based distributions fall within the range of 2100 to 3400 lbs/ft with an average of 2800 lbs/ft. In contrast, the $\phi' = 30°$, c' = 0 psf resultant is nearly twice that value.

Based on this comparison, it is proposed that the parameters from the triaxial and/or BST be used in the Rankine earth pressure equations for computing earth pressure in residual soils. In the context of the load test results where little or no true earth pressure was mobilized, these distributions would still represent a level of conservatism while at the same time provide substantial savings to NCDOT.

7.4 Impact on Numerical Models

Using the proposed simple model, the bending moments and maximum deflections are recomputed at an excavation depth of 16 feet for the Statesville and Monroe sites. Figures 7.7 and 7.8 show the resulting distributions of bending moment and deflection from both the SSI and FEM models using triaxial and borehole shear test parameters, respectively. The bending moments and deflections are far below those obtained in figure 7.1.

7.5 Impact on Retaining Structure Design

NCDOT routinely constructs gravity, pile panel, and mechanically stabilized

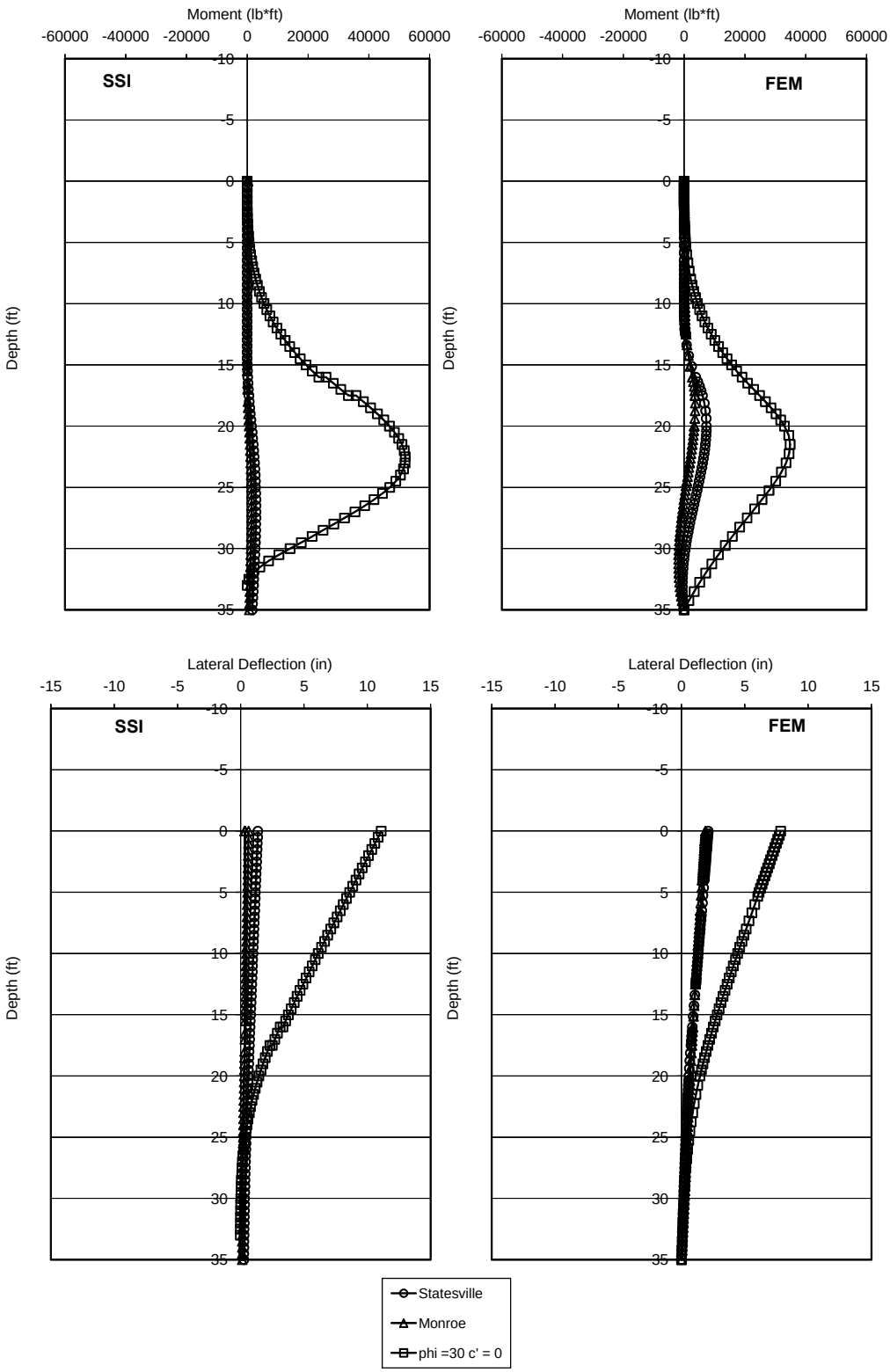

Figure 7.7 Numerical prediction of bending moment and deflection using triaxial parameters.

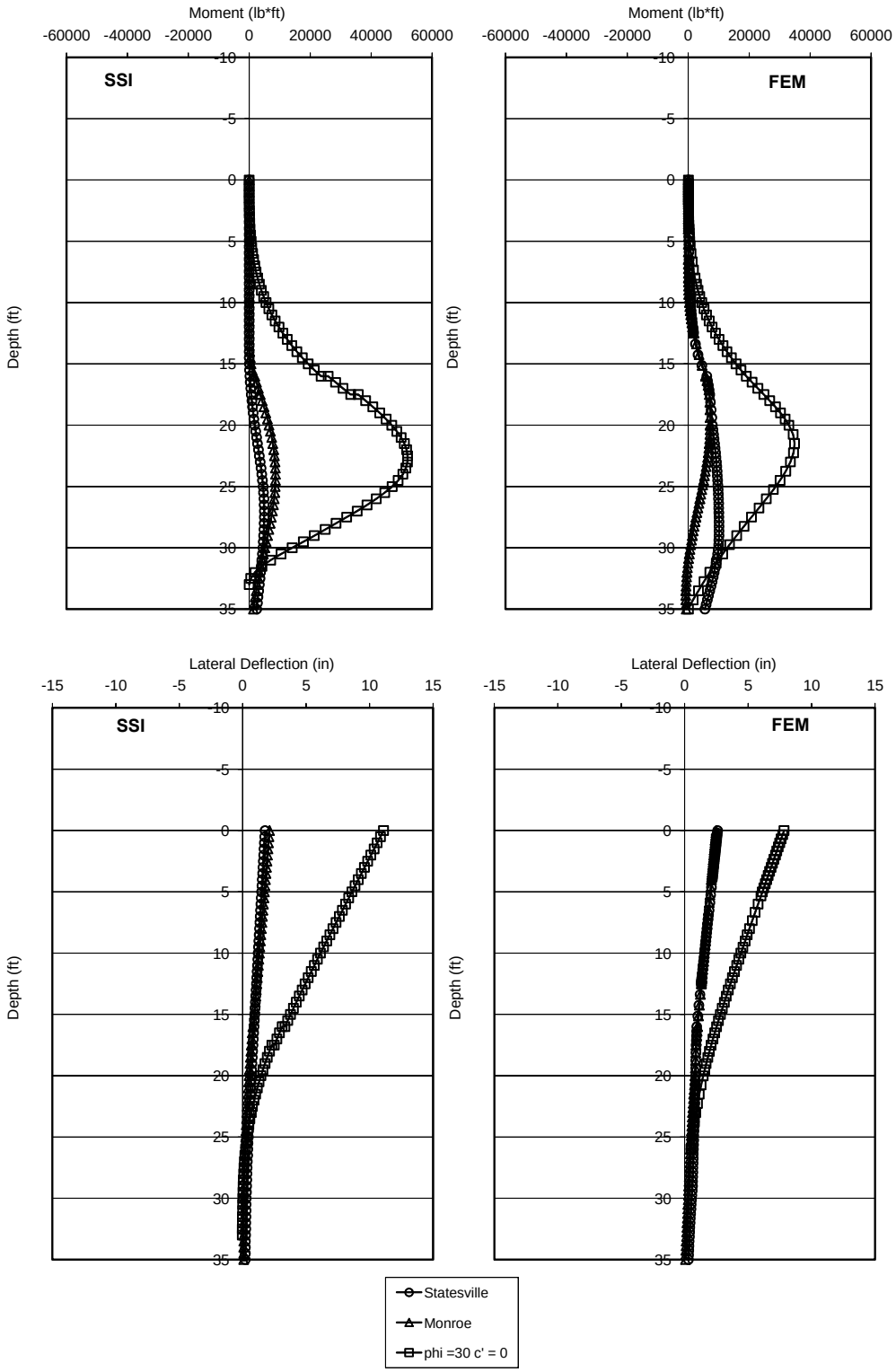

Figure 7.8 Numerical prediction of bending moment and deflection using BST parameters

walls in Piedmont residual soils. To demonstrate the impacts of the proposed models on wall design, it is convenient and simpler to focus on gravity walls. As simple case study of a gravity wall designed and built in the Piedmont to resist sliding and overturning can best illustrate the significant change in factors of safety for the parameters used in wall design. Consistent with the modeled cut, a wall of 16 feet designed for cases of c' = 0 and $\phi' = 30°$; c' = 250 psf and $\phi' = 28°$; c' = 0.

Starting with a factor of safety (FS) of 1.5 for overturning and sliding for the case in which the soil parameters are c' = 0 and $\phi' = 30°$, the corresponding FS for overturning and sliding are approximately 7.8 and 4.5 respectively for the case of soil parameters of c' = 250 psf and $\phi' = 28°$. Designing to the code prescribed FS will reduce the level of conservatism of the wall and result in substantial cost savings to NCDOT.

7.6 Parameter Selection

Key to this method is the selection of soil parameters. As previously stated the triaxial and borehole shear tests provide two parameter measurements of shear strength and therefore would be suitable for use with the two parameter model. Two issues then become important: 1) the number of tests needed to determine the design value for a structure and 2) the development of parameters from the test data.

The number of triaxial tests required to determine the representative c' and ϕ values should be based upon the length and height of structure as well as the judgment of the geologist. It is typical practice for NCDOT to perform borings at 50 to 100 foot intervals for the design of retaining structures. These borings extend the depth of the retaining structure including the potential foundation. After the initial borings are complete, the geologist/engineer should examine the spoon samples make note of any

particular changes in the character of the residual soil i.e. significant parent material changes, marked differences in particle distribution, or other geological anomalies.

It would make the most sense then to prescribe the number of tests based upon a criteria that includes the height and length of the wall and also reflects the judgment of the geologist/engineer. It is therefore recommended that a three point triaxial test should be performed for every 1000 square feet of wall face, with minimum of two tests for any structure. Additional tests may be recommended by the geologist/engineer based upon significant changes in stratigraphy. Additional specifications on performing triaxial tests on residual specimens are included as Appendix E.

The BST provides an insitu measure of ϕ and c as well. However, questions regarding drainage and whether there are unsaturated effects are difficult to answer, thus the parameters may or may not represent effective conditions. The parameters, on average compare well with the triaxial tests having slightly higher friction angles and lower c. While the triaxial test appears to be the standard, the BST may be recommended to complement the triaxial tests, or in exceptional cases, substitute for it.

Being that the tests represent discrete points within the soil mass, the SPT blowcounts, along with the descriptive information included in the boring logs, should be used to verify that the individual tests are representative.

When interpreting the results of the tests, the strength should be determined based upon application of the Mohr Coulomb failure criteria. Historically, the c component has been neglected by arbitrarily drawing the failure envelope through the origin. Use of a tool such as a spreadsheet that automatically determines the angle and intercept of the Mohr-coulomb envelope is suggested.

CHAPTER 8
CONCLUSION

8.1 Research Summary

The objective of this research project was to develop an earth pressure model for retaining structures in Piedmont residual soils. The scope of work included literature review, numerical models, insitu and laboratory soil testing, and full scale load testing of cantilever sheet pile retaining structures.

8.2 Conclusions

The following statements are made based upon the results of the research program:

1) The earth pressure currently used in design of retaining structures in Piedmont soils is greater than earth pressure measured during load tests. Field measurements from the instrumented wall load tests demonstrated that the retained soils exerted little or no pressure on the structure.
2) The Piedmont soils that were tested in this research had significant strength. The average friction angle was 28^{o} and the average drained cohesion intercept was above 300 psf. These values were consistent with those found in the literature for similar soils.
3) Based on the soil test results as well as the minimal earth pressure detected during the load tests, the soil strength parameters, ϕ and c' should be used together in Rankine's earth pressure equation to predict the earth pressure in Piedmont soils.
4) Triaxial tests provided the most consistent measurement of ϕ' and c'. The borehole shear tests also measure ϕ and c but should only be used when triaxial testing is unavailable.

8.3 Recommendations

Section 2.3 listed the limitations of this study. In order to address these, two primary recommendations for future work are put forward. First, it is suggested that a broader database of triaxial tests in Piedmont soils be developed. This data can be generated from historic test records as well as tests performed based on the recommendations of this study. This database will give NCDOT engineers confidence in the parameters, especially c', while at the same time provide a statistical context for the parameters for the development of a standard.

Second, the long term behavior of these soils must be examined. The constraints of this study were such that the retaining structures could not remain for a long enough period to evaluate the time-dependency of the ϕ and c' components of the soil. A follow up study using an instrumented retaining structure or cut, that can stand for several years would, at the minimum, help develop trends in the behavior of the materials. Within the study, soils would be tested at the outset of the project, and yearly to determine the changes in parameters, while the wall or cut is continuously monitored for changes in pore air and water pressures, movements or failures.

9 LIST OF REFERENCES

ASCE, (1982). *Engineering and construction in tropical and residual soils.* Proceedings of the ASCE Geotechnical Engineering Division Specialty Conference, *New York, ASCE*, 735 pp.

ASTM Standard D4767, (2004), "Standard Test Method for Consolidated Undrained Triaxial Compression Test for Cohesive Soils," ASTM International, West Conshohocken, PA.

Baldi, G., Bellotti, R., Ghionna, V., Jamiolkowski, M. and Pasqualini, E., (1981). "Cone Resistance of a Dry Medium Sand," *Proc.10th International Conference on Soil Mechanics and Foundation Engineering, Stockholm*, Vol. 2, pp. 427-432.

Bishop, A.W. and Henkel, D.J., (1957). *The triaxial test*. William Clowes 7 Sons, London.

Borden, R. H., Shao, L., and Gupta, A., (1996). "Dynamic properties of piedmont residual soils." *Journal of Geotechnical Engineering*, ASCE, Vol. 122(10), pp.813-821.

Brand, E. W. and Phillipson, H. B., (1985). *Sampling and testing of residual soils: a review of international practice*. Southeast Asian Geotechnical Society, Scorpion Press, Hong Kong.

Clough, G.W., and O'Rourke, T.D. (1990). "Construction induced movements of insitu walls." Design and Performance of Earth Retaining Structures, GSP No. 25, ASCE, New York, NY, pp. 439-470.

Crowther, C. L., (1963). *The design, construction, and use of a static penetrometer in micaceous silts of the southern Piedmont region.* MS Thesis, Georgia Institute of Technology, Atlanta.

Cruz, N., Figueiredo, S. and Viana da Fonseca, A., (2004a). "Deriving geotechnical parameters of residual soils from granite by interpreting DMT+CPTU tests." *Proc., ISC-2 on Geotechnical and Geophysical Site Characterization*, Porto Portugal, September 19-22, pp. 1799-1803.

Cruz, N., Viana da Fonseca, A., and Neves, E., (2004b). "Evaluation of effective cohesive intercept on residual soils by DMT and CPT." *Proc., ISC-2 on Geotechnical and Geophysical Site Characterization*, Porto Portugal, September 19-22, pp. 1275-1278.

Cruz, N., and Viana da Fonseca, A., (2006). "Portuguese experience in residual soil characterization by DMT tests", DMT06 – The Second International Conference on the Flat Dilatometer, Washington, D.C., 2-5 April, 2006.

Failmezger, R. A., Rom, D., and Ziegler, S. B., (1999). "SPT? - A better approach to site characterization of residual soils using other insitu tests." *Behavioral Characteristics of Residual Soils,* Geotechnical Special Publication No. 92, ASCE, pp. 158-175.

Fang, Y., Chen, T., and Wu, B., (1994). "Passive earth pressures with various wall movements." *Journal of Geotechnical Engineering*, Vol. 120(8), p. 1307 - 1323.

Fang, Y., Chen, J., and Chen, C., (1997). "Earth pressures with sloping backfill." *Journal of Geotechnical Engineering*, Vol. 123(3), p. 250 - 259.

Finke, K. A., Mayne, P.W., and Klopp, R. A., (1999). "Characteristic piezocone response in Piedmont residual soils." *Behavioral Characteristics of Residual Soils*, Geotechnical Special Publication No. 92, ASCE, pp. 1-11.

Finke, K. A., Mayne, P.W., and Klopp, R. A., (2001). "Piezocone penetration testing in Atlantic Piedmont residuum." *Journal of Geotechnical & Geoenvironmental Engineering*, Vol. 127(1), pp. 48 - 54.

Frank, A.R. (1990). *Development of an automated data acquisition system for an electric cone used for the correlation of the SPT, DMT, and CPT in Piedmont residual soils*. MS Thesis, Georgia Institute of Technology, Atlanta.

Gan, J. K. M., and Fredlund, D.G. (1996). "Shear strength characteristics of two saprolitic soils." *Canadian Geotechnical Journal*, 33(4), 595-609.

Garga, V. K. (1988). "Effect of Sample Size on Shear Strength of Basaltic Residual Soils." *Canadian Geotechnical Journal*, 25(3), August, 478-487.

Georgiadis, M. and Anagnostopoulos, C., (1998). "Lateral pressure on sheet pile walls due to strip load." *Journal of Geotechnical & Geoenvironmental Engineering*, Vol. 124(1), pp. 95 - 98.

Gomes Correia, A. , Viana da Fonseca, A., and Gambin, M., (2004). "Routine and advanced analysis of mechanical in situ tests. Results on saprolitic soils from granites more or less mixed in Portugal." *Proceedings ISC-2 on Geotechnical and Geophysical Site Characterization*, Porto Portugal, September 19-22, pp. 75-95.

Gupta, A., (1995). *Radial strain measurement and its significance in the study of dynamic behavior of Piedmont residual soils.* MS Thesis, North Carolina State University, Raleigh.

Hansen, J.B. (1961). *Earth pressure calculation 2nd ed.*, The Danish Technical Press, Copenhagen, Denmark.

Harshman, D.S., (1989). *Settlement predictions in residual soils : an evaluation of deformation modulus and stress distribution from the analysis of two case studies.* MS Thesis, North Carolina State University, Raleigh.

Heartz, W. T. (1986), *Properties of a Piedmont residual soil*. PhD Dissertation, North Carolina State University, Raleigh.

Hoyos Jr., L. and Macari, E. J., (1999). "Influence of insitu factors on dynamic response of Piedmont residual soils." *Journal of Geotechnical & Geoenvironmental Engineering*, ASCE Vol. 125(4), pp. 271-279.

Jaky, J., (1948). "Pressure in silos." Proc. 2nd ICSMFE, Vol. 1 pp. 103-107.

Kelly, S. P. and Lutenegger, A.J., (1999). "Enhanced site characterization in residual soils using the SPT-T and drive cone tests." *Behavioral Characteristics of Residual Soils,* Geotechnical Special Publication No. 92, ASCE, pp. 88-100.

Kort, D. A. (2002). *Steel sheet pile walls in soft soil*. Delft University Press, Delft, The Netherlands.

Lambe, P. C. and Heartz, W. T., (1988). "Consolidated drained triaxial testing of Piedmont residual soil." *Advanced Triaxial Testing of Soil and Rock*, ASTM STP 977: 311-320.

Lee, I. K., and Coop, M. R. (1995). "Intrinsic behaviour of a decomposed granite soil." *Geotechnique*, 45(1), 117-130.

Liu C. and Evett, J. B, (2001). *Soils and Foundations*, Prentice Hall, Upper Saddle River.

Long, M. (2001). "Database for retaining wall and ground movements due to deep excavations." *Journal of Geotechnical and Geoenvironmental Engineering*, Vol. 127, No. 3, ASCE, March, pp. 203-224.

Marchetti, S., (1980). "Insitu tests by flat dilatometer." *Journal of the Geotechnical Engineering Division*, ASCE, Vol. 106(3), pp. 299-321.

Marchetti, S. (1997). "The Flat Dilatometer: Design Applications", *Proc. Third International Geotechnical Engineering Conference*, Cairo University, Jan., 421-448.

Martin, G.K., and Mayne, P.W. (1998). "Seismic flat dilatometer tests in Piedmont residual soils." *Geotechnical Site Characterization,* Vol. 2, Balkema Rotterdam, 837-843.

Mayne, P.W., Brown, D., Vinson, J., Schneider, J.A., and Finke, K.A. (2000). "Site characterization of Piedmont residual soils at the NGES, Opelika, Alabama." *National Geotechnical Experimentation Sites,* GSP 93, ASCE, Reston,VA, 160-185.

Kulhawy, F. H. and Mayne, P.W., (1990). *Manual on Estimating Soil Properties for Foundation Design*, EPRI-EL-6800, Electric Power Research Institute, Palo Alto.

McCarthy, D. F., (2002). *Essentials of Soil Mechanics and Foundations: basic geotechnics 6th ed.*, Prentice Hall, Upper Saddle River, NJ

Miller, E. T., (1957). *A study of shear characteristics of the soils of the Piedmont region determined by rotating vanes*. MS Thesis, Georgia Institute of Technology, Atlanta.

Mohamedzein, Y., and Mohammed H. A. (2006). "Compressibility and shear strength of a residual soil." *Geotechnical and Geological Engineering*, 24, 1385 -1401.

Peck, R.B. (1969). "Deep excavations and tunneling in soft ground." *Proceedings of the 7th International Conference of Soil Mechanics and Foundation Engineering*. Mexico City, pp. 225-290.

Peck, R. B., Hanson, W. E., and Thornburn, T. H., (1974). *Foundation Engineering*, John Wiley and Sons, New York.

PLAXIS, (1998). *PLAXIS Version 7 Users Guide.* Eds. Brinkgreve, R. B. J., and Vermeer, P. A., A.A., Balkema, Rotterdam.

Rahardjo, H., Aung, K. K., Leong, E. C., and Rezaur, R. B. (2004a). "Characteristics of Residual Soils in Singapore as formed by weathering." *Engineering Geology*, 73, 157-169.

Rahardjo, H., Ong, B. H., and Leong E. C. (2004b). "Shear strength of a compacted residual soil from consolidated drained and constant water content triaxial tests." *Canadian Geotechnical Journal*, 41(3), 421-436.

Robertson, P. K. and Campanella, R. G., (1983). "Interpretation of Cone Penetration Tests: Parts 1 and 2," *Canadian Geotechnical Journal*, Vol. 20, pp 718-745.

Rodrigues, C.M.G. and Lemos, L.J.L., (2004). "SPT, CPT and CH tests results on saprolitic granite soils from Guarda, Portugal." *Proceedings ISC-2 on Geotechnical and Geophysical Site Characterization*, Porto Portugal, September 19-22, pp. 1345-1351.

Schneider, J. A., Hoyos Jr., L., Mayne, P.W., Macari, E.J. and Rix, G.J., (1999). "Field and laboratory measurements of dynamic shear modulus of piedmont residual soils." *Behavioral Characteristics of Residual Soils,* Geotechnical Special Publication No. 92, ASCE, pp. 158-175.

Sowers, G.F., (1954). "Soil problems in the southern Piedmont region." *Proc., Soil Mech. and Found Div.*, ASCE, Vol, 80, Separate No. 416, New York.

Sowers, G.F., (1963). "Engineering properties of residual soils derived from igneous and metamorphic rocks." *Proc., 2nd Panamerican Conf. on Soil Mech. and Found. Engrg.*, Sao Paulo, Brazil.

Sowers, G.F., (1979). *Introductory Soil Mechanics and Foundations: Geotechnical Engineering*, MacMillan, New York.

Viana da Fonseca, A., (2001). "Load tests on residual soil and settlement prediction on shallow foundation." *ASCE Journal of Geotechnical and Geoenvironmental Engineering*, Vol. 127(10), pp. 869-883.

Viana da Fonseca, A., Carvalho, J., Ferreira, C., Costa, E., Tuna, C., and J.A. Santos, (2004). "Geotechnical characterization of a residual soil profile: the ISC'2 experimental site, FEUP." *Proceedings ISC-2 on Geotechnical and Geophysical Site Characterization*, Porto Portugal, September 19-22, pp. 1361-1369.

Vinson, J.L and Brown, D.A., (1997). "Site characterization of the Spring Villa geotechnical test site and a comparison of strength and stiffness parameters for a Piedmont residual soil." Report No. IR-97-04, Highway Research Center, Harbert Engineering Center, Auburn University, AL, 385 p.

Wang, C. E., (1995). *Deformation characteristics and elastic settlement of piedmont residual soils*. MS Thesis, North Carolina State University, Raleigh.

Wang, C. E. and Borden, R.H., (1996). "Deformation characteristics of Piedmont residual soils." *ASCE Journal of Geotechnical Engineering*, Vol. 122(10), pp. 822-830.

Wang, S., and Reese, L. C., (1993). *Com624P- laterally loaded pile analysis program for the microcomputer version 2.0.* USDOT Publication No. FHWA-SA-91-048.

Wang, Y. H., and Yan, W. M. (2006). "Laboratory studies of two common saprolitic soils in Hong Kong." *Journal of Geotechnical and Geoenvironmental Engineering*, 132(7), 923-930.

Wilson, B.V., (1988) *Evaluation of in-situ testing of residual soils and prediction of settlement.* MS Thesis, North Carolina State University, Raleigh.

APPENDIX A
STATESVILLE SOIL TEST DATA

(included as separate attachment)

APPENDIX B
MONROE SOIL TEST DATA

(included as separate attachment)

APPENDIX C
STRAIN GAGE DATA

Table C.1 - Strain gage set data - Statesville

Pile #1

Tension				Compression			
Gage	Frequency (Hz)	Microstrain (με)	Δ με (set)	Gage	Frequency (Hz)	Microstrain (με)	Δ με (set)
1		1500.000	0.000	9		4500.000	0.000
2		1500.000	0.000	10		4500.000	0.000
3		1500.000	0.000	11		4500.000	0.000
4		1500.000	0.000	12		4500.000	0.000
5		1500.000	0.000	13		4500.000	0.000
6		1500.000	0.000	14		4500.000	0.000
7		1500.000	0.000	15		4500.000	0.000
8		1500.000	0.000	16		4500.000	0.000

Pile #2

Tension				Compression			
Gage	Frequency (Hz)	Microstrain (με)	Δ με (set)	Gage	Frequency (Hz)	Microstrain (με)	Δ με (set)
17		1500.000	0.000	25		4500.000	0.000
18		1500.000	0.000	26		4500.000	0.000
19		1500.000	0.000	27			
20		1500.000	0.000	28		4500.000	0.000
21		1500.000	0.000	29		4500.000	0.000
22		1500.000	0.000	30		4500.000	0.000
23		1500.000	0.000	31		4500.000	0.000
24		1500.000	0.000	32		4500.000	0.000

Pile #3

Compression				Tension			
Gage	Frequency (Hz)	Microstrain (με)	Δ με (set)	Gage	Frequency (Hz)	Microstrain (με)	Δ με (set)
33		4500.000	0.000	41		1500.000	0.000
34		4500.000	0.000	42		1500.000	0.000
35		4500.000	0.000	43		1500.000	0.000
36		4500.000	0.000	44		1500.000	0.000
37		4500.000	0.000	45		1500.000	0.000
38		4500.000	0.000	46		1500.000	0.000
39		4500.000	0.000	47		1500.000	0.000
40		4500.000	0.000	48		1500.000	0.000

Pile #4

Compression				Tension			
Gage	Frequency (Hz)	Microstrain (με)	Δ με (set)	Gage	Frequency (Hz)	Microstrain (με)	Δ με (set)
49		4500.000	0.000	57		1500.000	0.000
50				58		1500.000	0.000
51				59		1500.000	0.000
52				60		1500.000	0.000
53		4500.000	0.000	61		1500.000	0.000
54		4500.000	0.000	62		1500.000	0.000
55		4500.000	0.000	63		1500.000	0.000
56				64		1500.000	0.000

Table C.2 - Post driving strain readings - Statesville

Pile #1

Tension	SW			Compression			
Gage	**Frequency (Hz)**	**Microstrain (με)**	**Δ με**	**Gage**	**Frequency (Hz)**	**Microstrain (με)**	**Δ με**
1	602.2	1473.063	-26.937	9	1029	4301.012	-198.988
2	551.1	1233.675	-266.325	10	1058	4546.857	46.857
3	574.9	1342.532	-157.468	11	1056	4529.682	29.682
4	563.2	1288.443	-211.557	12	1038	4376.578	-123.422
5	494.3	992.479	-507.521	13	1060	4564.063	64.063
6	523.9	1114.902	-385.098	14	1065	4607.222	107.222
7	480.4	937.445	-562.555	15	1078	4720.385	220.385
8	467.2	886.636	-613.364	16	1040	4393.459	-106.541

Pile #2

Tension	SW			Compression			
Gage	**Frequency (Hz)**	**Microstrain (με)**	**Δ με**	**Gage**	**Frequency (Hz)**	**Microstrain (με)**	**Δ με**
17	580.1	1366.928	-133.072	25	1040	4393.459	-106.541
18	580.9	1370.701	-129.299	26	1062	4581.302	81.302
19	557.9	1264.307	-235.693	27			
20	659.2	1765.120	265.120	28	1040	4393.459	-106.541
21	579.9	1365.986	-134.014	29	1058	4546.857	46.857
22	487.6	965.756	-534.244	30	1064	4598.574	98.574
23	531.6	1147.915	-352.085	31	1081	4746.695	246.695
24	470.3	898.442	-601.558	32	1059	4555.456	55.456

Pile #3

Compressi	SE			Tension			
Gage	**Frequency (Hz)**	**Microstrain (με)**	**Δ με**	**Gage**	**Frequency (Hz)**	**Microstrain (με)**	**Δ με**
33	1029	4301.012	-198.988	41	603.4	1478.940	-21.060
34	1060	4564.063	64.063	42	581.2	1372.117	-127.883
35	1028	4292.657	-207.343	43	631.2	1618.355	118.355
36	1009	4135.445	-364.555	44	647.9	1705.124	205.124
37	1029	4301.012	-198.988	45	591.2	1419.740	-80.260
38	1031	4317.748	-182.252	46	626.5	1594.344	94.344
39	1028	4292.657	-207.343	47	693.5	1953.587	453.587
40	1024	4259.316	-240.684	48	611.6	1519.410	19.410

Pile #4

Compressi	NE			Tension			
Gage	**Frequency (Hz)**	**Microstrain (με)**	**Δ με**	**Gage**	**Frequency (Hz)**	**Microstrain (με)**	**Δ με**
49	1073	4676.698	176.698	57	583.7	1383.947	-116.053
50				58	650.5	1718.836	218.836
51				59	701.9	2001.200	501.200
52				60	534.1	1158.738	-341.262
53	1032	4326.127	-173.873	61	763.5	2367.871	867.871
54	1016	4193.024	-306.976	62	733.9	2187.831	687.831
55	1136	5241.995	741.995	63	593.7	1431.773	-68.227
56				64	517.3	1086.988	-413.012

Table C.3 - Strain after 4 foot excavation - Statesville

Pile #1

Tension				Compression			
Gage	**Frequency (Hz)**	**Microstrain (με)**	**Δ με**	**Gage**	**Frequency (Hz)**	**Microstrain (με)**	**Δ με**
1	602.0	1472.085	-27.915	9	1029	4301.012	-198.988
2	556.6	1258.422	-241.578	10	1057	4538.265	38.265
3	578.8	1360.808	-139.192	11	1056	4529.682	29.682
4	564.8	1295.774	-204.226	12	1038	4376.578	-123.422
5	496.1	999.720	-500.280	13	1061	4572.679	72.679
6	525.4	1121.295	-378.705	14	1066	4615.878	115.878
7	482.8	946.835	-553.165	15	1079	4729.147	229.147
8	470.1	897.678	-602.322	16	1041	4401.912	-98.088

Pile #2

Tension				Compression			
Gage	**Frequency (Hz)**	**Microstrain (με)**	**Δ με**	**Gage**	**Frequency (Hz)**	**Microstrain (με)**	**Δ με**
17	575.7	1346.271	-153.729	25	1042	4410.373	-89.627
18	578.7	1360.338	-139.662	26	1064	4598.574	98.574
19	561.2	1279.308	-220.692	27			
20	661.6	1777.997	277.997	28	1039	4385.014	-114.986
21	582.0	1375.897	-124.103	29	1059	4555.456	55.456
22	490.5	977.278	-522.722	30	1065	4607.222	107.222
23	534.8	1161.777	-338.223	31	1083	4764.275	264.275
24	475.0	916.489	-583.511	32	1060	4564.063	64.063

Pile #3

Compression				Tension			
Gage	**Frequency (Hz)**	**Microstrain (με)**	**Δ με**	**Gage**	**Frequency (Hz)**	**Microstrain (με)**	**Δ με**
33	1034.0	4342.912	-157.088	41	617.5	1548.866	48.866
34	1060.0	4564.063	64.063	42	584.2	1386.319	-113.681
35	1026.0	4275.970	-224.030	43	639.7	1662.236	162.236
36	1008.0	4127.252	-372.748	44	658.0	1758.700	258.700
37	1029.0	4301.012	-198.988	45	593.9	1432.737	-67.263
38	1032.0	4326.127	-173.873	46	627.3	1598.418	98.418
39	1050.0	4478.355	-21.645	47	691.2	1940.651	440.651
40	1025.0	4267.639	-232.361	48	612.3	1522.890	22.890

Pile #4

Compression				Tension			
Gage	**Frequency (Hz)**	**Microstrain (με)**	**Δ με**	**Gage**	**Frequency (Hz)**	**Microstrain (με)**	**Δ με**
49	1077	4711.632	211.632	57	591.4	1420.701	-79.299
50				58	649.9	1715.667	215.667
51				59	705.4	2021.207	521.207
52				60	538.8	1179.221	-320.779
53	1032	4326.127	-173.873	61	764.4	2373.456	873.456
54	1017	4201.282	-298.718	62	731.7	2174.733	674.733
55	1136	5241.995	741.995	63	594.7	1436.600	-63.400
56				64	518.2	1090.774	-409.226

Table C.4 - Strain after 8 foot excavation - Statesville

Pile #1

Tension				Compression			
Gage	**Frequency (Hz)**	**Microstrain (με)**	**Δ με**	**Gage**	**Frequency (Hz)**	**Microstrain (με)**	**Δ με**
1	599.8	1461.345	-38.655	9	1029	4301.012	-198.988
2	562.9	1287.071	-212.929	10	1053	4503.982	3.982
3	608.1	1502.069	2.069	11	1050	4478.355	-21.645
4	578.7	1360.338	-139.662	12	1037	4368.149	-131.851
5	504.2	1032.632	-467.368	13	1062	4581.302	81.302
6	528.8	1135.855	-364.145	14	1068	4633.215	133.215
7	485.9	959.033	-540.967	15	1080	4737.917	237.917
8	472.2	905.716	-594.284	16	1042	4410.373	-89.627

Pile #2

Tension				Compression			
Gage	**Frequency (Hz)**	**Microstrain (με)**	**Δ με**	**Gage**	**Frequency (Hz)**	**Microstrain (με)**	**Δ με**
17	579.0	1361.749	-138.251	25	1040	4393.459	-106.541
18	582.5	1378.262	-121.738	26	1064	4598.574	98.574
19	549.5	1226.522	-273.478	27			
20	669.8	1822.343	322.343	28	1036	4359.728	-140.272
21	591.8	1422.623	-77.377	29	1055	4521.108	21.108
22	496.7	1002.140	-497.860	30	1065	4607.222	107.222
23	538.4	1177.470	-322.530	31	1084	4773.077	273.077
24	479.1	932.379	-567.621	32	1060	4564.063	64.063

Pile #3

Compression				Tension			
Gage	**Frequency (Hz)**	**Microstrain (με)**	**Δ με**	**Gage**	**Frequency (Hz)**	**Microstrain (με)**	**Δ με**
33	1031.0	4317.748	-182.252	41	607.7	1500.094	0.094
34	1060.0	4564.063	64.063	42	584.6	1388.218	-111.782
35	1028.0	4292.657	-207.343	43	629.0	1607.094	107.094
36	1007.0	4119.067	-380.933	44	664.8	1795.238	295.238
37	1024.0	4259.316	-240.684	45	609.0	1506.519	6.519
38	1030.0	4309.376	-190.624	46	632.7	1626.056	126.056
39	1029.0	4301.012	-198.988	47	691.3	1941.212	441.212
40	1025.0	4267.639	-232.361	48	612.2	1522.392	22.392

Pile #4

Compression				Tension			
Gage	**Frequency (Hz)**	**Microstrain (με)**	**Δ με**	**Gage**	**Frequency (Hz)**	**Microstrain (με)**	**Δ με**
49	1074	4685.420	185.420	57	588.3	1405.846	-94.154
50				58	648.0	1705.650	205.650
51				59	697.3	1975.055	475.055
52				60	552.3	1239.053	-260.947
53	1026	4275.970	-224.030	61	771.5	2417.752	917.752
54	1014	4176.532	-323.468	62	732.8	2181.277	681.277
55	1136	5241.995	741.995	63	595.1	1438.533	-61.467
56				64	518.7	1092.880	-407.120

Table C.5 - Strain after 12 foot excavation - Statesville

Pile #1

Tension				Compression			
Gage	**Frequency (Hz)**	**Microstrain (με)**	**Δ με**	**Gage**	**Frequency (Hz)**	**Microstrain (με)**	**Δ με**
1	598.0	1452.587	-47.413	9	1032	4326.127	-173.873
2	566.5	1303.586	-196.414	10	1056	4529.682	29.682
3	591.4	1420.701	-79.299	11	1052	4495.432	-4.568
4	610.6	1514.445	14.445	12	1025	4267.639	-232.361
5	536.3	1168.303	-331.697	13	1054	4512.541	12.541
6	540.9	1188.431	-311.569	14	1068	4633.215	133.215
7	494.4	992.880	-507.120	15	1083	4764.275	264.275
8	478.1	928.490	-571.510	16	1043	4418.843	-81.157

Pile #2

Tension				Compression			
Gage	**Frequency (Hz)**	**Microstrain (με)**	**Δ με**	**Gage**	**Frequency (Hz)**	**Microstrain (με)**	**Δ με**
17	577.4	1354.233	-145.767	25	1041	4401.912	-98.088
18	586.4	1396.779	-103.221	26	1064	4598.574	98.574
19	554.1	1247.143	-252.857	27			
20	658.1	1759.234	259.234	28	1038	4376.578	-123.422
21	610.6	1514.445	14.445	29	1047	4452.801	-47.199
22	522.5	1108.951	-391.049	30	1055	4521.108	21.108
23	554.0	1246.693	-253.307	31	1081	4746.695	246.695
24	489.2	972.104	-527.896	32	1060	4564.063	64.063

Pile #3

Compression				Tension			
Gage	**Frequency (Hz)**	**Microstrain (με)**	**Δ με**	**Gage**	**Frequency (Hz)**	**Microstrain (με)**	**Δ με**
33	1030.0	4309.376	-190.624	41	605.4	1488.760	-11.240
34	1059.0	4555.456	55.456	42	585.9	1394.399	-105.601
35	1031.0	4317.748	-182.252	43	627.0	1596.890	96.890
36	1017.0	4201.282	-298.718	44	639.7	1662.236	162.236
37	1023.0	4251.001	-248.999	45	609.9	1510.975	10.975
38	1018.0	4209.548	-290.452	46	668.1	1813.105	313.105
39	1022.0	4242.694	-257.306	47	706.6	2028.090	528.090
40	1024.0	4259.316	-240.684	48	612.9	1525.876	25.876

Pile #4

Compression				Tension			
Gage	**Frequency (Hz)**	**Microstrain (με)**	**Δ με**	**Gage**	**Frequency (Hz)**	**Microstrain (με)**	**Δ με**
49	1073	4676.698	176.698	57	582.8	1379.682	-120.318
50				58	646.5	1697.763	197.763
51				59	704.5	2016.053	516.053
52				60	549.4	1226.076	-273.924
53	1020	4226.105	-273.895	61	780.7	2475.758	975.758
54	999	4053.880	-446.120	62	746.5	2263.599	763.599
55	1129	5177.592	677.592	63	601.8	1471.107	-28.893
56				64	519.9	1097.942	-402.058

Table C.6 - Strain after 16 foot excavation - Statesville

Pile #1

Tension				Compression			
Gage	**Frequency (Hz)**	**Microstrain (με)**	**Δ με**	**Gage**	**Frequency (Hz)**	**Microstrain (με)**	**Δ με**
1	594.4	1435.151	-64.849	9	1035	4351.316	-148.684
2	562.4	1284.785	-215.215	10	1061	4572.679	72.679
3	584.5	1387.743	-112.257	11	1057	4538.265	38.265
4	603.5	1479.430	-20.570	12	1027	4284.309	-215.691
5	578.7	1360.338	-139.662	13	1041	4401.912	-98.088
6	567.6	1308.654	-191.346	14	1062	4581.302	81.302
7	513.9	1072.747	-427.253	15	1083	4764.275	264.275
8	487.0	963.380	-536.620	16	1046	4444.299	-55.701

Pile #2

Tension				Compression			
Gage	**Frequency (Hz)**	**Microstrain (με)**	**Δ με**	**Gage**	**Frequency (Hz)**	**Microstrain (με)**	**Δ με**
17	573.9	1337.865	-162.135	25	1043	4418.843	-81.157
18	581.2	1372.117	-127.883	26	1065	4607.222	107.222
19	548.9	1223.845	-276.155	27			
20	658.2	1759.769	259.769	28	1038	4376.578	-123.422
21	595.8	1441.919	-58.081	29	1048	4461.311	-38.689
22	556.6	1258.422	-241.578	30	1042	4410.373	-89.627
23	595.5	1440.467	-59.533	31	1065	4607.222	107.222
24	507.8	1047.431	-452.569	32	1054	4512.541	12.541

Pile #3

Compression				Tension			
Gage	**Frequency (Hz)**	**Microstrain (με)**	**Δ με**	**Gage**	**Frequency (Hz)**	**Microstrain (με)**	**Δ με**
33	1031.0	4317.748	-182.252	41	604.7	1485.319	-14.681
34	1059.0	4555.456	55.456	42	585.3	1391.544	-108.456
35	1030.0	4309.376	-190.624	43	626.4	1593.835	93.835
36	1019.0	4217.822	-282.178	44	634.9	1637.384	137.384
37	1035.0	4351.316	-148.684	45	591.1	1419.260	-80.740
38	1031.0	4317.748	-182.252	46	659.4	1766.192	266.192
39	1022.0	4242.694	-257.306	47	736.0	2200.369	700.369
40	1019.0	4217.822	-282.178	48	628.0	1601.988	101.988

Pile #4

Compression				Tension			
Gage	**Frequency (Hz)**	**Microstrain (με)**	**Δ με**	**Gage**	**Frequency (Hz)**	**Microstrain (με)**	**Δ με**
49	1076	4702.886	202.886	57	578.8	1360.808	-139.192
50				58	645.7	1693.564	193.564
51				59	701.0	1996.071	496.071
52				60	548.7	1222.953	-277.047
53	1030	4309.376	-190.624	61	769.1	2402.733	902.733
54	1002	4078.264	-421.736	62	742.7	2240.613	740.613
55	1119	5086.278	586.278	63	613.2	1527.370	27.370
56				64	530.4	1142.739	-357.261

Table C.7 - Strain after 20 foot excavation - Statesville

Pile #1

Tension				Compression			
Gage	**Frequency (Hz)**	**Microstrain (με)**	**Δ με**	**Gage**	**Frequency (Hz)**	**Microstrain (με)**	**Δ με**
1	595.5	1440.467	-59.533	9	1041	4401.912	-98.088
2	565.4	1298.529	-201.471	10	1068	4633.215	133.215
3	581.8	1374.951	-125.049	11	1065	4607.222	107.222
4	601.3	1468.664	-31.336	12	1033	4334.516	-165.484
5	581.4	1373.061	-126.939	13	1042	4410.373	-89.627
6	596.5	1445.309	-54.691	14	1047	4452.801	-47.199
7	544.3	1203.418	-296.582	15	1173	5589.024	1089.024
8	500.1	1015.906	-484.094	16	1045	4435.806	-64.194

Pile #2

Tension				Compression			
Gage	**Frequency (Hz)**	**Microstrain (με)**	**Δ με**	**Gage**	**Frequency (Hz)**	**Microstrain (με)**	**Δ με**
17	570.4	1321.597	-178.403	25	1045	4435.806	-64.194
18	578.3	1358.458	-141.542	26	1069	4641.895	141.895
19	545.9	1210.504	-289.496	27			
20	651.6	1724.654	224.654	28	1043	4418.843	-81.157
21	591.9	1423.104	-76.896	29	1052	4495.432	-4.568
22	543.7	1200.767	-299.233	30	1046	4444.299	-55.701
23	612.9	1525.876	25.876	31	1057	4538.265	38.265
24	531.9	1149.211	-350.789	32	1047	4452.801	-47.199

Pile #3

Compression				Tension			
Gage	**Frequency (Hz)**	**Microstrain (με)**	**Δ με**	**Gage**	**Frequency (Hz)**	**Microstrain (με)**	**Δ με**
33	1034.0	4342.912	-157.088	41	615.1	1536.850	36.850
34	1061.0	4572.679	72.679	42	585.9	1394.399	-105.601
35	1032.0	4326.127	-173.873	43	628.8	1606.072	106.072
36	1023.0	4251.001	-248.999	44	629.1	1607.605	107.605
37	1045.0	4435.806	-64.194	45	578.4	1358.928	-141.072
38	1056.0	4529.682	29.682	46	626.9	1596.381	96.381
39	1047.0	4452.801	-47.199	47	700.9	1995.501	495.501
40	1022.0	4242.694	-257.306	48	645.6	1693.039	193.039

Pile #4

Compression				Tension			
Gage	**Frequency (Hz)**	**Microstrain (με)**	**Δ με**	**Gage**	**Frequency (Hz)**	**Microstrain (με)**	**Δ με**
49	1078	4720.385	220.385	57	581.4	1373.061	-126.939
50				58	644.0	1684.658	184.658
51				59	699.5	1987.538	487.538
52				60	546.9	1214.943	-285.057
53	1039	4385.014	-114.986	61	761.3	2354.245	854.245
54	1030	4309.376	-190.624	62	708.0	2036.134	536.134
55	1140	5278.975	778.975	63	576.6	1350.483	-149.517
56				64	534.0	1158.304	-341.696

Table C.8 - Strain gage set data - Monroe

Pile #1 (SE)

Tension				Compression			
Gage	Frequency (Hz)	Microstrain (με)	Δ με (set)	Gage	Frequency (Hz)	Microstrain (με)	Δ με (set)
1		1500.000	0.000	9		4500.000	0.000
65		1500.000	0.000	72			
2		1500.000	0.000	10		4500.000	0.000
66		1500.000	0.000	73		4500.000	0.000
3		1500.000	0.000	11		4500.000	0.000
67		1500.000	0.000	74		4500.000	0.000
4		1500.000	0.000	12		4500.000	0.000
68		1500.000	0.000	75		4500.000	0.000
5				13		4500.000	0.000
69		1500.000	0.000	76		4500.000	0.000
6		1500.000	0.000	14		4500.000	0.000
70				77		4500.000	0.000
7		1500.000	0.000	15		4500.000	0.000
71		1500.000	0.000	78		4500.000	0.000
8		1500.000	0.000	16		4500.000	0.000

Pile #2 (NE)

Tension				Compression			
Gage	Frequency (Hz)	Microstrain (με)	Δ με (set)	Gage	Frequency (Hz)	Microstrain (με)	Δ με (set)
17		1500.000	0.000	25		4500.000	0.000
79		1500.000	0.000	86		4500.000	0.000
18		1500.000	0.000	26		4500.000	0.000
80		1500.000	0.000	87		4500.000	0.000
19		1500.000	0.000	27		4500.000	0.000
81		1500.000	0.000	88		4500.000	0.000
20		1500.000	0.000	28		4500.000	0.000
82				89		4500.000	0.000
21				29			
83		1500.000	0.000	90		4500.000	0.000
22		1500.000	0.000	30		4500.000	0.000
84		1500.000	0.000	91		4500.000	0.000
23		1500.000	0.000	31		4500.000	0.000
85		1500.000	0.000	92		4500.000	0.000
24		1500.000	0.000	32		4500.000	0.000

Pile #3 (SW)

Compression				Tension			
Gage	Frequency (Hz)	Microstrain (με)	Δ με (set)	Gage	Frequency (Hz)	Microstrain (με)	Δ με (set)
33		4500.000	0.000	41		1500.000	0.000
93		4500.000	0.000	100		1500.000	0.000
34		4500.000	0.000	42			
94		4500.000	0.000	101		1500.000	0.000
35		4500.000	0.000	43		1500.000	0.000
95		4500.000	0.000	102		1500.000	0.000
36		4500.000	0.000	44		1500.000	0.000
96		4500.000	0.000	103		1500.000	0.000
37		4500.000	0.000	45		1500.000	0.000
97		4500.000	0.000	104		1500.000	0.000
38		4500.000	0.000	46		1500.000	0.000
98		4500.000	0.000	105		1500.000	0.000
39		4500.000	0.000	47		1500.000	0.000
99		4500.000	0.000	106		1500.000	0.000
40				48		1500.000	0.000

Pile #4 (NW)

Compression				Tension			
Gage	Frequency (Hz)	Microstrain (με)	Δ με (set)	Gage	Frequency (Hz)	Microstrain (με)	Δ με (set)
49		4500.000	0.000	57		1500.000	0.000
107				114			
50				58		1500.000	0.000
108		4500.000	0.000	115			
51				59		1500.000	0.000
109		4500.000	0.000	116		1500.000	0.000
52				60		1500.000	0.000
110		4500.000	0.000	117		1500.000	0.000
53		4500.000	0.000	61			
111		4500.000	0.000	118		1500.000	0.000
54		4500.000	0.000	62			
112		4500.000	0.000	119		1500.000	0.000
55		4500.000	0.000	63		1500.000	0.000
113		4500.000	0.000	120		1500.000	0.000
56		4500.000	0.000	64		1500.000	0.000

Table C.9 - Post driving strain readings - Monroe

Pile #1 (SE)

Tension				Compression			
Gage	Frequency (Hz)	Microstrain (με)	Δ με (set)	Gage	Frequency (Hz)	Microstrain (με)	Δ με (set)
1	605.9	1491.220	-8.780	9	1022	4242.694	-257.306
65	610.2	1512.461	12.461	72			
2	585.4	1392.020	-107.980	10	1046	4444.299	-55.701
66	650.6	1719.365	219.365	73	1055	4521.108	21.108
3	588.2	1405.368	-94.632	11	1041	4401.912	-98.088
67	659.4	1766.192	266.192	74	1036	4359.728	-140.272
4	542.2	1194.150	-305.850	12	1027	4284.309	-215.691
68	579.1	1362.219	-137.781	75	1047	4452.801	-47.199
5				13	1026	4275.970	-224.030
69	581.2	1372.117	-127.883	76	1053	4503.982	3.982
6	585.9	1394.399	-105.601	14	1033	4334.516	-165.484
70				77	1044	4427.320	-72.680
7	608.4	1503.552	3.552	15	1048	4461.311	-38.689
71	677.6	1865.034	365.034	78	1040	4393.459	-106.541
8	624.0	1581.645	81.645	16	1032	4326.127	-173.873

Pile #2 (NE)

Tension				Compression			
Gage	Frequency (Hz)	Microstrain (με)	Δ με (set)	Gage	Frequency (Hz)	Microstrain (με)	Δ με (set)
17	528.3	1133.708	-366.292	25	1015	4184.774	-315.226
79	620.7	1564.961	64.961	86	1070	4650.584	150.584
18	616.4	1543.353	43.353	26	1064	4598.574	98.574
80	598.9	1456.963	-43.037	87	1041	4401.912	-98.088
19	613.4	1528.366	28.366	27	1002	4078.264	-421.736
81	522.2	1107.678	-392.322	88	1061	4572.679	72.679
20	521.0	1102.593	-397.407	28	1001	4070.128	-429.872
82				89	1019	4217.822	-282.178
21				29			
83	613.1	1526.872	26.872	90	1018	4209.548	-290.452
22	536.8	1170.483	-329.517	30	1023	4251.001	-248.999
84	674.0	1845.269	345.269	91	1060	4564.063	64.063
23	637.6	1651.340	151.340	31	1079	4729.147	229.147
85	663.8	1789.841	289.841	92	1038	4376.578	-123.422
24	584.3	1386.793	-113.207	32	1026	4275.970	-224.030

Pile #3 (SW)

Compression				Tension			
Gage	Frequency (Hz)	Microstrain (με)	Δ με (set)	Gage	Frequency (Hz)	Microstrain (με)	Δ με (set)
33	1034	4342.912	-157.088	41	601.4	1469.152	-30.848
93	1037	4368.149	-131.851	100	636.5	1645.647	145.647
34	1053	4503.982	3.982	42			
94	998	4045.768	-454.232	101	611.5	1518.913	18.913
35	999	4053.880	-446.120	43	662.8	1784.452	284.452
95	1010	4143.646	-356.354	102	649.1	1711.446	211.446
36	1015	4184.774	-315.226	44	599.0	1457.450	-42.550
96	1024	4259.316	-240.684	103	690.7	1937.844	437.844
37	1039	4385.014	-114.986	45	583.7	1383.947	-116.053
97	1070	4650.584	150.584	104	662.4	1782.299	282.299
38	1057	4538.265	38.265	46	571.1	1324.842	-175.158
98	1043	4418.843	-81.157	105	641.3	1670.561	170.561
39	1077	4711.632	211.632	47	699.2	1985.833	485.833
99	1052	4495.432	-4.568	106	656.4	1750.157	250.157
40				48	626.0	1591.800	91.800

Pile #4 (NW)

Compression				Tension			
Gage	Frequency (Hz)	Microstrain (με)	Δ με (set)	Gage	Frequency (Hz)	Microstrain (με)	Δ με (set)
49	1054	4512.541	12.541	57	562.9	1287.071	-212.929
107				114			
50				58	673.3	1841.438	341.438
108	1017	4201.282	-298.718	115			
51				59	722.4	2119.802	619.802
109	999	4053.880	-446.120	116	693.2	1951.898	451.898
52				60	723.8	2128.027	628.027
110	998	4045.768	-454.232	117	710.6	2051.116	551.116
53	1010	4143.646	-356.354	61			
111	1005	4102.722	-397.278	118	717.9	2093.475	593.475
54	1015	4184.774	-315.226	62			
112	1019	4217.822	-282.178	119	700.9	1995.501	495.501
55	1066	4615.878	115.878	63	683.9	1899.875	399.875
113	1064	4598.574	98.574	120	662.2	1781.223	281.223
56	1042	4410.373	-89.627	64	721.6	2115.110	615.110

Table C.10 - Strain after 4 foot excavation - Monroe

Pile #1 (SE)

Tension				Compression			
Gage	Frequency (Hz)	Microstrain (με)	Δ με	Gage	Frequency (Hz)	Microstrain (με)	Δ με
1	609.7	1509.984	9.984	9	1024	4259.316	-240.684
65	608.6	1504.540	4.540	72			
2	584.6	1388.218	-111.782	10	1044	4427.320	-72.680
66	652.9	1731.543	231.543	73	1054	4512.541	12.541
3	590.0	1413.982	-86.018	11	1042	4410.373	-89.627
67	658.9	1763.514	263.514	74	1037	4368.149	-131.851
4	542.4	1195.031	-304.969	12	1027	4284.309	-215.691
68	579.6	1364.573	-135.427	75	1048	4461.311	-38.689
5				13	1027	4284.309	-215.691
69	582.3	1377.316	-122.684	76	1054	4512.541	12.541
6	586.6	1397.732	-102.268	14	1034	4342.912	-157.088
70				77	1045	4435.806	-64.194
7	608.3	1503.057	3.057	15	1049	4469.829	-30.171
71	677.8	1866.135	366.135	78	1041	4401.912	-98.088
8	624.3	1583.166	83.166	16	1033	4334.516	-165.484

Pile #2 (NE)

Tension				Compression			
Gage	Frequency (Hz)	Microstrain (με)	Δ με	Gage	Frequency (Hz)	Microstrain (με)	Δ με
17	527.6	1130.705	-369.295	25	1014	4176.532	-323.468
79	624.3	1583.166	83.166	86	1069	4641.895	141.895
18	618.1	1551.877	51.877	26	1065	4607.222	107.222
80	599.4	1459.397	-40.603	87	1042	4410.373	-89.627
19	614.2	1532.356	32.356	27	1004	4094.561	-405.439
81	523.2	1111.925	-388.075	88	1062	4581.302	81.302
20	521.1	1103.017	-396.983	28	1002	4078.264	-421.736
82				89	1020	4226.105	-273.895
21				29			
83	614.4	1533.354	33.354	90	1019	4217.822	-282.178
22	538.7	1178.783	-321.217	30	1024	4259.316	-240.684
84	675.4	1852.943	352.943	91	1060	4564.063	64.063
23	639.4	1660.677	160.677	31	1080	4737.917	237.917
85	665.1	1796.858	296.858	92	1039	4385.014	-114.986
24	585.7	1393.447	-106.553	32	1026	4275.970	-224.030

Pile #3 (SW)

Compression				Tension			
Gage	Frequency (Hz)	Microstrain (με)	Δ με	Gage	Frequency (Hz)	Microstrain (με)	Δ με
33	1034.0	4342.912	-157.088	41	604.4	1483.846	-16.154
93	1037.0	4368.149	-131.851	100	637.5	1650.822	150.822
34	1052.0	4495.432	-4.568	42			
94	998.0	4045.768	-454.232	101	610.9	1515.934	15.934
35	999.0	4053.880	-446.120	43	662.4	1782.299	282.299
95	1011.0	4151.856	-348.144	102	648.1	1706.177	206.177
36	1017.0	4201.282	-298.718	44	598.8	1456.477	-43.523
96	1025	4267.639	-232.361	103	691.0	1939.528	439.528
37	1040	4393.459	-106.541	45	583.6	1383.472	-116.528
97	1071	4659.281	159.281	104	663.1	1786.068	286.068
38	1057	4538.265	38.265	46	572.4	1330.881	-169.119
98	1044	4427.320	-72.680	105	642.5	1676.819	176.819
39	1078	4720.385	220.385	47	703.6	2010.905	510.905
99	1053	4503.982	3.982	106	657.8	1757.631	257.631
40				48	627.1	1597.399	97.399

Pile #4 (NW)

Compression				Tension			
Gage	Frequency (Hz)	Microstrain (με)	Δ με	Gage	Frequency (Hz)	Microstrain (με)	Δ με
49	1055	4521.108	21.108	57	564.4	1293.939	-206.061
107				114			
50				58	675.0	1850.749	350.749
108	1016	4193.024	-306.976	115			
51				59	723.2	2124.500	624.500
109	999	4053.880	-446.120	116	693.9	1955.842	455.842
52				60	724.6	2132.733	632.733
110	999	4053.880	-446.120	117	711.8	2058.050	558.050
53	1011	4151.856	-348.144	61			
111	1007	4119.067	-380.933	118	719.3	2101.648	601.648
54	1016	4193.024	-306.976	62			
112	1020	4226.105	-273.895	119	702.6	2005.193	505.193
55	1067	4624.542	124.542	63	685.7	1909.889	409.889
113	1065	4607.222	107.222	120	663.8	1789.841	289.841
56	1043	4418.843	-81.157	64	722.9	2122.738	622.738

Table C.11 - Strain after 8 foot excavation - Monroe

Pile #1 (SE)

Tension				Compression			
Gage	Frequency (Hz)	Microstrain (με)	Δ με	Gage	Frequency (Hz)	Microstrain (με)	Δ με
1	610.3	1512.957	12.957	9	1022	4242.694	-257.306
65	610.8	1515.437	15.437	72			
2	581.6	1374.006	-125.994	10	1047	4452.801	-47.199
66	638.2	1654.450	154.450	73	1057	4538.265	38.265
3	570.6	1322.524	-177.476	11	1045	4435.806	-64.194
67	631.5	1619.894	119.894	74	1036	4359.728	-140.272
4	536.0	1166.996	-333.004	12	1022	4242.694	-257.306
68	580.1	1366.928	-133.072	75	1044	4427.320	-72.680
5				13	1024	4259.316	-240.684
69	581.1	1371.645	-128.355	76	1052	4495.432	-4.568
6	584.2	1386.319	-113.681	14	1032	4326.127	-173.873
70				77	1044	4427.320	-72.680
7	605.3	1488.268	-11.732	15	1047	4452.801	-47.199
71	676.0	1856.237	356.237	78	1040	4393.459	-106.541
8	622.9	1576.074	76.074	16	1032	4326.127	-173.873

Pile #2 (NE)

Tension				Compression			
Gage	Frequency (Hz)	Microstrain (με)	Δ με	Gage	Frequency (Hz)	Microstrain (με)	Δ με
17	531.9	1149.211	-350.789	25	1013	4168.298	-331.702
79	628.2	1603.008	103.008	86	1068	4633.215	133.215
18	620.5	1563.952	63.952	26	1066	4615.878	115.878
80	600.5	1464.758	-35.242	87	1040	4393.459	-106.541
19	617.1	1546.860	46.860	27	1001	4070.128	-429.872
81	532.0	1149.643	-350.357	88	1058	4546.857	46.857
20	523.1	1111.500	-388.500	28	1001	4070.128	-429.872
82				89	1021	4234.395	-265.605
21				29			
83	613.8	1530.360	30.360	90	1020	4226.105	-273.895
22	537.0	1171.355	-328.645	30	1024	4259.316	-240.684
84	673.5	1842.532	342.532	91	1060	4564.063	64.063
23	638.5	1656.005	156.005	31	1080	4737.917	237.917
85	664.9	1795.778	295.778	92	1039	4385.014	-114.986
24	585.6	1392.971	-107.029	32	1026	4275.970	-224.030

Pile #3 (SW)

Compression				Tension			
Gage	Frequency (Hz)	Microstrain (με)	Δ με	Gage	Frequency (Hz)	Microstrain (με)	Δ με
33	1034	4342.912	-157.088	41	603.2	1477.960	-22.040
93	1037	4368.149	-131.851	100	635.4	1639.964	139.964
34	1056	4529.682	29.682	42			
94	1002	4078.264	-421.736	101	594.9	1437.566	-62.434
35	1002	4078.264	-421.736	43	654.6	1740.572	240.572
95	1010	4143.646	-356.354	102	645.6	1693.039	193.039
36	1015	4184.774	-315.226	44	599.8	1461.345	-38.655
96	1024	4259.316	-240.684	103	689.6	1931.677	431.677
37	1039	4385.014	-114.986	45	578.9	1361.279	-138.721
97	1070	4650.584	150.584	104	661.2	1775.847	275.847
38	1057	4538.265	38.265	46	571.1	1324.842	-175.158
98	1043	4418.843	-81.157	105	641.5	1671.603	171.603
39	1078	4720.385	220.385	47	700.3	1992.086	492.086
99	1053	4503.982	3.982	106	657.5	1756.028	256.028
40				48	627.0	1596.890	96.890

Pile #4 (NW)

Compression				Tension			
Gage	Frequency (Hz)	Microstrain (με)	Δ με	Gage	Frequency (Hz)	Microstrain (με)	Δ με
49	1054	4512.541	12.541	57	566.0	1301.286	-198.714
107				114			
50				58	672.9	1839.251	339.251
108	1014	4176.532	-323.468	115			
51				59	729.5	2161.676	661.676
109	993	4005.331	-494.669	116	698.5	1981.859	481.859
52				60	726.6	2144.523	644.523
110	997	4037.665	-462.335	117	712.3	2060.942	560.942
53	1010	4143.646	-356.354	61			
111	1007	4119.067	-380.933	118	718.9	2099.312	599.312
54	1017	4201.282	-298.718	62			
112	1020	4226.105	-273.895	119	702.5	2004.622	504.622
55	1068	4633.215	133.215	63	686.0	1911.561	411.561
113	1066	4615.878	115.878	120	664.1	1791.459	291.459
56	1043	4418.843	-81.157	64	723.4	2125.675	625.675

Table C.12 - Strain after 12 foot excavation - Monroe

Pile #1 (SE)

Tension				Compression			
Gage	Frequency (Hz)	Microstrain (με)	Δ με	Gage	Frequency (Hz)	Microstrain (με)	Δ με
1	605.7	1490.236	-9.764	9	1019	4217.822	-282.178
65	611.4	1518.416	18.416	72			
2	582.4	1377.789	-122.211	10	1045	4435.806	-64.194
66	639.2	1659.638	159.638	73	1057	4538.265	38.265
3	570.6	1322.524	-177.476	11	1046	4444.299	-55.701
67	631.3	1618.868	118.868	74	1036	4359.728	-140.272
4	536.2	1167.867	-332.133	12	1022	4242.694	-257.306
68	580.4	1368.342	-131.658	75	1044	4427.320	-72.680
5				13	1024	4259.316	-240.684
69	581.0	1371.173	-128.827	76	1052	4495.432	-4.568
6	584.1	1385.844	-114.156	14	1032	4326.127	-173.873
70				77	1044	4427.320	-72.680
7	605.1	1487.285	-12.715	15	1047	4452.801	-47.199
71	675.9	1855.687	355.687	78	1040	4393.459	-106.541
8	622.8	1575.568	75.568	16	1032	4326.127	-173.873

Pile #2 (NE)

Tension				Compression			
Gage	Frequency (Hz)	Microstrain (με)	Δ με	Gage	Frequency (Hz)	Microstrain (με)	Δ με
17	532.5	1151.805	-348.195	25	1012	4160.073	-339.927
79	629.3	1608.627	108.627	86	1069	4641.895	141.895
18	621.4	1568.492	68.492	26	1066	4615.878	115.878
80	602.7	1475.510	-24.490	87	1038	4376.578	-123.422
19	614.1	1531.857	31.857	27	998	4045.768	-454.232
81	538.6	1178.345	-321.655	88	1054	4512.541	12.541
20	525.9	1123.431	-376.569	28	998	4045.768	-454.232
82				89	1018	4209.548	-290.452
21				29			
83	613.2	1527.370	27.370	90	1019	4217.822	-282.178
22	535.5	1164.820	-335.180	30	1024	4259.316	-240.684
84	671.5	1831.606	331.606	91	1060	4564.063	64.063
23	637.4	1650.304	150.304	31	1080	4737.917	237.917
85	664.3	1792.538	292.538	92	1039	4385.014	-114.986
24	585.3	1391.544	-108.456	32	1026	4275.970	-224.030

Pile #3 (SW)

Compression				Tension			
Gage	Frequency (Hz)	Microstrain (με)	Δ με	Gage	Frequency (Hz)	Microstrain (με)	Δ με
33	1032	4326.127	-173.873	41	603.0	1476.980	-23.020
93	1037	4368.149	-131.851	100	635.9	1642.546	142.546
34	1056	4529.682	29.682	42			
94	1003	4086.409	-413.591	101	593.4	1430.326	-69.674
35	1003	4086.409	-413.591	43	653.5	1734.727	234.727
95	1010	4143.646	-356.354	102	645.2	1690.942	190.942
36	1015	4184.774	-315.226	44	599.8	1461.345	-38.655
96	1023	4251.001	-248.999	103	689.3	1929.996	429.996
37	1038	4376.578	-123.422	45	578.2	1357.989	-142.011
97	1070	4650.584	150.584	104	660.6	1772.626	272.626
38	1056	4529.682	29.682	46	570.5	1322.060	-177.940
98	1043	4418.843	-81.157	105	640.9	1668.478	168.478
39	1078	4720.385	220.385	47	699.8	1989.243	489.243
99	1053	4503.982	3.982	106	657.2	1754.426	254.426
40				48	626.8	1595.871	95.871

Pile #4 (NW)

Compression				Tension			
Gage	Frequency (Hz)	Microstrain (με)	Δ με	Gage	Frequency (Hz)	Microstrain (με)	Δ με
49	1052	4495.432	-4.568	57	563.2	1288.443	-211.557
107				114			
50				58	671.6	1832.151	332.151
108	1012	4160.073	-339.927	115			
51				59	733.7	2186.638	686.638
109	987	3957.074	-542.926	116	715.0	2076.596	576.596
52				60	739.3	2220.145	720.145
110	991	3989.213	-510.787	117	715.7	2080.664	580.664
53	1007	4119.067	-380.933	61			
111	1005	4102.722	-397.278	118	717.0	2088.230	588.230
54	1016	4193.024	-306.976	62			
112	1019	4217.822	-282.178	119	699.9	1989.811	489.811
55	1067	4624.542	124.542	63	683.9	1899.875	399.875
113	1065	4607.222	107.222	120	662.7	1783.914	283.914
56	1043	4418.843	-81.157	64	722.7	2121.563	621.563

Table C.13 - Strain after 16 foot excavation - Monroe

Pile #1 (SE)

Tension				Compression			
Gage	Frequency (Hz)	Microstrain (με)	Δ με	Gage	Frequency (Hz)	Microstrain (με)	Δ με
1	611.6	1519.410	19.410	9	1022	4242.694	-257.306
65	612.2	1522.392	22.392	72			
2	583.6	1383.472	-116.528	10	1048	4461.311	-38.689
66	638.3	1654.968	154.968	73	1061	4572.679	72.679
3	567.3	1307.271	-192.729	11	1051	4486.889	-13.111
67	609.8	1510.479	10.479	74	1044	4427.320	-72.680
4	508.9	1051.974	-448.026	12	1023	4251.001	-248.999
68	538.3	1177.033	-322.967	75	1043	4418.843	-81.157
5				13	1022	4242.694	-257.306
69	580.5	1368.814	-131.186	76	1048	4461.311	-38.689
6	575.9	1347.206	-152.794	14	1027	4284.309	-215.691
70				77	1039	4385.014	-114.986
7	601.2	1468.175	-31.825	15	1044	4427.320	-72.680
71	672.8	1838.704	338.704	78	1037	4368.149	-131.851
8	620.1	1561.937	61.937	16	1030	4309.376	-190.624

Pile #2 (NE)

Tension				Compression			
Gage	Frequency (Hz)	Microstrain (με)	Δ με	Gage	Frequency (Hz)	Microstrain (με)	Δ με
17	535.6	1165.255	-334.745	25	1014	4176.532	-323.468
79	628.3	1603.519	103.519	86	1070	4650.584	150.584
18	618.4	1553.384	53.384	26	1068	4633.215	133.215
80	602.6	1475.021	-24.979	87	1041	4401.912	-98.088
19	612.0	1521.398	21.398	27	1001	4070.128	-429.872
81	533.2	1154.836	-345.164	88	1054	4512.541	12.541
20	524.2	1116.179	-383.821	28	993	4005.331	-494.669
82				89	1010	4143.646	-356.354
21				29			
83	614.7	1534.851	34.851	90	1014	4176.532	-323.468
22	531.6	1147.915	-352.085	30	1021	4234.395	-265.605
84	669.6	1821.255	321.255	91	1058	4546.857	46.857
23	635.7	1641.513	141.513	31	1078	4720.385	220.385
85	663.2	1786.607	286.607	92	1038	4376.578	-123.422
24	584.3	1386.793	-113.207	32	1025	4267.639	-232.361

Pile #3 (SW)

Compression				Tension			
Gage	Frequency (Hz)	Microstrain (με)	Δ με	Gage	Frequency (Hz)	Microstrain (με)	Δ με
33	1034	4342.912	-157.088	41	605.7	1490.236	-9.764
93	1039	4385.014	-114.986	100	635.8	1642.030	142.030
34	1057	4538.265	38.265	42			
94	1007	4119.067	-380.933	101	588.6	1407.280	-92.720
35	1008	4127.252	-372.748	43	648.7	1709.337	209.337
95	1022	4242.694	-257.306	102	621.3	1567.988	67.988
36	1022	4242.694	-257.306	44	585.1	1390.593	-109.407
96	1019	4217.822	-282.178	103	698.5	1981.859	481.859
37	1032	4326.127	-173.873	45	575.7	1346.271	-153.729
97	1066	4615.878	115.878	104	654.6	1740.572	240.572
38	1053	4503.982	3.982	46	565.0	1296.692	-203.308
98	1040	4393.459	-106.541	105	636.7	1646.682	146.682
39	1076	4702.886	202.886	47	697.9	1978.456	478.456
99	1052	4495.432	-4.568	106	654.1	1737.914	237.914
40				48	624.3	1583.166	83.166

Pile #4 (NW)

Compression				Tension			
Gage	Frequency (Hz)	Microstrain (με)	Δ με	Gage	Frequency (Hz)	Microstrain (με)	Δ με
49	1054	4512.541	12.541	57	557.7	1263.401	-236.599
107				114			
50				58	665.9	1801.183	301.183
108	1017	4201.282	-298.718	115			
51				59	729.9	2164.047	664.047
109	986	3949.060	-550.940	116	710.1	2048.231	548.231
52				60	753.1	2303.802	803.802
110	985	3941.054	-558.946	117	747.2	2267.846	767.846
53	1004	4094.561	-405.439	61			
111	1003	4086.409	-413.591	118	719.0	2099.896	599.896
54	1015	4184.774	-315.226	62			
112	1019	4217.822	-282.178	119	699.6	1988.106	488.106
55	1068	4633.215	133.215	63	683.0	1894.878	394.878
113	1066	4615.878	115.878	120	661.8	1779.072	279.072
56	1044	4427.320	-72.680	64	722.3	2119.216	619.216

Table C.14 - Strain after 20 foot excavation - Monroe

Pile #1 (SE)

Tension				Compression			
Gage	Frequency (Hz)	Microstrain (με)	Δ με	Gage	Frequency (Hz)	Microstrain (με)	Δ με
1	611.1	1516.926	16.926	9	1021	4234.395	-265.605
65	614.1	1531.857	31.857	72			
2	585.1	1390.593	-109.407	10	1049	4469.829	-30.171
66	638.1	1653.931	153.931	73	1061	4572.679	72.679
3	565.7	1299.907	-200.093	11	1053	4503.982	3.982
67	610.3	1512.957	12.957	74	1047	4452.801	-47.199
4	504.4	1033.451	-466.549	12	1027	4284.309	-215.691
68	530.4	1142.739	-357.261	75	1047	4452.801	-47.199
5				13	1028	4292.657	-207.343
69	556.3	1257.066	-242.934	76	1051	4486.889	-13.111
6	567.9	1310.037	-189.963	14	1028	4292.657	-207.343
70				77	1037	4368.149	-131.851
7	598.4	1454.531	-45.469	15	1040	4393.459	-106.541
71	671.1	1829.424	329.424	78	1034	4342.912	-157.088
8	618.8	1555.394	55.394	16	1028	4292.657	-207.343

Pile #2 (NE)

Tension				Compression			
Gage	Frequency (Hz)	Microstrain (με)	Δ με	Gage	Frequency (Hz)	Microstrain (με)	Δ με
17	532.6	1152.238	-347.762	25	1014	4176.532	-323.468
79	626.6	1594.853	94.853	86	1070	4650.584	150.584
18	616.2	1542.351	42.351	26	1068	4633.215	133.215
80	600.5	1464.758	-35.242	87	1040	4393.459	-106.541
19	617.7	1549.869	49.869	27	1004	4094.561	-405.439
81	534.6	1160.908	-339.092	88	1056	4529.682	29.682
20	519.4	1095.832	-404.168	28	990	3981.166	-518.834
82				89	1011	4151.856	-348.144
21				29			
83	633.1	1628.113	128.113	90	1008	4127.252	-372.748
22	542.9	1197.236	-302.764	30	1018	4209.548	-290.452
84	667.1	1807.681	307.681	91	1057	4538.265	38.265
23	634.7	1636.353	136.353	31	1078	4720.385	220.385
85	662.9	1784.991	284.991	92	1037	4368.149	-131.851
24	584.1	1385.844	-114.156	32	1025	4267.639	-232.361

Pile #3 (SW)

Compression				Tension			
Gage	Frequency (Hz)	Microstrain (με)	Δ με	Gage	Frequency (Hz)	Microstrain (με)	Δ με
33	1034	4342.912	-157.088	41	603.0	1476.980	-23.020
93	1039	4385.014	-114.986	100	633.9	1632.230	132.230
34	1059	4555.456	55.456	42			
94	1008	4127.252	-372.748	101	585.8	1393.923	-106.077
35	1010	4143.646	-356.354	43	636.8	1647.199	147.199
95	1027	4284.309	-215.691	102	618.0	1551.375	51.375
36	1029	4301.012	-198.988	44	566.7	1304.507	-195.493
96	1030	4309.376	-190.624	103	682.3	1890.996	390.996
37	1031	4317.748	-182.252	45	571.1	1324.842	-175.158
97	1059	4555.456	55.456	104	660.0	1769.407	269.407
38	1048	4461.311	-38.689	46	560.2	1274.753	-225.247
98	1038	4376.578	-123.422	105	629.9	1611.696	111.696
39	1074	4685.420	185.420	47	691.6	1942.897	442.897
99	1050	4478.355	-21.645	106	650.4	1718.308	218.308
40				48	621.7	1570.007	70.007

Pile #4 (NW)

Compression				Tension			
Gage	Frequency (Hz)	Microstrain (με)	Δ με	Gage	Frequency (Hz)	Microstrain (με)	Δ με
49	1055	4521.108	21.108	57	552.4	1239.502	-260.498
107				114			
50				58	660.2	1770.480	270.480
108	1021	4234.395	-265.605	115			
51				59	721.8	2116.283	616.283
109	992	3997.268	-502.732	116	698.2	1980.157	480.157
52				60	753.2	2304.414	804.414
110	981	3909.110	-590.890	117	710.7	2051.694	551.694
53	1000	4062.000	-438.000	61			
111	999	4053.880	-446.120	118	719.7	2103.986	603.986
54	1013	4168.298	-331.702	62			
112	1019	4217.822	-282.178	119	696.0	1967.698	467.698
55	1067	4624.542	124.542	63	680.3	1879.926	379.926
113	1066	4615.878	115.878	120	659.8	1768.335	268.335
56	1044	4427.320	-72.680	64	721.0	2111.594	611.594

Table C.15 - Strain after 20 foot excavation and 8 foot surcharge - Monroe

Pile #1 (SE)

Tension				Compression			
Gage	Frequency (Hz)	Microstrain (με)	Δ με	Gage	Frequency (Hz)	Microstrain (με)	Δ με
1	611.1	1516.926	16.926	9	1021	4234.395	-265.605
65	614.1	1531.857	31.857	72			
2	585.1	1390.593	-109.407	10	1049	4469.829	-30.171
66	638.1	1653.931	153.931	73	1061	4572.679	72.679
3	565.7	1299.907	-200.093	11	1053	4503.982	3.982
67	610.3	1512.957	12.957	74	1047	4452.801	-47.199
4	504.4	1033.451	-466.549	12	1027	4284.309	-215.691
68	530.4	1142.739	-357.261	75	1047	4452.801	-47.199
5				13	1028	4292.657	-207.343
69	556.3	1257.066	-242.934	76	1051	4486.889	-13.111
6	567.9	1310.037	-189.963	14	1028	4292.657	-207.343
70				77	1037	4368.149	-131.851
7	598.4	1454.531	-45.469	15	1040	4393.459	-106.541
71	671.1	1829.424	329.424	78	1034	4342.912	-157.088
8	618.8	1555.394	55.394	16	1028	4292.657	-207.343

Pile #2 (NE)

Tension				Compression			
Gage	Frequency (Hz)	Microstrain (με)	Δ με	Gage	Frequency (Hz)	Microstrain (με)	Δ με
17	532.6	1152.238	-347.762	25	1014	4176.532	-323.468
79	626.6	1594.853	94.853	86	1070	4650.584	150.584
18	616.2	1542.351	42.351	26	1068	4633.215	133.215
80	600.5	1464.758	-35.242	87	1040	4393.459	-106.541
19	617.7	1549.869	49.869	27	1004	4094.561	-405.439
81	534.6	1160.908	-339.092	88	1056	4529.682	29.682
20	519.4	1095.832	-404.168	28	990	3981.166	-518.834
82				89	1011	4151.856	-348.144
21				29			
83	633.1	1628.113	128.113	90	1008	4127.252	-372.748
22	542.9	1197.236	-302.764	30	1018	4209.548	-290.452
84	667.1	1807.681	307.681	91	1057	4538.265	38.265
23	634.7	1636.353	136.353	31	1078	4720.385	220.385
85	662.9	1784.991	284.991	92	1037	4368.149	-131.851
24	584.1	1385.844	-114.156	32	1025	4267.639	-232.361

Pile #3 (SW)

Compression				Tension			
Gage	Frequency (Hz)	Microstrain (με)	Δ με	Gage	Frequency (Hz)	Microstrain (με)	Δ με
33	1034	4342.912	-157.088	41	602.5	1474.531	-25.469
93	1039	4385.014	-114.986	100	633.6	1630.686	130.686
34	1058	4546.857	46.857	42			
94	1008	4127.252	-372.748	101	585.5	1392.495	-107.505
35	1010	4143.646	-356.354	43	636.8	1647.199	147.199
95	1026	4275.970	-224.030	102	618.1	1551.877	51.877
36	1028	4292.657	-207.343	44	566.7	1304.507	-195.493
96	1029	4301.012	-198.988	103	682.2	1890.442	390.442
37	1030	4309.376	-190.624	45	570.8	1323.451	-176.549
97	1058	4546.857	46.857	104	659.5	1766.727	266.727
38	1048	4461.311	-38.689	46	559.4	1271.115	-228.885
98	1037	4368.149	-131.851	105	629.2	1608.116	108.116
39	1074	4685.420	185.420	47	691.3	1941.212	441.212
99	1049	4469.829	-30.171	106	649.6	1714.083	214.083
40				48	621.0	1566.474	66.474

Pile #4 (NW)

Compression				Tension			
Gage	Frequency (Hz)	Microstrain (με)	Δ με	Gage	Frequency (Hz)	Microstrain (με)	Δ με
49	1055	4521.108	21.108	57	552.7	1240.849	-259.151
107				114			
50				58	660.6	1772.626	272.626
108	1021	4234.395	-265.605	115			
51				59	721.4	2113.938	613.938
109	992	3997.268	-502.732	116	698.0	1979.023	479.023
52				60	753.1	2303.802	803.802
110	981	3909.110	-590.890	117	709.9	2047.077	547.077
53	999	4053.880	-446.120	61			
111	998	4045.768	-454.232	118	719.3	2101.648	601.648
54	1013	4168.298	-331.702	62			
112	1018	4209.548	-290.452	119	695.2	1963.177	463.177
55	1067	4624.542	124.542	63	679.3	1874.404	374.404
113	1065	4607.222	107.222	120	659.0	1764.049	264.049
56	1043	4418.843	-81.157	64	720.3	2107.496	607.496

APPENDIX D
INCLINOMETER DATA

Table D. 1 - NW inclinometer Statesville

Plot Coordinates for Inclinometer NW
Relative to initial reading on 6 Oct2005 at 1206

UNC Charlotte - J. Brian Anderson, Ph.D., P.E.

Printed 11-09-2005 at 18:02:53

skew = 135deg

	18	Oct-05	19	Oct-05	20	Oct-05		21-Oct-05		25-Oct-05		27-Oct-05
Depth	Cum X	Cum Y	Cum X	Cum Y	Cum X	Cum Y	Cum X	Cum Y	Cum X	Cum Y	Cum X	Cum Y
1	0.042	-0.033	0.174	0.02	0.401	0.035	0.643	-0.003	0.729	0.003	0.942	0.005
3	0.045	-0.035	0.16	0.016	0.365	0.032	0.59	-0.006	0.668	0.001	0.894	-0.011
5	0.041	-0.028	0.141	0.008	0.317	0.026	0.522	-0.007	0.587	0	0.818	-0.02
7	0.036	-0.022	0.12	0.006	0.266	0.02	0.446	-0.01	0.501	-0.003	0.726	-0.024
9	0.028	-0.02	0.093	0.003	0.219	0.017	0.381	-0.006	0.431	0.002	0.647	-0.02
11	0.023	-0.016	0.065	0.001	0.169	0.011	0.313	-0.005	0.359	0	0.564	-0.017
13	0.022	-0.014	0.044	-0.002	0.13	0.006	0.265	-0.002	0.307	0	0.496	-0.011
15	0.021	-0.014	0.029	-0.012	0.087	-0.006	0.215	-0.012	0.249	-0.012	0.431	-0.017
17	0.02	-0.014	0.022	-0.011	0.058	-0.008	0.172	-0.016	0.198	-0.016	0.374	-0.02
19	0.022	-0.013	0.019	-0.008	0.041	-0.006	0.121	-0.014	0.142	-0.014	0.317	-0.021
21	0.019	-0.011	0.014	-0.005	0.027	-0.003	0.074	-0.011	0.091	-0.011	0.246	-0.021
23	0.017	-0.011	0.011	-0.004	0.019	-0.002	0.042	-0.011	0.053	-0.01	0.157	-0.014
25	0.014	-0.008	0.008	-0.003	0.01	0	0.022	-0.01	0.028	-0.008	0.083	-0.009
27	0.008	-0.003	0.005	0	0.002	0.003	0.007	-0.006	0.014	-0.005	0.038	-0.006
29	0.005	-0.003	0.003	-0.001	-0.001	0.004	0.001	-0.002	0.006	-0.003	0.013	-0.001
31	0	0	0	0	0	0	0	0	0	0	0	0

Table D. 2 - SW inclinometer Statesville

Plot Coordinates for Inclinometer SW
Relative to initial reading on 4 Oct2005 at 1443

UNC Charlotte - J. Brian Anderson, Ph.D., P.E.

Printed 11-09-2005 at 18:19:29

skew = 135deg

Depth	10/18/2005 Cum X	10/18/2005 Cum Y	10/19/2005 Cum X	10/19/2005 Cum Y	10/20/2005 Cum X	10/20/2005 Cum Y	10/21/2005 Cum X	10/21/2005 Cum Y	10/21/2005 Cum X	10/21/2005 Cum Y	10/25/2005 Cum X	10/25/2005 Cum Y	10/27/2005 Cum X	10/27/2005 Cum Y
----(ft)-----	-----(in)-----	-----(in)-----	-----(in)-----	-----(in)-----	-----(in)-----	-----(in)-----	-----(in)-----	-----(in)-----	-----(in)-----	-----(in)-----	-----(in)-----	-----(in)-----	-----(in)-----	-----(in)-----
3	0.02	0.007	0.081	0.027	0.182	0.027	0.247	0.04	0.303	0.02	0.398	0.035	0.588	-0.005
5	0.014	0.006	0.071	0.022	0.165	0.026	0.231	0.042	0.283	0.024	0.367	0.038	0.55	0.019
7	0.01	0.006	0.054	0.017	0.143	0.024	0.209	0.045	0.261	0.028	0.336	0.041	0.518	0.034
9	0.008	0.006	0.034	0.016	0.119	0.022	0.188	0.044	0.241	0.029	0.307	0.039	0.496	0.04
11	0.007	0.006	0.021	0.012	0.093	0.016	0.169	0.04	0.22	0.025	0.28	0.03	0.484	0.034
13	0.008	0.006	0.015	0.008	0.064	0.011	0.151	0.032	0.2	0.017	0.256	0.018	0.475	0.025
15	0.008	0.003	0.011	0.006	0.043	0.01	0.123	0.026	0.172	0.008	0.223	0.01	0.458	0.015
17	0.007	0.003	0.01	0.005	0.027	0.007	0.081	0.028	0.119	0.009	0.165	0.01	0.411	0.014
19	0.005	0.004	0.009	0.004	0.018	0.006	0.047	0.025	0.067	0.011	0.108	0.013	0.333	0.016
21	0.004	0.005	0.006	0.003	0.012	0.003	0.029	0.022	0.037	0.008	0.075	0.008	0.247	0.019
23	0.004	0.007	0.009	0.001	0.011	0.003	0.02	0.016	0.021	0.008	0.059	0.001	0.17	0.014
25	0.003	0.006	0.008	0.001	0.008	0.003	0.012	0.015	0.015	0.004	0.045	-0.003	0.114	0.007
27	0.004	0.006	0.01	0	0.01	0.001	0.01	0.012	0.01	0.001	0.031	0	0.074	-0.001
29	0	0.006	0.007	0	0.008	0.002	0.009	0.007	0.004	-0.002	0.021	-0.002	0.043	-0.003
31	0	0.003	0.001	0.001	0.006	-0.001	0.005	0.003	-0.003	-0.003	0.011	-0.002	0.019	-0.002
33	0	0	0	0	0	0	0	0	0	0	0	0	0	0

Table D. 3 - NE inclinometer Statesville

Plot Coordinates for Inclinometer NE
Relative to initial reading on 4 Oct2005 at 1215

UNC Charlotte - J. Brian Anderson, Ph.D., P.E.

Printed 11-09-2005 at 18:11:55

skew = -45deg

Depth	10/18/2005 Cum X	10/18/2005 Cum Y	10/19/2005 Cum X	10/19/2005 Cum Y	10/20/2005 Cum X	10/20/2005 Cum Y	10/21/2005 Cum X	10/21/2005 Cum Y	10/25/2005 Cum X	10/25/2005 Cum Y	10/27/2005 Cum X	10/27/2005 Cum Y
----(ft)-----	-----(in)-----	-----(in)-----	-----(in)-----	-----(in)-----	-----(in)-----	-----(in)-----	-----(in)-----	-----(in)-----	-----(in)-----	-----(in)-----	-----(in)-----	-----(in)-----
1	0.062	0.003	0.319	-0.038	0.901	-0.118	1.628	-0.153	1.944	-0.155	3.288	-0.215
3	0.048	-0.004	0.28	-0.027	0.823	-0.105	1.485	-0.147	1.767	-0.15	3.019	-0.216
5	0.033	-0.006	0.227	-0.027	0.72	-0.098	1.318	-0.138	1.565	-0.141	2.731	-0.202
7	0.019	-0.006	0.177	-0.036	0.613	-0.106	1.143	-0.14	1.358	-0.139	2.434	-0.193
9	-0.001	-0.008	0.132	-0.038	0.504	-0.106	0.969	-0.136	1.152	-0.132	2.14	-0.18
11	-0.014	-0.007	0.079	-0.028	0.399	-0.092	0.808	-0.122	0.963	-0.119	1.867	-0.16
13	-0.02	-0.005	0.036	-0.023	0.327	-0.076	0.678	-0.111	0.807	-0.107	1.627	-0.139
15	-0.02	-0.002	-0.004	-0.007	0.241	-0.038	0.551	-0.065	0.656	-0.061	1.391	-0.086
17	-0.022	0.002	-0.019	0	0.148	-0.013	0.426	-0.028	0.505	-0.02	1.156	-0.042
19	-0.011	-0.004	-0.019	0.001	0.067	-0.008	0.305	-0.014	0.364	-0.008	0.928	-0.024
21	-0.007	-0.005	-0.015	0	0.023	-0.003	0.185	-0.014	0.226	-0.008	0.706	-0.018
23	-0.005	-0.003	-0.01	0.001	0.005	0.005	0.087	-0.011	0.115	-0.008	0.507	-0.015
25	-0.004	-0.002	-0.008	-0.001	0	0.007	0.035	-0.003	0.051	-0.002	0.332	-0.019
27	-0.002	-0.001	-0.006	0	-0.005	0.003	0.012	0.003	0.018	0.004	0.188	-0.016
29	-0.002	-0.001	-0.003	0	-0.004	0.002	0.003	0.006	0.004	0.006	0.087	-0.011
31	-0.001	0	-0.001	0	-0.002	0.001	0	0.004	0	0.005	0.031	-0.003
33	0	0	0	0	0	0	0	0	0	0	0	0

Table D. 4 - SE inclinometer Statesville

Plot Coordinates for Inclinometer SE
Relative to initial reading on 4 Oct2005 at 1454

UNC Charlotte - J. Brian Anderson, Ph.D., P.E.

Printed 11-11-2005 at 14:19:33

skew = -45deg

Depth	10/18/2005 Cum X	10/18/2005 Cum Y	10/19/2005 Cum X	10/19/2005 Cum Y	10/20/2005 Cum X	10/20/2005 Cum Y	10/20/2005 Cum X	10/20/2005 Cum Y	10/21/2005 Cum X	10/21/2005 Cum Y	10/21/2005 Cum X	10/21/2005 Cum Y	10/25/2005 Cum X	10/25/2005 Cum Y	10/27/2005 Cum X	10/27/2005 Cum Y
----(ft)-----	-----(in)-----	-----(in)-----	-----(in)-----	-----(in)-----	-----(in)-----	-----(in)-----	-----(in)-----	-----(in)-----	-----(in)-----	-----(in)-----	-----(in)-----	-----(in)-----	-----(in)-----	-----(in)-----	-----(in)-----	-----(in)-----
-8.2	0.163	0.063	0.37	0.057	1.056	0.484	1.045	0.372	1.456	0.548	1.745	0.664	1.985	0.79	3.805	1.191
-6.2	0.117	0.032	0.324	0.051	0.93	0.423	0.94	0.341	1.306	0.5	1.585	0.612	1.819	0.728	3.525	1.073
-4.2	0.073	0.022	0.279	0.046	0.803	0.365	0.838	0.299	1.165	0.445	1.441	0.547	1.655	0.663	3.241	0.966
-2.2	0.042	0.013	0.232	0.038	0.68	0.303	0.727	0.248	1.024	0.384	1.289	0.48	1.485	0.593	2.963	0.86
-0.2	0.024	0.013	0.192	0.029	0.556	0.239	0.613	0.192	0.878	0.311	1.135	0.403	1.302	0.51	2.679	0.751
1.8	0.015	0.012	0.148	0.022	0.435	0.182	0.497	0.135	0.735	0.241	0.98	0.325	1.127	0.429	2.395	0.639
3.8	0.003	0.011	0.112	0.012	0.343	0.124	0.399	0.087	0.608	0.178	0.833	0.252	0.964	0.331	2.14	0.536
5.8	-0.004	0.01	0.081	0.011	0.274	0.086	0.324	0.052	0.507	0.126	0.702	0.19	0.825	0.261	1.903	0.449
7.8	-0.005	0.003	0.043	0.003	0.22	0.063	0.262	0.035	0.419	0.087	0.583	0.139	0.69	0.199	1.667	0.364
9.8	-0.006	-0.001	0.012	-0.006	0.177	0.049	0.208	0.027	0.344	0.063	0.473	0.1	0.566	0.144	1.437	0.291
11.8	-0.005	-0.002	-0.006	-0.005	0.125	0.047	0.148	0.029	0.281	0.055	0.377	0.08	0.449	0.112	1.213	0.23
13.8	-0.006	-0.002	-0.013	-0.005	0.062	0.034	0.076	0.022	0.211	0.048	0.281	0.065	0.333	0.084	0.985	0.171
15.8	-0.006	-0.003	-0.013	-0.005	0.014	0.02	0.02	0.011	0.132	0.031	0.182	0.045	0.216	0.052	0.757	0.106
17.8	-0.006	-0.003	-0.011	-0.005	-0.003	0.012	-0.003	0.008	0.061	0.016	0.09	0.024	0.111	0.023	0.538	0.054
19.8	-0.003	-0.002	-0.007	-0.004	-0.007	0.007	-0.006	0.006	0.023	0.011	0.032	0.01	0.044	0.008	0.339	0.022
21.8	-0.002	-0.002	-0.003	-0.001	-0.005	0.004	-0.005	0.005	0.006	0.005	0.01	0.005	0.014	0.004	0.156	0.005
23.8	0	0	0	0	0	0	0	0	0	0	0	0	0	0	0	0

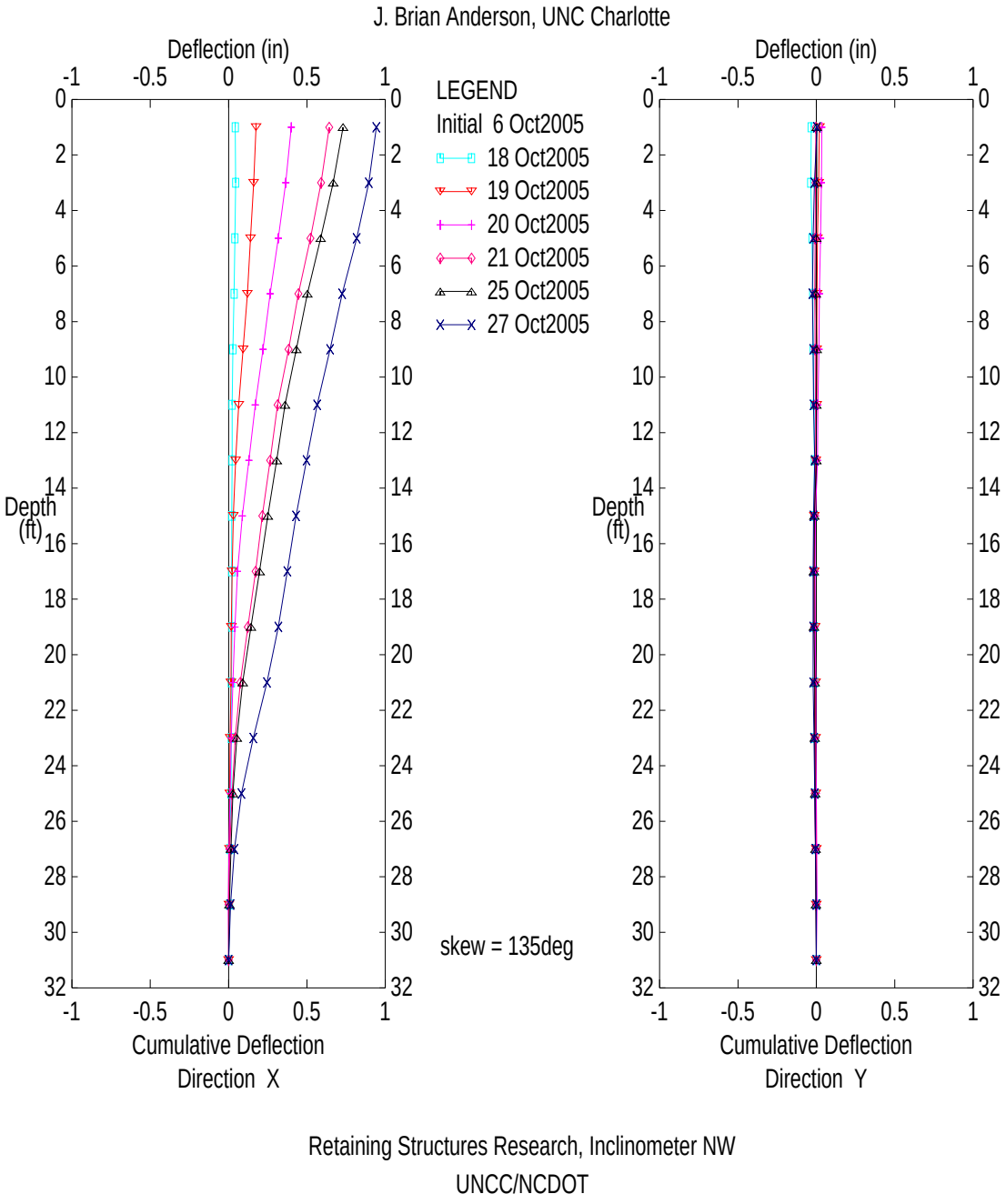

Figure D.1 - NW inclinometer Statesville

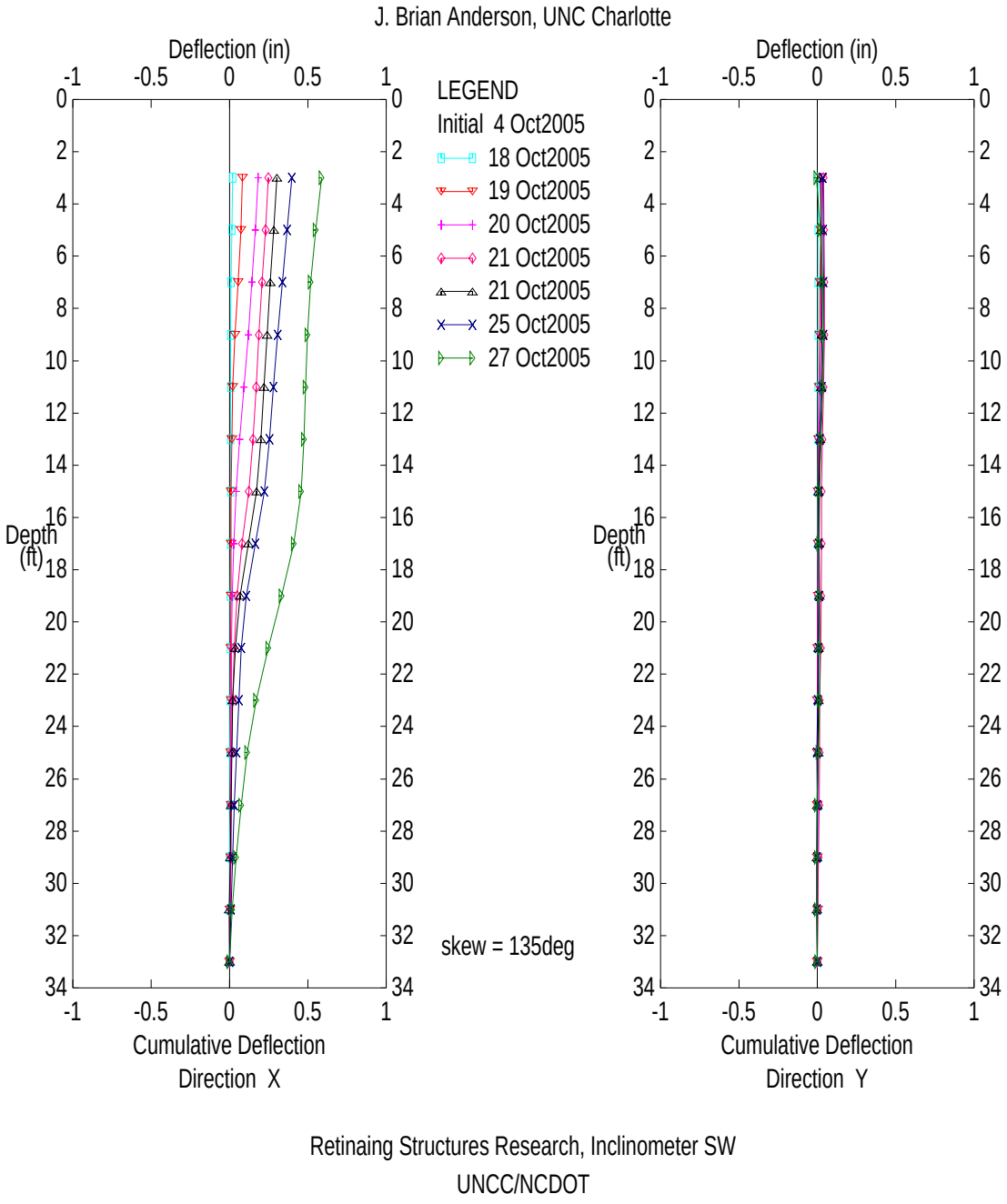

Figure D.2 - SW inclinometer Statesville

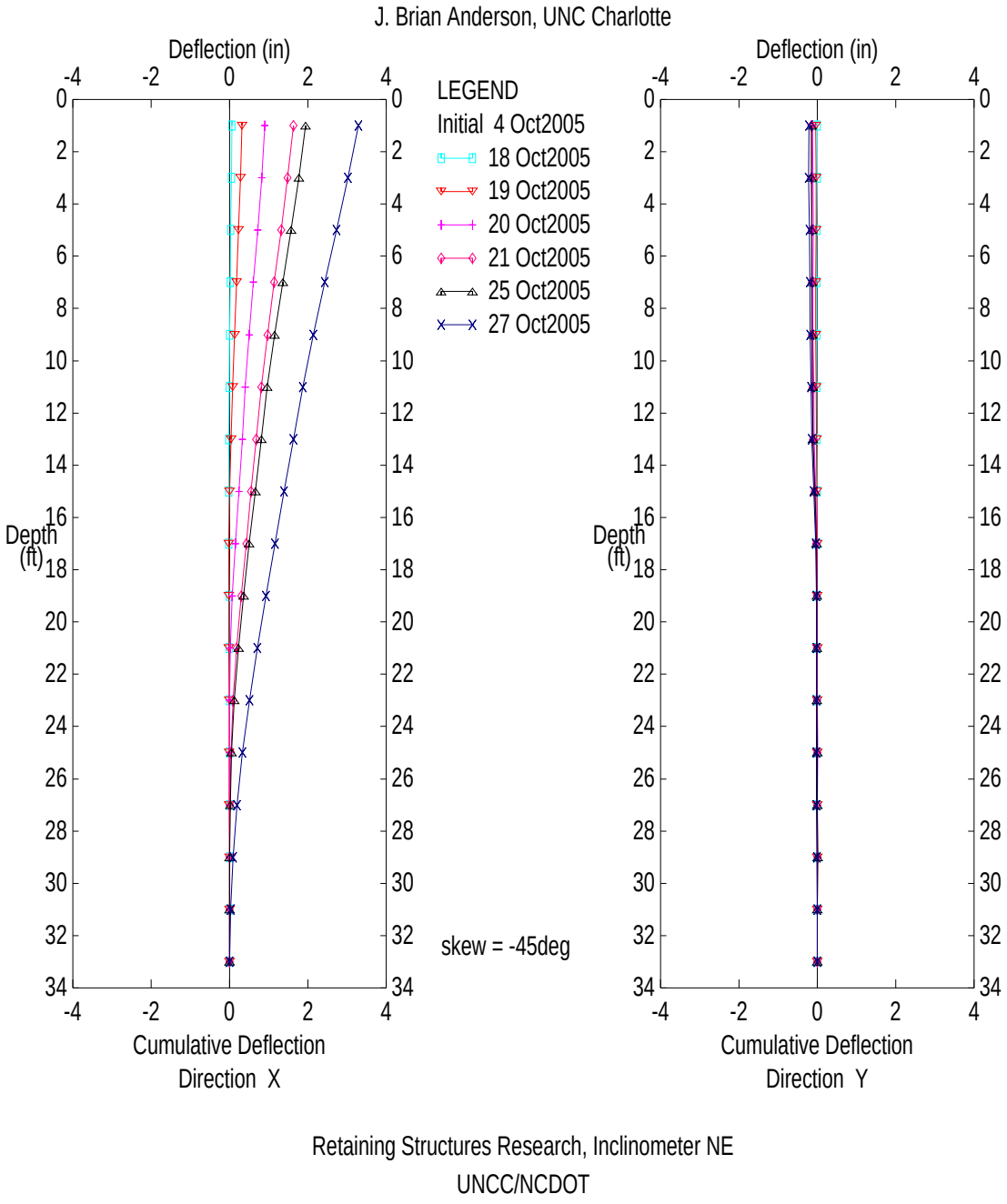

Figure D.3 - NE inclinometer Statesville

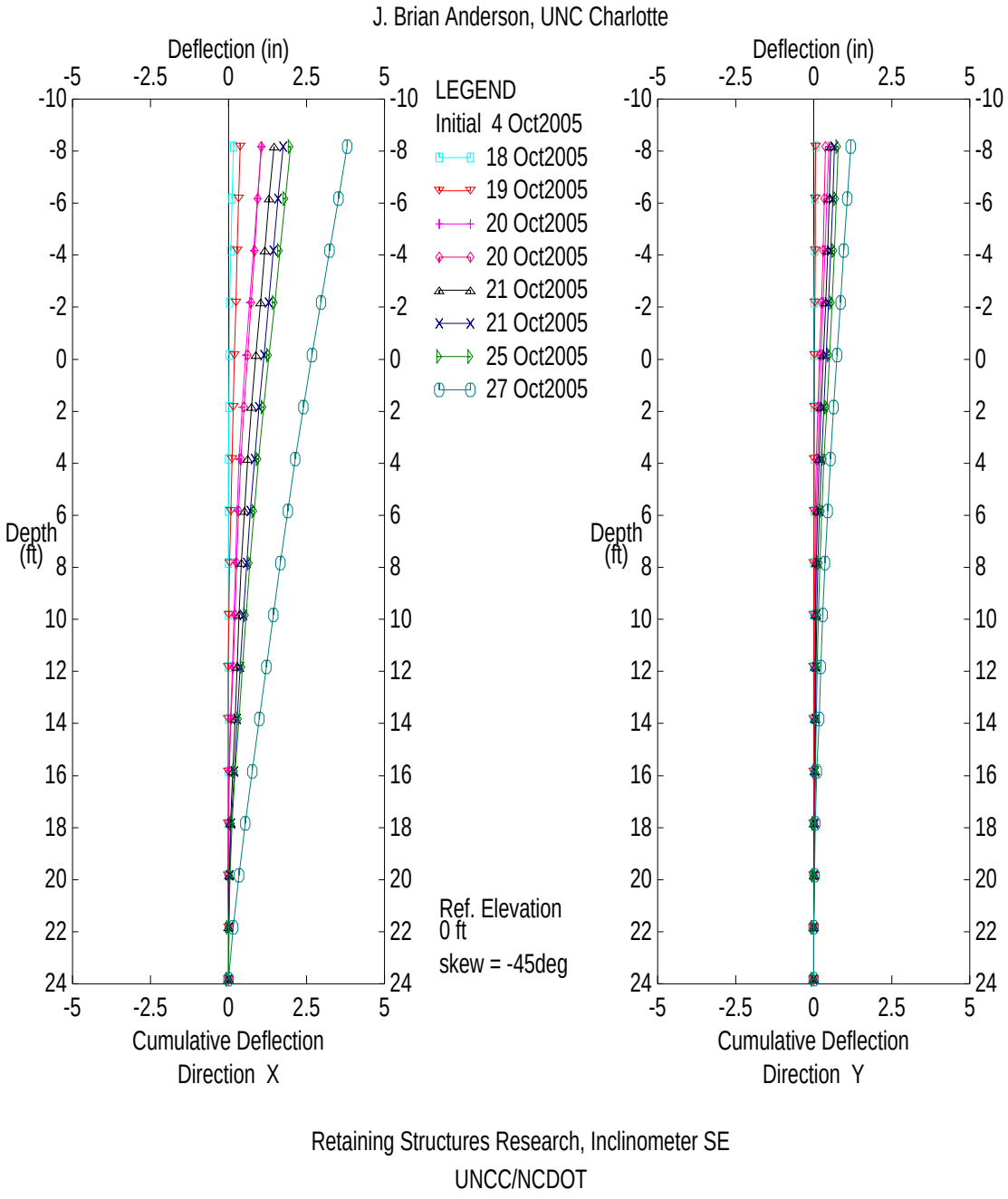

Figure D.4 - SE inclinometer Statesville

Table D. 5 - NW inclinometer Monroe

Plot Coordinates for Inclinometer NW
Relative to initial reading on 7 Dec2006 at 1421

J. Brian Anderson, UNC Charlotte

Printed 09-03-2007 at 17:01:18

skew = 135deg

Depth	12/11/2006 Cum X	12/11/2006 Cum Y	12/12/2006 Cum X	12/12/2006 Cum Y	12/12/2006 Cum X	12/12/2006 Cum Y	12/13/2006 Cum X	12/13/2006 Cum Y	12/14/2006 Cum X	12/14/2006 Cum Y	12/14/2006 Cum X	12/14/2006 Cum Y	12/17/2006 Cum X	12/17/2006 Cum Y
----(ft)-----	-----(in)-----	-----(in)-----	-----(in)-----	-----(in)-----	-----(in)-----	-----(in)-----	-----(in)-----	-----(in)-----	-----(in)-----	-----(in)-----	-----(in)-----	-----(in)-----	-----(in)-----	-----(in)-----
5	0	0.034	0.015	0.039	0.18	-0.059	0.309	-0.141	0.607	-0.263	0.656	-0.248	0.651	-0.265
7	0.001	0.03	0.004	0.043	0.133	-0.028	0.244	-0.108	0.493	-0.213	0.534	-0.195	0.533	-0.213
9	0.001	0.027	-0.002	0.043	0.092	-0.013	0.185	-0.093	0.391	-0.188	0.425	-0.166	0.426	-0.185
11	0.003	0.025	-0.008	0.044	0.048	0.003	0.12	-0.069	0.278	-0.141	0.306	-0.118	0.309	-0.135
13	0.003	0.024	-0.011	0.043	0.019	0.009	0.071	-0.053	0.184	-0.104	0.205	-0.078	0.21	-0.094
15	0.003	0.024	-0.012	0.044	0	0.014	0.03	-0.043	0.101	-0.074	0.116	-0.046	0.12	-0.061
17	-0.001	0.025	-0.015	0.043	0	0.015	0.01	-0.035	0.045	-0.048	0.056	-0.015	0.057	-0.031
19	-0.005	0.024	-0.017	0.044	-0.001	0.016	0.011	-0.027	0.019	-0.023	0.023	0.014	0.018	0
21	-0.003	0.026	-0.014	0.046	-0.005	0.023	0.018	-0.012	0.015	0	0.018	0.039	0.01	0.028
23	0	0.027	-0.009	0.048	-0.007	0.03	0.017	-0.005	0.027	0.009	0.009	0.051	0.003	0.041
25	-0.001	0.039	-0.001	0.052	-0.006	0.039	0.02	0.001	0.021	0.014	0.009	0.053	0.006	0.044
27	-0.003	0.039	-0.001	0.056	-0.011	0.047	0.013	0.008	0.015	0.014	0.003	0.052	0	0.043
29	0.008	0.031	0.008	0.045	-0.001	0.041	0.009	0.016	0.019	0.008	0.001	0.051	0.006	0.032
31	-0.006	0.025	-0.004	0.038	-0.008	0.038	-0.003	0.018	-0.002	0.021	-0.011	0.042	-0.006	0.025
33	0	0	0	0	0	0	0	0	0	0	0	0	0	0

Table D. 6- SW inclinometer Monroe

Plot Coordinates for Inclinometer SW
Relative to initial reading on 7 Dec2006 at 1412

J. Brian Anderson, UNC Charlotte

Printed 09-03-2007 at 17:01:42

skew = 135deg

Depth	12/11/2006 Cum X	12/11/2006 Cum Y	12/12/2006 Cum X	12/12/2006 Cum Y	12/12/2006 Cum X	12/12/2006 Cum Y	12/13/2006 Cum X	12/13/2006 Cum Y	12/14/2006 Cum X	12/14/2006 Cum Y	12/14/2006 Cum X	12/14/2006 Cum Y	12/17/2006 Cum X	12/17/2006 Cum Y
----(ft)-----	-----(in)-----	-----(in)-----	-----(in)-----	-----(in)-----	-----(in)-----	-----(in)-----	-----(in)-----	-----(in)-----	-----(in)-----	-----(in)-----	-----(in)-----	-----(in)-----	-----(in)-----	-----(in)-----
1	-0.087	0.022	-0.063	-0.034	-0.061	0.012	-0.041	0.003	-0.074	0.083	-0.035	0.088	-0.022	0.074
3	-0.088	0.017	-0.058	-0.039	-0.046	-0.001	-0.023	0.001	0.013	0.071	0.037	0.081	0.054	0.071
5	-0.079	0.012	-0.05	-0.041	-0.034	-0.004	0.021	0.003	0.09	0.073	0.112	0.084	0.13	0.074
7	-0.074	0.012	-0.045	-0.043	-0.03	-0.003	0.06	0.013	0.162	0.084	0.18	0.098	0.202	0.085
9	-0.068	0.011	-0.048	-0.043	-0.032	0	0.099	0.032	0.232	0.104	0.25	0.118	0.272	0.105
11	-0.065	0.011	-0.052	-0.042	-0.036	0.008	0.147	0.066	0.307	0.14	0.323	0.154	0.346	0.143
13	-0.063	0.01	-0.053	-0.04	-0.04	0.016	0.179	0.101	0.355	0.18	0.373	0.193	0.394	0.183
15	-0.062	0.007	-0.053	-0.042	-0.053	0.01	0.158	0.095	0.345	0.176	0.36	0.189	0.378	0.181
17	-0.057	0.004	-0.05	-0.043	-0.056	0.002	0.075	0.045	0.254	0.124	0.268	0.138	0.28	0.129
19	-0.054	0.008	-0.048	-0.04	-0.053	0.001	-0.014	-0.004	0.121	0.05	0.131	0.067	0.14	0.059
21	-0.051	0.003	-0.043	-0.043	-0.051	-0.002	-0.044	-0.027	0.014	-0.011	0.02	0.008	0.027	-0.002
23	-0.045	-0.005	-0.038	-0.043	-0.044	-0.011	-0.039	-0.036	-0.033	-0.03	-0.028	-0.015	-0.024	-0.021
25	-0.029	-0.017	-0.034	-0.037	-0.032	-0.017	-0.034	-0.032	-0.039	-0.025	-0.028	-0.018	-0.031	-0.022
27	-0.029	-0.021	-0.034	-0.036	-0.025	-0.032	-0.031	-0.032	-0.037	-0.025	-0.025	-0.025	-0.026	-0.029
29	-0.025	-0.033	-0.031	-0.041	-0.023	-0.045	-0.025	-0.04	-0.033	-0.03	-0.022	-0.032	-0.022	-0.035
31	-0.026	-0.031	-0.027	-0.042	-0.026	-0.041	-0.024	-0.04	-0.026	-0.036	-0.022	-0.037	-0.025	-0.038
33	0	0	0	0	0	0	0	0	0	0	0	0	0	0

Table D. 7 - NE inclinometer Monroe

Plot Coordinates for Inclinometer NE
Relative to initial reading on 7 Dec2006 at 1439

J. Brian Anderson, UNC Charlotte

Printed 09-03-2007 at 16:58:30

skew = -45deg

Depth	12/11/2006 Cum X	12/11/2006 Cum Y	12/12/2006 Cum X	12/12/2006 Cum Y	12/12/2006 Cum X	12/12/2006 Cum Y	12/13/2006 Cum X	12/13/2006 Cum Y	12/14/2006 Cum X	12/14/2006 Cum Y	12/14/2006 Cum X	12/14/2006 Cum Y	12/17/2006 Cum X	12/17/2006 Cum Y
----(ft)-----	-----(in)-----	-----(in)-----	-----(in)-----	-----(in)-----	-----(in)-----	-----(in)-----	-----(in)-----	-----(in)-----	-----(in)-----	-----(in)-----	-----(in)-----	-----(in)-----	-----(in)-----	-----(in)-----
1	0.036	-0.021	0.258	-0.081	0.466	-0.196	1.17	-0.414	1.936	-0.72	1.977	-0.695	1.951	-0.686
3	0.043	-0.026	0.241	-0.09	0.43	-0.198	1.041	-0.406	1.732	-0.702	1.779	-0.68	1.759	-0.674
5	0.042	-0.028	0.207	-0.088	0.376	-0.192	0.894	-0.385	1.51	-0.665	1.557	-0.644	1.542	-0.64
7	0.031	-0.022	0.148	-0.068	0.276	-0.158	0.703	-0.329	1.24	-0.586	1.288	-0.566	1.279	-0.567
9	0.024	-0.018	0.07	-0.033	0.147	-0.105	0.476	-0.244	0.925	-0.466	0.977	-0.45	0.972	-0.454
11	0.025	-0.019	0.028	-0.011	0.043	-0.06	0.266	-0.157	0.627	-0.339	0.681	-0.327	0.678	-0.33
13	0.026	-0.017	0.021	-0.008	-0.014	-0.034	0.116	-0.095	0.403	-0.236	0.451	-0.235	0.446	-0.235
15	0.028	-0.015	0.018	-0.008	-0.038	-0.022	0.02	-0.056	0.243	-0.168	0.291	-0.172	0.284	-0.171
17	0.029	-0.016	0.013	-0.009	-0.04	-0.021	-0.018	-0.039	0.144	-0.125	0.188	-0.129	0.176	-0.125
19	0.031	-0.019	0.014	-0.011	-0.024	-0.022	-0.041	-0.024	0.085	-0.088	0.117	-0.09	0.102	-0.086
21	0.032	-0.017	0.017	-0.01	-0.011	-0.023	-0.034	-0.016	0.034	-0.051	0.051	-0.053	0.038	-0.048
23	0.021	-0.012	0.016	-0.011	-0.009	-0.02	-0.014	-0.014	-0.001	-0.024	0.015	-0.025	-0.004	-0.02
25	0.014	-0.011	0.008	-0.01	-0.009	-0.013	-0.014	-0.015	-0.004	-0.018	0.008	-0.017	-0.013	-0.012
27	0.012	-0.01	0.003	-0.008	-0.002	-0.008	0.004	-0.013	0.006	-0.014	0.008	-0.014	-0.006	-0.011
29	0.011	-0.008	0.01	-0.007	0.008	-0.008	0.008	-0.008	0.009	-0.009	0.008	-0.009	0.01	-0.008
31	0	0	0	0	0	0	0	0	0	0	0	0	0	0

Table D. 8 - SE inclinometer Monroe

Plot Coordinates for Inclinometer SE
Relative to initial reading on 7 Dec2006 at 1431

J. Brian Anderson, UNC Charlotte

Printed 09-03-2007 at 16:59:47

skew = -45deg

Depth	12/11/2006 Cum X	12/11/2006 Cum Y	12/12/2006 Cum X	12/12/2006 Cum Y	12/12/2006 Cum X	12/12/2006 Cum Y	12/13/2006 Cum X	12/13/2006 Cum Y	12/14/2006 Cum X	12/14/2006 Cum Y	12/14/2006 Cum X	12/14/2006 Cum Y	12/17/2006 Cum X	12/17/2006 Cum Y
----(ft)-----	-----(in)-----	-----(in)-----	-----(in)-----	-----(in)-----	-----(in)-----	-----(in)-----	-----(in)-----	-----(in)-----	-----(in)-----	-----(in)-----	-----(in)-----	-----(in)-----	-----(in)-----	-----(in)-----
1	0	-0.042	0.032	-0.084	0.064	-0.063	0.228	-0.025	0.709	0.261	0.633	0.241	0.594	0.213
3	0.009	-0.041	0.021	-0.078	0.062	-0.05	0.201	-0.026	0.66	0.242	0.594	0.229	0.56	0.207
5	0.02	-0.045	0.014	-0.071	0.073	-0.046	0.185	-0.021	0.608	0.224	0.556	0.217	0.521	0.198
7	0.023	-0.042	0.006	-0.062	0.067	-0.036	0.164	-0.01	0.559	0.218	0.522	0.213	0.487	0.198
9	0.024	-0.033	0.002	-0.049	0.059	-0.023	0.148	0.004	0.52	0.216	0.494	0.212	0.465	0.203
11	0.027	-0.025	-0.002	-0.03	0.053	-0.008	0.14	0.019	0.484	0.213	0.467	0.213	0.449	0.209
13	0.025	-0.026	-0.006	-0.024	0.046	0	0.14	0.032	0.46	0.21	0.453	0.215	0.443	0.215
15	0.028	-0.028	-0.008	-0.026	0.04	-0.002	0.146	0.04	0.451	0.208	0.445	0.215	0.446	0.218
17	0.026	-0.026	-0.007	-0.026	0.019	-0.004	0.137	0.042	0.417	0.196	0.416	0.202	0.42	0.207
19	0.028	-0.026	0.001	-0.027	0.011	-0.009	0.098	0.025	0.359	0.165	0.363	0.168	0.365	0.177
21	0.029	-0.028	0.003	-0.025	0.013	-0.021	0.053	-0.003	0.271	0.111	0.279	0.115	0.28	0.127
23	0.024	-0.021	0.005	-0.015	0.009	-0.014	0.024	-0.008	0.156	0.064	0.16	0.067	0.161	0.073
25	0.02	-0.012	0.005	-0.005	0.008	-0.01	0.012	-0.006	0.057	0.021	0.059	0.021	0.061	0.023
27	0.011	-0.005	0.001	-0.001	0.003	-0.003	0.004	-0.001	0.011	0.004	0.01	0.004	0.012	0.004
29	0	0	0	0	0	0	0	0	0	0	0	0	0	0

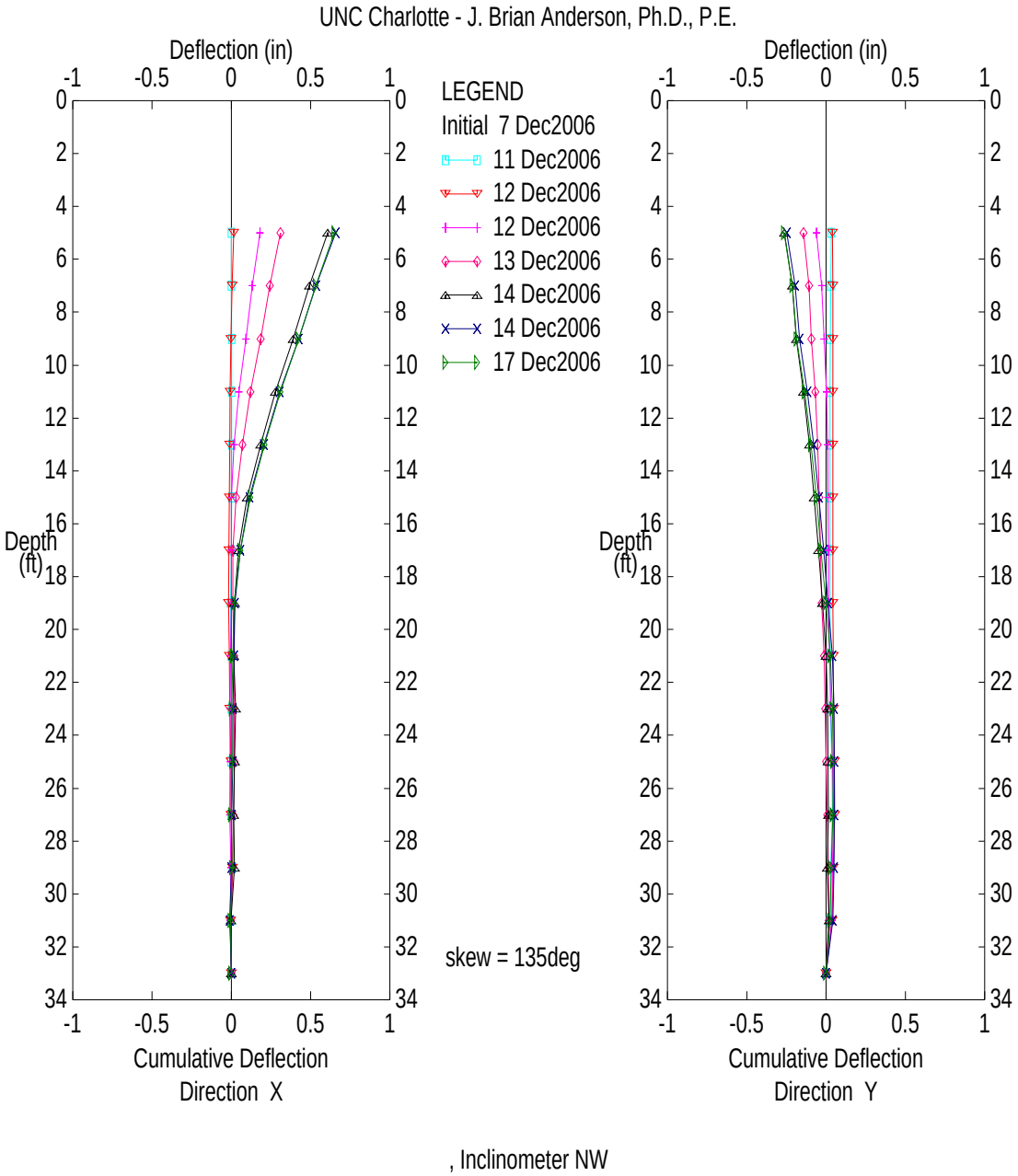

Figure D.5 - NW inclinometer Monroe

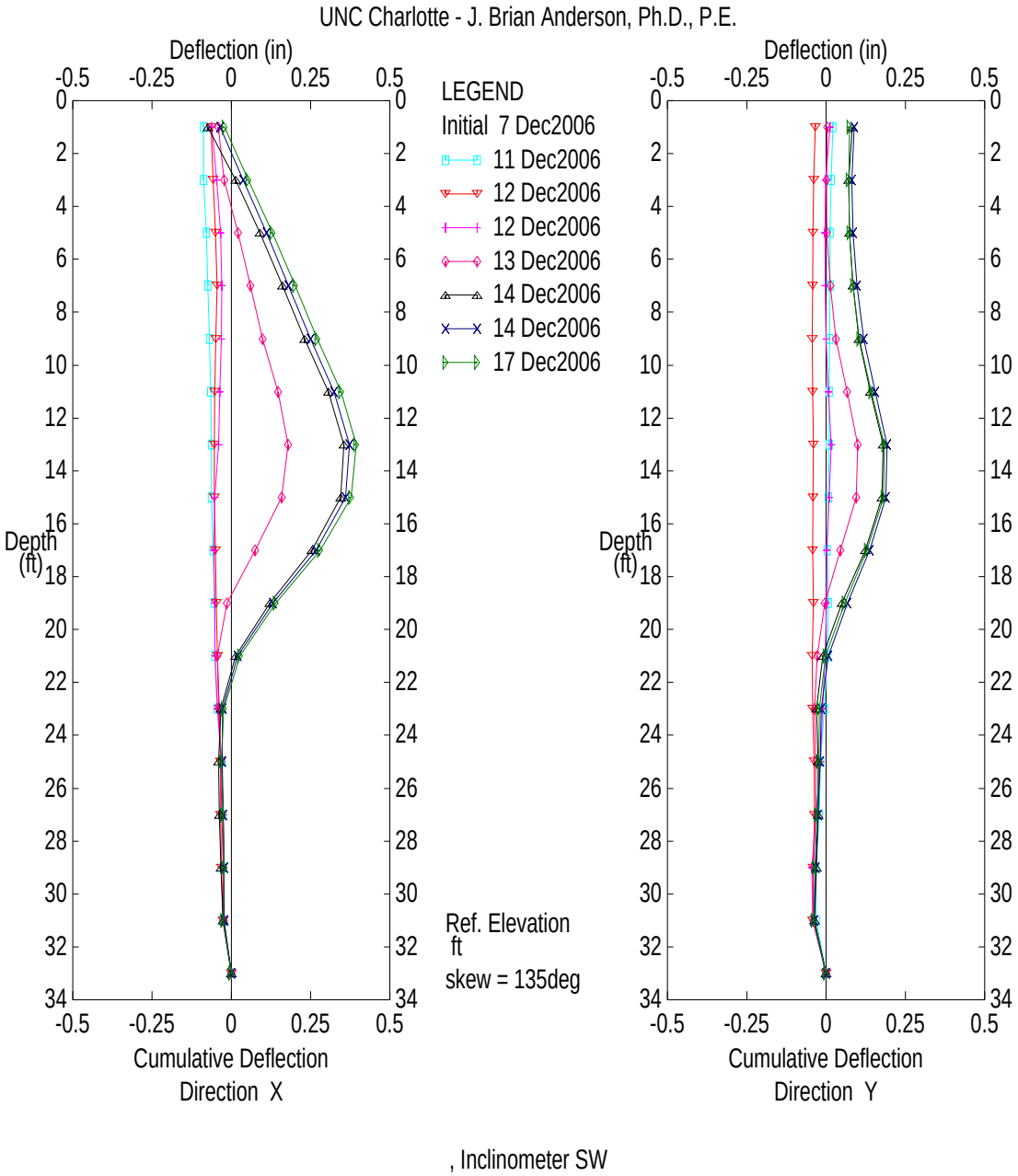

Figure D.6 - SW inclinometer Monroe

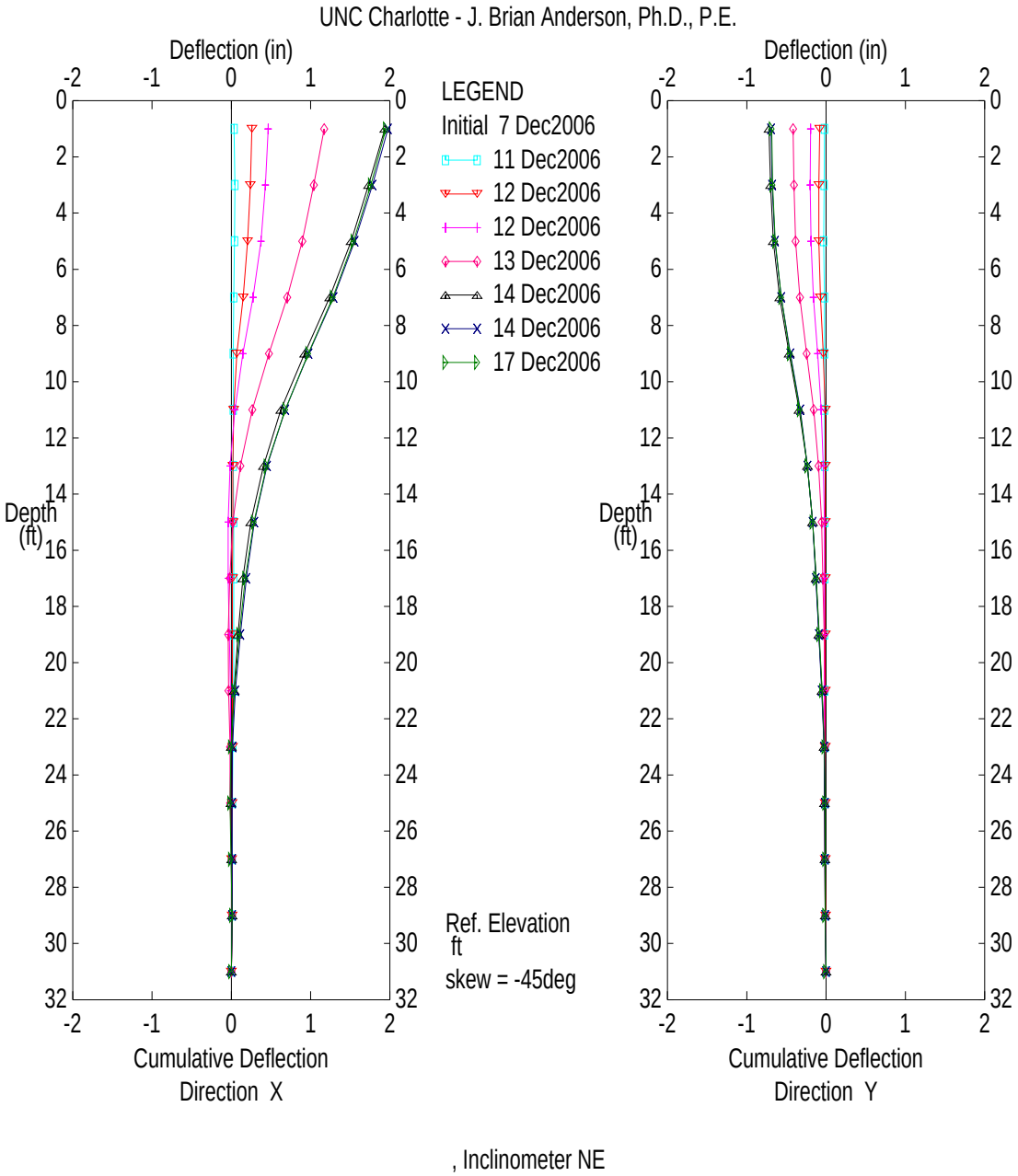

Figure D.7 - NE inclinometer Monroe

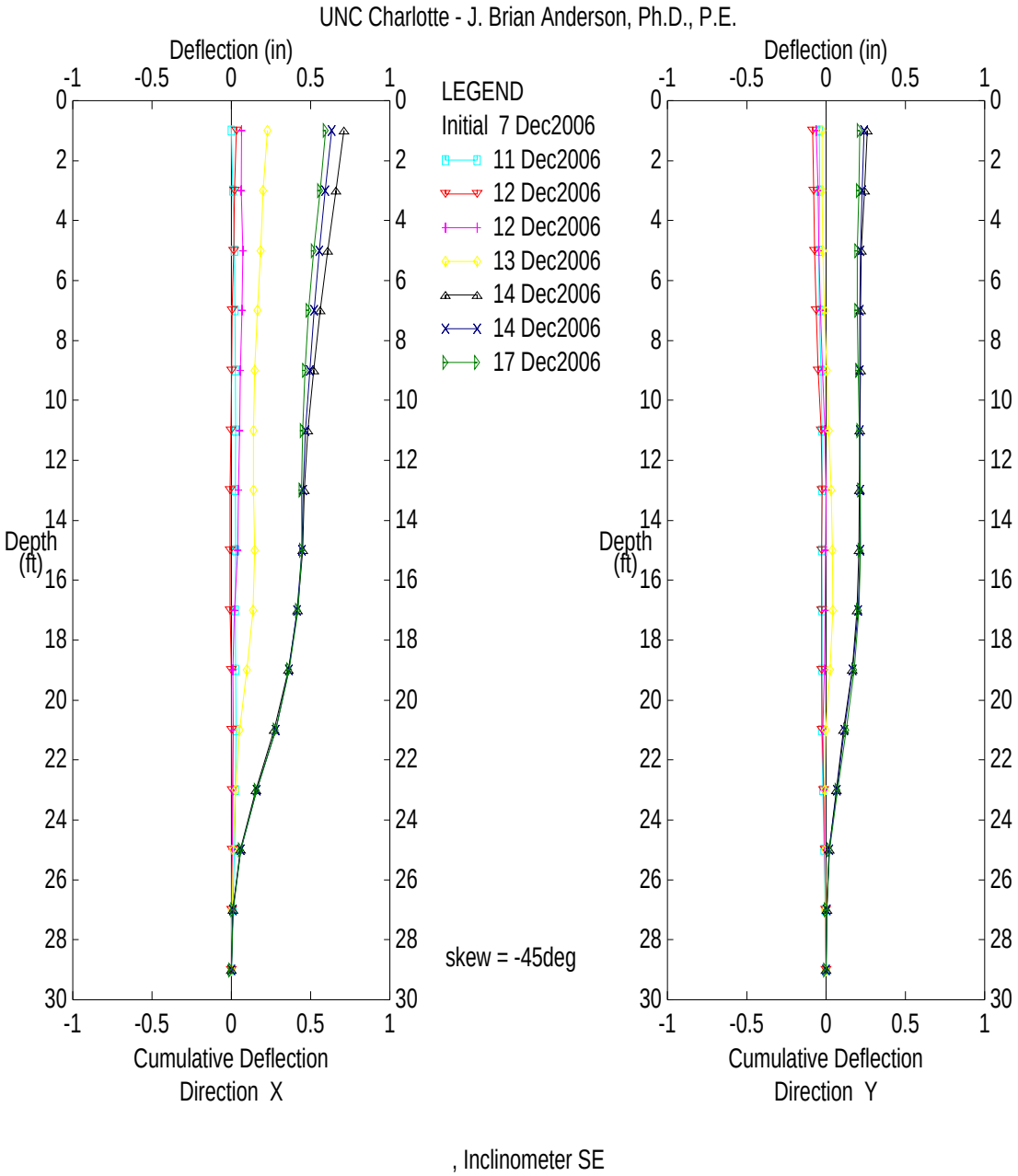

Figure D.8 - SE inclinometer Monroe

APPENDIX E
RECOMMENDATIONS FOR TRIAXIAL TESTS IN PIEDMONT RESIDUAL SOILS

Residual soils should be sampled in accordance with AASHTO T207 or ASTM D1587 specifications. Unlike clays that are typically sampled using Shelby tubes, residual soils require delicate and deliberate handling to insure the viability of test specimens. The procedure currently used by the Materials and Tests Unit of NCDOT to cut and extract specimens from Shelby Tubes utilizes a custom manufactured Shelby tube vise and large pipe cutter, shown in figure E.1, has proven to effective in creation of triaxial specimens.

The method is as follows:

1) If this is the first specimen from the Shelby tube, cut one inch from the beveled end with a 3 inch pipe cutter to remove disturbed/contaminated soil.
2) Mark a six inch length from the cut end of the tube and note the direction the orientation of the tube.
3) Place the Shelby tube in the tube vise and use a 3 inch pipe cutter to cut the Shelby tube at the six inch mark. Tighten the clamp slowly to insure even cutting and limit deformation of the tube. It should take more than 25 turns to cut the tube.
4) When cutter penetrates the tube and the entire circumference is separated, use a wire saw or knife edge to cut the soil inside.
5) Reseal the remaining tube length with a protective cap.
6) Using a vertically oriented jack extractor with a retaining ring appropriate for Shelby tubes, extrude the soil specimen insuring the soil moves in the same direction as when it was sampled.

Each triaxial test should be conducted using AASHTO T297 or ASTM D4767. Strain rates, and time to failure, can be determined based upon those specified by ASTM D4767 (2004), equation E.1, and recommendations by Bishop and Henkel (1957), equation E.2.

$$'\varepsilon = \frac{4\%}{10t_{50}} \tag{E.1}$$

Where ‘ε is the strain rate
t_{50} is the time to 50% consolidation of the triaxial specimen

$$t_f = \frac{20h^2}{\eta c_v} \tag{E.2}$$

Where t_f is time to failure
h is half height of the triaxial specimen
η = 3 drainage at both ends or 35 for radial and drainage at both ends
c_v is the coefficient of consolidation

Using 15% strain as the arbitrary failure point, the time to failure and strain rate for increasing values of t_{50} for a 3 x 6 inch specimen are shown in table E - 1. The quickest practical time to failure is 90 minutes for 15% strain. On the other hand, tests with a duration longer than 6 hours are impractical as well. Therefore if t_{50} during consolidation is 10 minutes or less (120 if filter strips are used), a drained test is recommended. For specimens with longer t_{50} values, undrained tests should be conducted. The strain rates and times to failure shown in table E.1 can be used as a guide. Generally, the addition of filter strips will enhance the ability to conduct drained tests on the specimens.

Figure E.1 – NCDOT Shelby Tube Vise and 3 inch pipe cutter

Table E.1 – Time to failure and strain rate recommendations for drained tests

		Bishop & Henkel CD Recommendation				ASTM CU		
		End Drainage		End and Radial Drainage				
t_{50}	c_v	t_f	ε'	t_f	ε'	t_f	ε'	ε'
(min)	(in^2/min)	(min)	(in/min)	(min)	(in/min)	(min)	(in/min)	(%/min)
0.1	17.64	3.4	0.2646	0.3	3.087	3.75	0.24	4.00
0.2	8.82	6.8	0.1323	0.6	1.5435	7.50	0.12	2.00
0.5	3.528	17.0	0.05292	1.5	0.6174	18.75	0.048	0.80
1	1.764	34.0	0.02646	2.9	0.3087	37.50	0.024	0.40
2	0.882	68.0	0.01323	5.8	0.15435	75.00	0.012	0.20
5	0.3528	170.1	0.005292	14.6	0.06174	187.50	0.0048	0.08
10	0.1764	340.1	0.002646	29.2	0.03087	375.00	0.0024	0.04
20	0.0882	680.3	0.001323	58.3	0.015435	750.00	0.0012	0.02
50	0.03528	1700.7	0.0005292	145.8	0.006174	1875.00	0.00048	0.01
100	0.01764	3401.4	0.0002646	291.5	0.003087	3750.00	0.00024	0.00
120	0.0147	4081.6	0.0002205	349.9	0.0025725	4500.00	0.0002	0.00